INFORMATION TO USERS

This manuscript has been reproduced from the microfilm master. UMI films the text directly from the original or copy submitted. Thus, some thesis and dissertation copies are in typewriter face, while others may be from any type of computer printer.

The quality of this reproduction is dependent upon the quality of the copy submitted. Broken or indistinct print, colored or poor quality illustrations and photographs, print bleedthrough, substandard margins, and improper alignment can adversely affect reproduction.

In the unlikely event that the author did not send UMI a complete manuscript and there are missing pages, these will be noted. Also, if unauthorized copyright material had to be removed, a note will indicate the deletion.

Oversize materials (e.g., maps, drawings, charts) are reproduced by sectioning the original, beginning at the upper left-hand corner and continuing from left to right in equal sections with small overlaps.

Photographs included in the original manuscript have been reproduced xerographically in this copy. Higher quality 6" x 9" black and white photographic prints are available for any photographs or illustrations appearing in this copy for an additional charge. Contact UMI directly to order.

ProQuest Information and Learning
300 North Zeeb Road, Ann Arbor, MI 48106-1346 USA
800-521-0600

BASEMENT-CORED UPLIFT DEFORMATION IN THE NORTHERN SIERRAS PAMPEANAS: THREE-DIMENSIONAL UPLIFT STRUCTURE, BASEMENT DEFORMATION, AND REGIONAL ANALYSIS

by

Pilar Elena García

A Dissertation Submitted to the Faculty of the

DEPARTMENT OF GEOSCIENCES

In Partial Fulfillment of the Requirements
For the Degree of

DOCTOR OF PHILOSOPHY

In the Graduate College

THE UNIVERSITY OF ARIZONA

2001

UMI Number: 3016470

UMI Microform 3016470

Bell & Howell Information and Learning Company
300 North Zeeb Road
P.O. Box 1346
Ann Arbor, MI 48106-1346

THE UNIVERSITY OF ARIZONA ®
GRADUATE COLLEGE

As members of the Final Examination Committee, we certify that we have read the dissertation prepared by Pilar Elena García

entitled Basement-Cored Uplift Deformation in the Northern Sierras Pampeanas: 3D Uplift Structure, Basement Deformation and Regional Analysis

and recommend that it be accepted as fulfilling the dissertation requirement for the Degree of Doctor of Philosophy

George H. Davis — Date 5/4/01

Charles Kluth — Date 05/04/01

Clem Chase — Date 4 May 2001

Susan Beck — Date 5/4/2001

George Zandt — Date 5/4/01

Peter DeCelles — Date 5/24/01

Final approval and acceptance of this dissertation is contingent upon the candidate's submission of the final copy of the dissertation to the Graduate College.

I hereby certify that I have read this dissertation prepared under my direction and recommend that it be accepted as fulfilling the dissertation requirement.

Dissertation Director George H. Davis — Date 5/4/01

STATEMENT BY AUTHOR

This dissertation has been submitted in partial fulfillment of requirements for an advanced degree at The University of Arizona and is deposited in the University Library to be made available to borrowers under rules of the Library.

Brief quotations from this dissertation are allowable without special permission, provided that accurate acknowledgment of the source is made. Requests for permission for extended quotation from or reproduction of this manuscript in whole or in part may be granted by the head of the major department or the Dean of the Graduate College when in his or her judgment the proposed use of the material is in the interests of scholarship. In all other instances, however, permission must be obtained from the author.

SIGNED: 

ACKNOWLEDGMENTS

"Well, how did I get myself into this?" There are several people who lured me into this study and who helped me along the way. First, my family who always led me to believe I could do anything I wanted (except play softball when I was eight) and who supported me and encouraged me in carrying out my endeavors. My dad, who taught me Spanish and algebra when I was little and made sure that I received just as good (if not better!) an education as anyone else, my mom who provided an example of an able and independent woman who ventured out into the world and who always prayed for me, my older brother Julio who taught me to expect only the best from myself and to fight for it, and my younger brother Guillermo, confidant, cohort and supporter throughout the years, an example of someone who stands by his word and his beliefs.

My advisor, "agent" and friend, George H. Davis, most noticeably lured me to the University of Arizona with his enthusiasm for geology and with his unselfish good-nature. George took me up to the Colorado Plateau with him before starting graduate school, as an introduction to the geology of the area, but also as an introduction to our relationship. It's an eleven hour drive to and from Kodachrome State Park, Plush Basecamp Accommodations. He has been a tremendous mentor as a scientist and even more importantly as a person; inspiration of the phrase, "I wanna be just like George."

George introduced me to one of my best geology cohorts, Shari Christofferson, who provided tremendous personal support, as well as scientific support in Argentina. Shari, role model of coolness, good-heartedness and humor, revived the New Yorker in me and has been a superb companion since we met. Many other friends provided support and helpful discussion, including (but not limited in any way) Elena Shoshitaishvili, Nadine McQuarrie, Matt Muller, Carlie Rodriguez, Steve Kidder, Alex Bump, Steve Ahlgren, Ofori Pearson, Delores Robinson, Catherine O'Reilly, Kirk Hoffman, Matt Spurlin, Frankie Ridolfi. In the midst of all their work, they always found time to talk, climb, help me move, discuss, drink tea. Mariam Maqsood and Andrea Chartock provided valuable support, endless encouragement, and excellent distractions throughout the years.

There are several other people (and agencies) who made my work in Argentina possible. Rick Allmendinger first suggested Sierra de Hualfín to George and myself, as an accessible area, good basement exposure and few pokey cactus plants. Rick generously continued to provide helpful discussion, references, airphotos, and helpful reviews of manuscripts. Ernesto Cristallini also provided helpful discussions, access to unpublished and soon-to-be published data, and logistical help in Argentina. Peter Coney was a great inspiration for this study. He gave me encouragement, and always had kind words and a smile just when I needed them. Pete DeCelles, Susan Beck and George Zandt also took time to discuss ideas and help improve the content of this study. Chuck Kluth and Greg Schoenborn generously took time to help me with ideas, discussions and electronic cross section consultations. Financial support for this study came from an NSF Minority Graduate Fellowship (1997-2000), an ARCO field study award (1999), GeoStructure Partnership fund (1998, 1999), an NSF Dissertation Enhancement Award (1999-2000).

Last, but greatest in overall contribution to the success of this work is my fiancé, Oleg Mikhailov. Oleg inspired me, supported me, comforted me, excitedly discussed ideas with me, helped me build models of the crust from books and a down bedspread. His enthusiasm knows no end; he is one of the most alive people I have ever met. His intelligence and rigor improved the ideas and content in this study. His creativity and crisis management skills got me out of trouble and helped me see problems as puzzles. His kindness helped me live better during the last few years. I am most fortunate to have met him and even more fortunate to be able to spend the rest of my life with him.
Thank you so much, Olezha.

...En la alameda
un manantial recita
su canto entre las hierbas.
Y el caracol, pacífico
burgués de la vereda,
ignorado y humilde,
el paisaje contempla.

La divina quietud
de la naturaleza
le dio valor y fe,
y olvidando las penas
de su hogar deseó
ver el fin de la senda...

Federico García Lorca
Los Encuentros de un Caracol Aventurero
Diciembre de 1918

Este trabajo ha sido inspirado por mis padres, Julio y María García.
Sin su amor, fe y apoyo, nunca hubiera podido explorar este mundo.
Se los dedico a Uds. con todo mi amor y devoción.

TABLE OF CONTENTS

TABLE OF CONTENTS - *Continued*

LIST OF FIGURES

LIST OF FIGURES - *Continued*

LIST OF FIGURES - *Continued*

LIST OF TABLES

ABSTRACT

The structure of basement-cored uplift mountains is fundamentally controlled by the geometry of the basement and the basement unconformity. In the Sierra de Hualfín, an uplift located in the Sierras Pampeanas of NW Argentina, the well-exposed basement unconformity displays along-strike structural variations. The Sierra de Hualfín is composed of a core of Ordovician granitoid overlain by and thrust over Tertiary sedimentary rocks. The range is uplifted by an east-directed thrust fault, creating a steep range-front on the east and a gently dipping backlimb on the west. In the central region, however, basement and cover rocks in the backlimb are folded. Cross sections across the uplift and a three-dimensional computer model show that the variations along strike are due to differences in the geometry of the underlying fault or faults that deform the basement unconformity.

Analysis of the folded basement unconformity on the west side of Sierra de Hualfín shows that brittle processes of faulting, cataclasis and fracture foliation help the basement attain a folded form. Pervasive and continuous joint fractures, and an unconformity-parallel fracture foliation at the surface, set up a condition for "flow" of granitic materials. Additionally, in order for basement to fold, the tip of the underlying fault must be located within the basement before it begins propagating towards the surface.

Using the knowledge gained from the detailed structural studies, two regional cross sections were constructed in the region of Sierra de Hualfín, showing spatial and geometric relations between the adjacent uplifts, and the thrust systems of the eastern Puna Plateau. The cross sections show detachment levels at 16 km and ~27 km for uplifts in the northern Sierras Pampeanas. Thrust faults of the northern Sierras Pampeanas, and of the eastern edge of the Puna can be interpreted as part of the same east-directed thrust system, with intervening west-directed backthrust development. The combination of the modeling of

Sierra de Hualfín and the regional cross sections with detachments at 16 to 27 km depth suggests that basement-cored uplifts can be formed, not by steep faults, but by gently-dipping faults detaching in the middle crust and near the base of the crust.

CHAPTER 1
INTRODUCTION

This work addresses the structure and regional context of the Sierra de Hualfín, a basement-cored uplift located in the northern Sierras Pampeanas, NW Argentina. The Sierras Pampeanas present an opportunity to study a modern (and active) basement-cored uplift province. Basement-cored uplift provinces occur in many places around the world and are composed of individual mountain ranges separated by wide, intervening basins. Attention was first drawn to basement-cored uplifts in the western United States because they occur far inboard from the North America-Pacific plate margin, perhaps too far for compressional forces to be uplifting these structures (Dickinson and Snyder, 1978). Thus, their tectonic significance and mechanism of formation were in question. The structure of the uplifts (i.e. fault geometry, basement geometry) as observed on the surface only added to debates on their origin, plate tectonic significance, and kinematic development (e.g. Stearns, 1978; Brown, 1988; Jordan et al., 1983; Jordan and Allmendinger, 1986).

With the recognition of the Sierras Pampeanas, first as basement-cored uplifts (González Bonorino, 1950), and subsequently as a possible modern analogue to the Rocky Mountain foreland (Sales, 1968; Dickinson and Snyder, 1978; Jordan and Allmendinger, 1986), the Sierras Pampeanas became a natural place to study active basement-cored uplifts. The Sierra de Hualfín was chosen for this study because it is one of the few uplifts in the Sierras Pampeanas where cover sedimentary rocks are preserved (Fig. 1.1). Additionally, the uplift is exposed at the level of the basement-cover interface. The basement-cover interface is a paleo-erosional surface in granite, and was presumably horizontal before basement-cored uplift deformation (Jordan et al., 1989). Thus the geometry of the basement unconformity records the deformation of the basement during development of the uplift. The basement unconformity in the Sierra de Hualfín is clearly

folded, and thus the question of how crystalline, granitic basement can achieve a fold shape (also a point of contention in the Rocky Mountain foreland) can be addressed.

The premise of the first and second studies presented herein is that a better understanding of the structure of these uplifts from analysis of field observations, and available subsurface data, will lead to better theories concerning the tectonic significance of the uplifts and the provinces they comprise. The third paper deals with the northern Sierras Pampeanas in their regional context, and suggests a deformational history related to adjacent thrust systems. These studies also suggest that basement-cored uplifts formed via low-angle thrust faults.

The first study, "*Along-strike variations in the Sierra de Hualfín, NW Argentina: Clues to the formation of a basement-cored uplift*," addresses the three-dimensional range-scale structure of the Sierra de Hualfín. Field mapping of the uplift uncovered along-strike variations in the geometry of the basement unconformity which can be divided into four structural domains. The along-strike structural variations appear to be the result of backthrust formation, and of complexities in the main thrust plane. Three-dimensional modeling of the main thrust shows that there is a kink in the west-dipping main fault plane that may be contributing to along-strike structural variations on the east side of the uplift. In addition, cross section balancing shows that the Sierra de Hualfín, and similar basement-cored uplifts, can be formed by gently-dipping thrust faults whose geometry reflects the geometry of the overlying basement and cover rocks.

The second study, "*Mechanisms of basement deformation as revealed in the Sierra de Hualfín basement-cored uplift, NW Argentina*," takes a close look at the geometry, kinematics, and deformation of the granitic basement in the Sierra de Hualfín. Brittle processes of faulting, cataclasis and fracture foliation development affect the basement and help it attain a folded form. However, it is the condition of the granitic basement prior to deformation that most influences how it deforms. The presence of pervasive and

continuous joint fractures, and of an unconformity-parallel fracture foliation at the surface, sets up a condition for "flow" of granitic materials, much the way grains in a sandstone facilitate bulk-rock flow during folding and deformation. Additionally, in order for basement to fold, the tip of the fault must be located (deep) within the basement before it begins propagating towards the surface. This is contrary to the depiction of basement-cored uplifts in the literature, where the fault tip is located at the basement-cover interface. This condition implies that, where basement is folded, the underlying faults must have been newly-formed or the tips of pre-existing faults must have been beneath the basement-cover interface. Thus, the development of models of basement-cored uplifts can include an assessment of the extent of folding of basement in these provinces and incorporate a buried fault tip into their models in order to more closely reproduce observed features.

The third study, "*The northern Sierras Pampeanas and their relation to the adjacent Puna Plateau and Eastern Cordillera-Santa Barbara System*," examines the regional context of basement-cored uplifts in the northern Sierras Pampeanas and their development through the construction and analysis of two regional cross sections. Previous studies of kinematics of the adjacent thrust systems of the Puna Plateau and the Eastern Cordillera-Santa Barbara System show a continuity of deformation (Allmendinger et al., 1997, Marrett et al., 1994), suggesting these systems have a related compressional history. The cross sections in this study show two detachment levels, at 16 km and ~27 km for uplifts in the study area of the northern Sierras Pampeanas. The cross sections can be restored and balanced using a general eastward progression of deformation from the eastern edge of the Puna to the northern Sierras Pampeanas. Thrust faults of the northern Sierras Pampeanas and of the eastern edge of the Puna can be interpreted as having similar detachment levels, and as part of the same east-directed thrust system, with intervening west-directed backthrust development. The combination of modeling of the Sierra de Hualfín from the first study, and the regional cross sections with detachments ranging from 16 to ~27 km depth

suggests that, in the northern Sierras Pampeanas, basement-cored uplifts can be formed, not by steep faults, but by gently-dipping faults detaching in the middle crust and near the base of the crust. Similar detachment levels have also been proposed for the uplifts in the Wyoming foreland (Stone, 1993; Erslev, 1993). Mechanisms for the formation of basement-cored uplifts must then address or account for varying levels of detachment for individual uplifts within a province.

CHAPTER 2

ALONG-STRIKE STRUCTURAL VARIATIONS IN THE SIERRA DE HUALFIN, NW ARGENTINA: CLUES TO THE FORMATION OF A BASEMENT-CORED UPLIFT

ABSTRACT

The Sierra de Hualfín is a basement-cored uplift located at the southern boundary of the Puna Plateau and the northwestern end of the Sierras Pampeanas province. Referred to as the Tucumán Lineament and the Tucumán Transfer Zone, this area is marked by NE-SW-trending structures, which depart from the general N-S trend of uplifts in the Sierras Pampeanas. The Sierra de Hualfín trends NNE to NE, and is a 22 km-long, thrust-bounded basement-cored uplift that places Ordovician granite over Tertiary sedimentary rocks. The uplift is characterized by a broad fold related to a large east-verging, listric reverse fault.

Field mapping in the Sierra de Hualfín revealed NW-SE trending tear faults with apparent dextral motion and/or NNE-NNW directed reverse motion. The main range-bounding reverse fault strikes NE and appears to have accommodated mainly dip-slip motion. The uplift is compartmentalized by tear faults into several basement blocks that have distinct characteristics. The arrays of basement blocks can be divided into four domains that are distinguished by changes in the orientation (and shape) of an originally planar basement unconformity. Movement on the tear faults, although minimal, imparted an overall right-lateral shear to the basement of the Sierra de Hualfín. Analysis of the compartmentalizing faults and the domains suggests that the Sierra de Hualfín was formed by (1) Major faulting of the uplift under NW-SE directed compression (1a) Development of

the backthrust on the west (2) Uplift of the Northern Domain block by local NNE-SSW compression (2a) Movement of the East-Central Domain block due to thrusting of the Northern Domain over the East-Central Domain. This is compatible with regional kinematic interpretations of two distinct shortening directions, one oriented E-W to WSW-ENE and the other oriented N-S.

The along-strike structural variations appear to be the result of backthrust formation, and of complexities in the main thrust plane. Three-dimensional modeling of the main thrust shows that there is a kink in the west-dipping main fault plane that may be contributing to along-strike structural variations on the east side of the uplift. In addition, cross section balancing shows that the Sierra de Hualfín, and similar basement-cored uplifts, can be formed by gently-dipping thrust faults whose geometry reflects the geometry of the overlying basement and cover rocks.

2.1. INTRODUCTION

The Sierras Pampeanas are a group of basement-cored uplifts (Fig. 2.1), analogous to the Laramide province in the western U.S. Basement-cored uplifts are typically located in the foreland of fold-thrust belts and consist of several major, and subsidiary, individual basement-cored uplifts. The two-dimensional structure of basement-cored uplifts has been studied most extensively in the Laramide province of the western United States (e.g. Brown, 1988; Schmidt and Perry, 1988; Schmidt and Erslev, 1993). In many cases, basement-cored uplifts are structurally complex or they display structural variation along strike.

The Sierra de Hualfín is located at the southern boundary of the Puna Plateau (Allmendinger, 1986) and at the northwestern end of the Sierras Pampeanas (Fig. 2.1). This area has been interpreted as the site of the Tucumán Lineament (Mon, 1976) and the

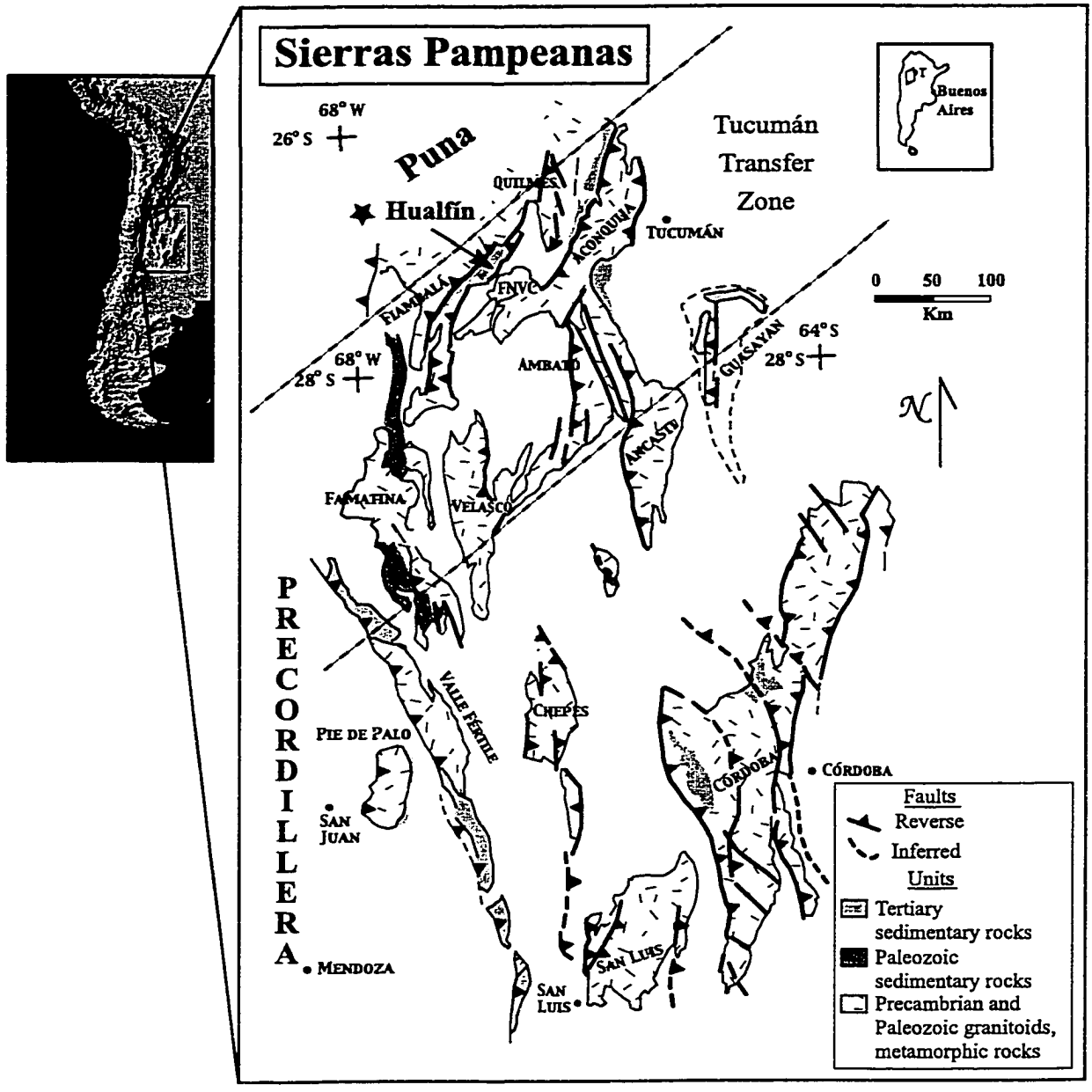

Figure 2.1. Shaded digital topographic image of the western margin of South America and simplified geologic map of the Sierras Pampeanas. Sierras Pampeanas are located in the black outline box. Adapted from Jordan and Allmendinger (1986) and the Geologic Map of Argentina (Achili et al., 1997) by the Servicio Geológico Argentino. Ranges are accompanied by their respective names. Sierra de Hualfín is located in the northern region. Tucumán Transfer Zone location from Urreiztieta et al. (1996).

Tucumán Transfer Zone (Urreiztieta et al., 1996) because of NE-SW-trending structures throughout the area, which depart from the general N-S trend of uplifts in the Sierras Pampeanas. The Transfer Zone is postulated to be a dextral transpressional zone that helps accommodate the southward narrowing of the Puna Plateau (Jordan et al., 1983; Urreiztieta et al., 1996, Gapais et al., 2000).

Sierra de Hualfín is one of the few uplifts in the Sierras Pampeanas where sedimentary cover rocks are preserved (Figs. 2.1, 2.2, 2.3) and where structures are exposed at the level of the basement-cover interface (Figs. 2.2, 2.3). Thus, it is an opportune place to study the structure of a typical basement-cored uplift, and to analyze how deformation of the basement defines the structural form of the uplift. Additionally, the topography can be directly correlated to the structure because of the youthful age of deformation (not older than ~ 10 Ma) and recent denudation of the area (Coughlin et al., 1998).

Structural variations seen in the Sierra de Hualfín have been recognized before (Urreiztieta et al., 1996); however, no attempts have been made to examine the transitions between these variations to interpret the development of the Sierra de Hualfín. The uplift can be divided into a southern portion characterized by bending of basement, a central area where there is kinking of the basement erosional surface and obvious folding of the overlying Tertiary rocks, and a northern area where there is "low-angle" thrusting of basement over Tertiary sedimentary rocks (Urreiztieta et al., 1996). The presence of the prominent along-strike variations in the Sierra de Hualfín lends to the definition of structural domains within the uplift. Results of field mapping at a scale of 1:55,000 show that structural variations along-strike of Sierra de Hualfin can be divided into four domains separated by transverse faults (Fig. 2.4, 2.5).

Regional kinematic interpretations (Allmendinger, 1986; Marrett et al., 1994; Urreiztieta et al., 1996; Gapais et al., 2000) suggest there are two distinct shortening

directions that have affected the region of the northern Sierras Pampeanas and the SE Puna Plateau. The shortening directions from these interpretations are oriented E-W to WSW-ENE and N-S. The present study integrates the results of mapping, cross sections and a three-dimensional model, and suggests that the Sierra de Hualfín was uplifted along a main, gently-dipping thrust fault, and other reverse faults, that are oriented consistently with respect to the regional shortening directions previously interpreted.

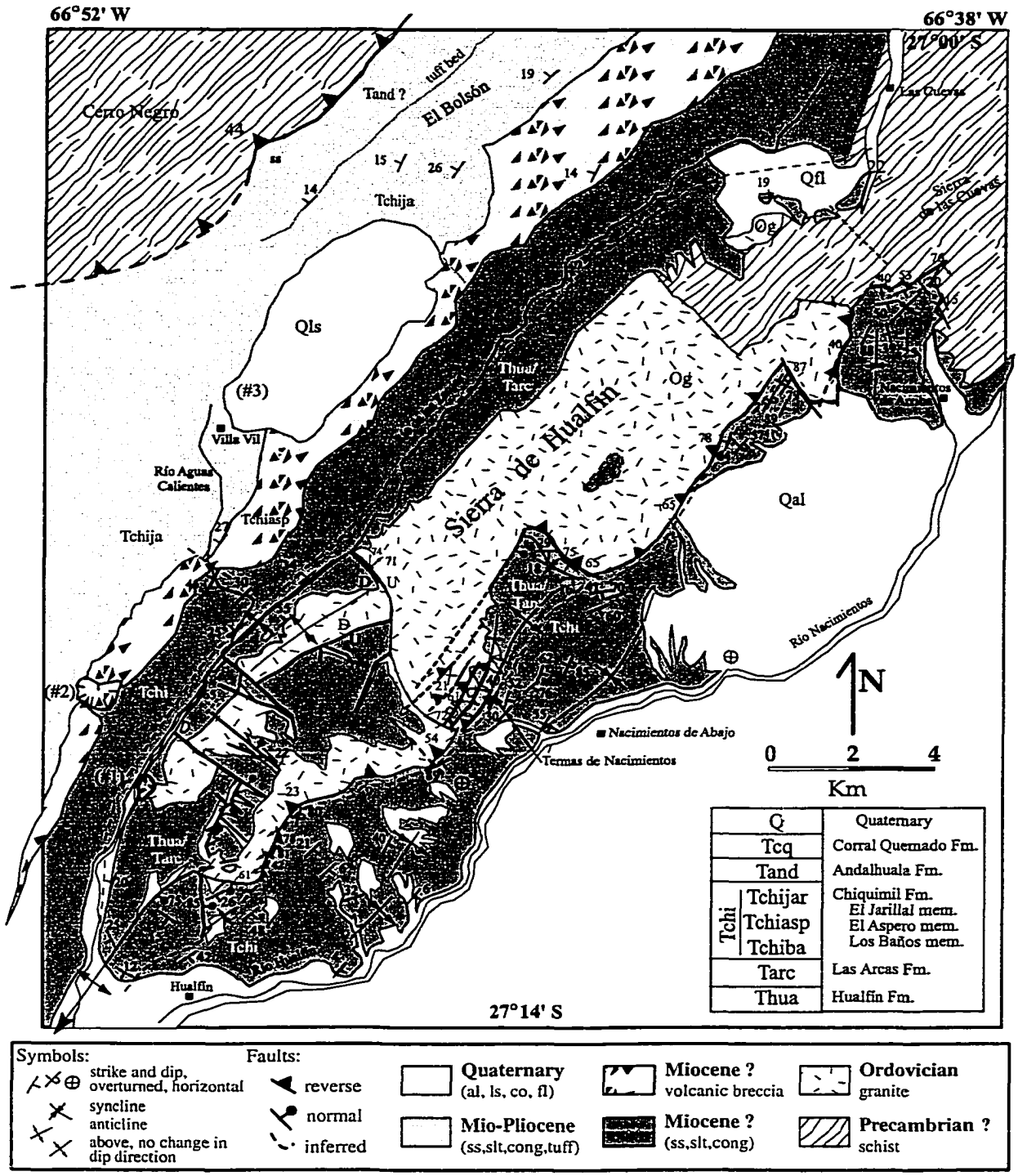

Figure 2.2. Geologic map of the Sierra de Hualfín. Stratigraphy and legend described in Figure 2.3.

Figure 2.3. Stratigraphic column of lithologies in the area of Sierra de Hualfín, showing classifications from González Bonorino (1950), Allmendinger (1986), and Muruaga (1998). The 100-m scale on the right corresponds to thicknesses reported in Muruaga (1999). Legend at right corresponds to mapped units in Figure 2. Abbreviations used for units (where identifiable) are: **Og** (Ordovician granite), **Thua** (Hualfín Fm.), **Tarc** (Las Arcas Fm.), **Tchiq** (Chiquimil Fm., undifferentiated), **Tchiba** (Los Baños member, Chiquimil Fm.), **Tchias** (El Aspero member, Chiquimil Fm.), **Tchija** (El Jarillal member, Chiquimil Fm.), **Tand** (Andalhuala Fm.), **Tcq** (Corral Quemado Fm.), **Q**(al, ls, fl).

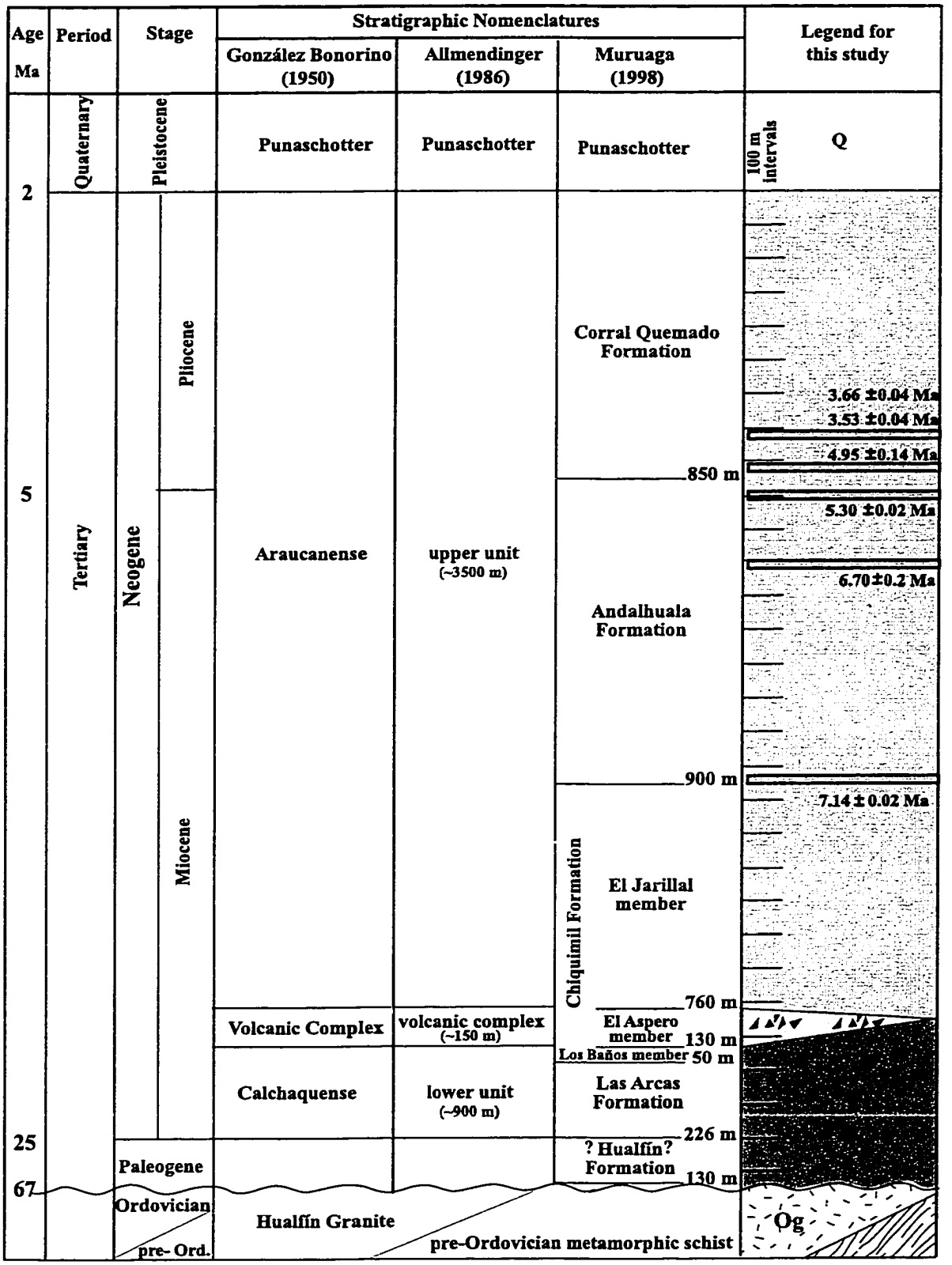
Age Ma
Period
Stage
Stratigraphic Nomenclatures
González Bonorino (1950)
Allmendinger (1986)
Muruaga (1998)
Legend for this study
2
5
25
67
Quaternary
Tertiary
Neogene
Paleogene
Pleistocene
Pliocene
Miocene
Ordovician
pre- Ord.
Punaschotter
Punaschotter
Punaschotter
100 m intervals
Q
Araucanense
upper unit (~3500 m)
Corral Quemado Formation
3.66 ±0.04 Ma
3.53 ±0.04 Ma
4.95 ±0.14 Ma
850 m
5.30 ±0.02 Ma
6.70±0.2 Ma
Andalhuala Formation
900 m
7.14 ± 0.02 Ma
Chiquimil Formation
El Jarillal member
760 m
Volcanic Complex
volcanic complex (~150 m)
El Aspero member
130 m
Los Baños member
50 m
Calchaquense
lower unit (~900 m)
Las Arcas Formation
226 m
? Hualfín? Formation
130 m
Hualfín Granite
pre-Ordovician metamorphic schist
Og

Figure 2.3

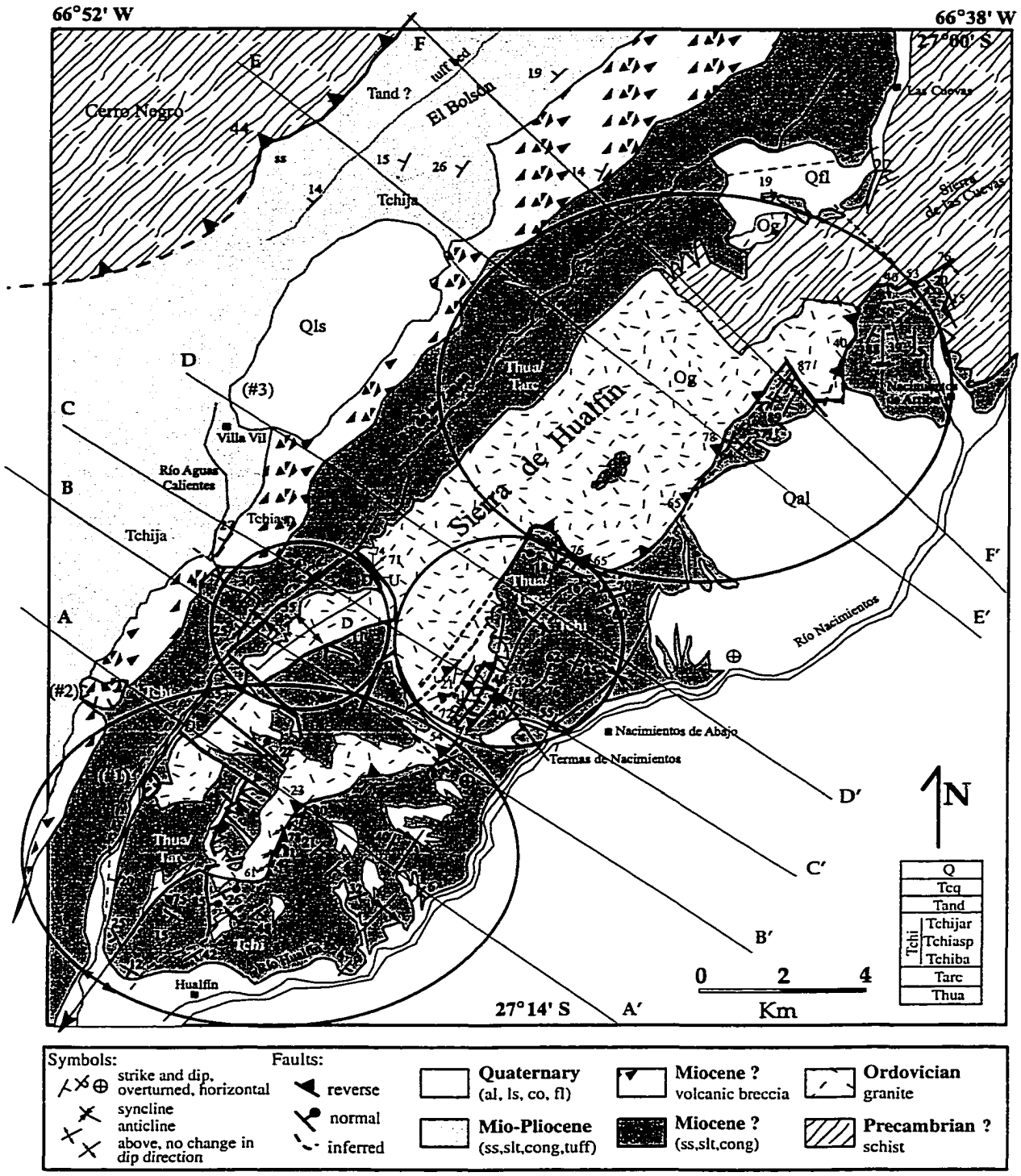

Figure 2.4. Geologic map of the Sierra de Hualfín with domain boundaries and cross section locations. See Figure 2.3 for legend details.

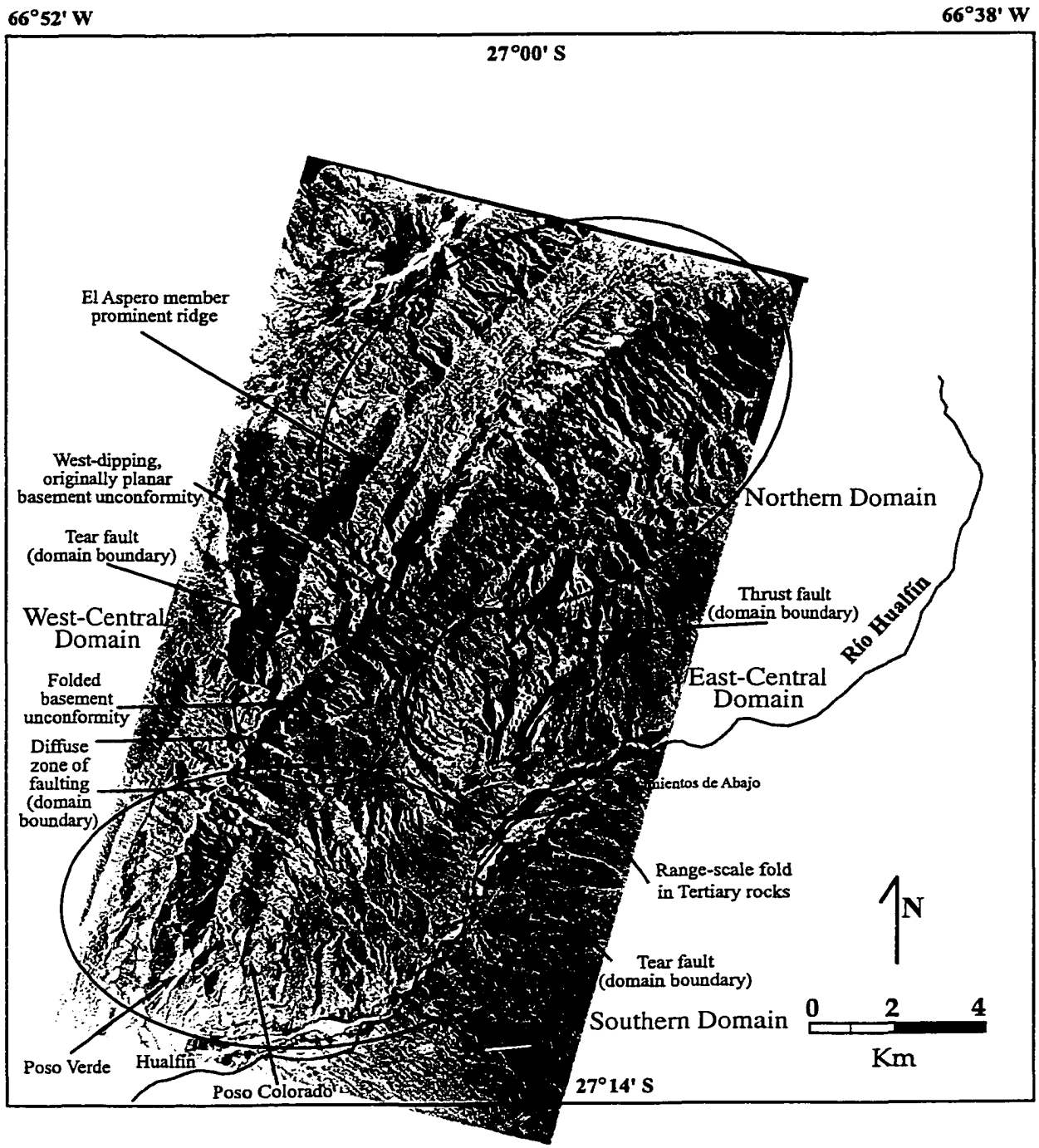

Figure 2.5. Aerial photo collage of the Sierra de Hualfín showing general domain locations, domain boundaries, and salient features of the uplift. Latitude and longitude bounding box corresponds to the same area in the geologic map of Figure 2.2. Aerial photos are from the Instituto Geográfico Militar in Buenos Aires, Argentina.

2.2. SIERRA DE HUALFIN

2.2.1. Tectonic and Geologic Setting:

The Sierras Pampeanas province is located in the foreland of the central Andes, between 26°S and 33°S, and comprises a modern and active orogenic system. Movements along reverse faults that place Precambrian to Ordovician metamorphic and granitic basement rocks (Omarini et al., 1984) over Paleozoic to Tertiary sedimentary rocks have formed the uplifts of the province. The majority of the uplifts of the Sierras Pampeanas are oriented approximately N-S and the range-bounding reverse faults verge both to the east and to the west (Fig. 2.1). The province borders the Puna plateau on the NW and the Eastern Cordillera-Santa Barbara thrust belts to the north. In general, it is thought that the uplifts of the province were produced in response to compressive stresses generated from the subduction of the Nazca plate underneath the South America plate. The ages of uplift of the Sierras Pampeanas have been loosely constrained to about 10 Ma, perhaps continuing through 2 Ma (Allmendinger, 1986; Jordan and Allmendinger, 1986). Dating of pediment surfaces (Strecker et al., 1989) and fission track ages of exhumation for several uplifts (Coughlin et al., 1998) are in agreement with these dates.

2.2.2. General Structure:

Sierra de Hualfin trends NNE to NE and is composed of a core of Ordovician granitoid rocks overlain by and thrust over Tertiary sedimentary rocks (Figs. 2.2, 2.3). Although the range is only 5 km wide, the complete structural entity is almost 20 km in width. Strata of the uppermost Tertiary section dip gently to the west in the hanging wall for at least 20 km farther west, at which point they become the footwall of the thrust beneath Cerro Negro (Fig. 2.2). On the eastern front of the uplift, the granite is thrust over

the sedimentary strata along 40° to 70° west-dipping faults that strike from N30°E to N50°E. This faulting produces a steep range front in the north and south and underlies a large fold in overlying sedimentary strata in the central part of the range (Figs. 2.2, 2.5). The west side of the uplift is characterized by a gently dipping (15° - 20°W) backlimb, departing from this geometry only in the central region. In the central region, the basement-cover unconformity and overlying sedimentary units are sharply folded (Fig. 2.6a, b).

Figure 2.6. (a) View ENE of the folded west limb of the Sierra de Hualfín. The basement unconformity is seen in the center of the photograph (lighter surface) among patches of remaining Hualfín Formation sandstones. Geologic sketch for reference to rock units (legend in Figure 2.3). (b) View NE of the same area as (a). The basement unconformity is the light area in the central part of the photograph. Note the folded geometry of the sedimentary rocks (pock-marked flat-irons) that track the folded unconformity.

a)

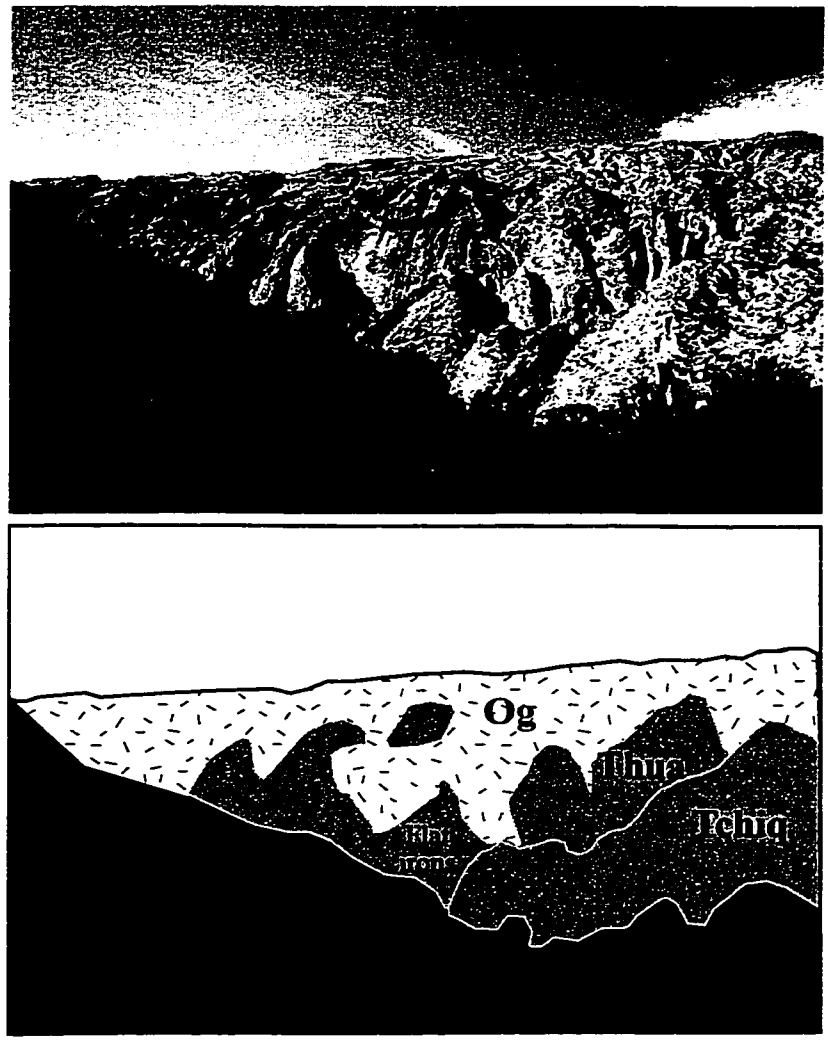
Og
Thua
Tchg

b)

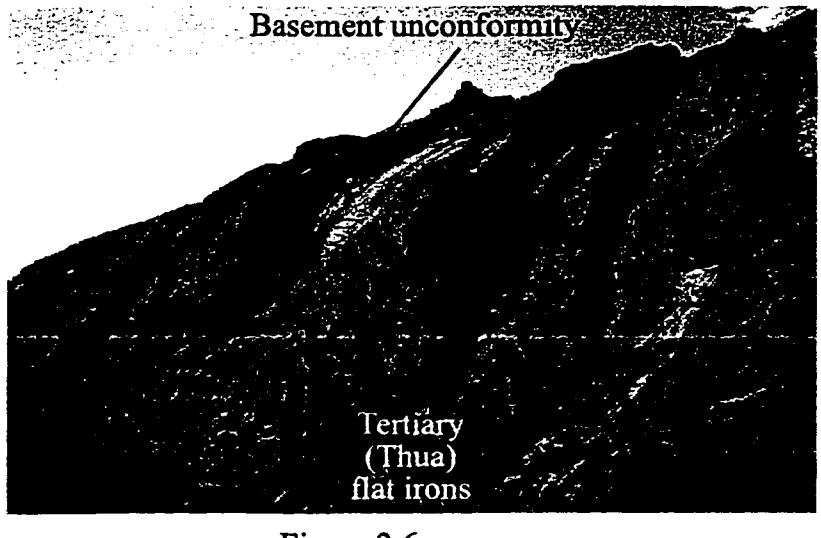
Basement unconformity
Tertiary
(Thua)
flat irons

Figure 2.6

2.2.3. General Relationships and Map Stratigraphy

Characteristic of basement-cored uplift provinces is the presence of basement rocks near the surface due to a lack of thick sedimentary rock cover. The basement rocks present in the Sierra de Hualfín are part of the Faja Eruptiva de la Puna (Mendez et al., 1973). Most of the basement rocks that are exposed in the Sierra de Hualfín are Ordovician granitoid rocks (Omarini et al., 1984). The rocks are generally coarse grained and equigranular with sporadic fine-grained sills. A mylonitic schist mapped in the northeastern end of the uplift likely represents the lower Paleozoic and/or upper Precambrian basement which makes up the cores of neighboring uplifts (e.g. Sierra de Aconquija, Sierra de Quilmes).

The sedimentary cover section is composed of Tertiary age continental deposits and is only 3 -4 km thick. The stratigraphy of the Tertiary section in combination with the geometry of the strata are important for constraining the geometry of the underlying fault. The Tertiary strata that unconformably overlie basement rocks are well exposed, and are variable in thickness and lateral extent (Allmendinger, 1986). There are several section localities that have been previously studied in detail. These are located near the town of Santa Maria (e.g. Bossi et al., 1993), on the outskirts of the village of Puerta de Corral Quemado (~10 km WNW of the village of Hualfín) (Marshall and Patterson, 1981; Butler et al., 1994; Latorre et al., 1997), and in the area of Río Villa Vil located on the west side of the Sierra de Hualfín (Muruaga, 1998; Muruaga, 1999). The names of the units and the unit boundaries related to these sections have been changed over the years with the addition of new information throughout the NW Sierras Pampeanas (Marshall and Patterson, 1981; Butler et al., 1984; Allmendinger 1986; Jordan and Alonso, 1987; Latorre et al., 1997; Muruaga, 1999).

At the time mapping was carried out for this study, the stratigraphy used was based on the studies by González Bonorino (1950), Caminos (1979), Butler et al. (1984) and Allmendinger (1986) (Fig. 2.3). Approximate locations of the revised stratigraphic

boundaries suggested by Muruaga (1999) are shown as dashed lines on Figure 2.2. A complication that arises from this interpretation is that the type section studied by Muruaga (1999), located on the west side of Sierra de Hualfín, may not exist in its entirety on the east side of the uplift. For example, other workers have noted the absence of the distinct volcanic breccia (El Aspero Member of the Chiquimil Formation) on the east side of Sierra de Hualfín (Bossi et al., 1993; Urreiztieta et al., 1996).

The Tertiary strata reflect a continental depositional environment and are composed of sandstones, siltstones and conglomerates. The section is approximately 3050 m thick in the western area of Sierra de Hualfín (Muruaga, 1999). The Tertiary section overlies the erosional basement surface (a nonconformity), and can be divided simply into three parts (González Bonorino, 1950; Allmendinger, 1986): the Calchaquense Formation or lower unit, the volcanic complex, and the Araucanense Formation or upper unit (Fig. 2.3). Muruaga (1998, 1999) completed a more detailed study in which she subdivided the section into the following five major formations (from older to younger): Hualfín, Las Arcas, Chiquimil, Andalhuala, and Corral Quemado Formations. Her work showed that the section in the Hualfín-Las Cuevas area is part of a sub-basin within the regional Santa María-Hualfín basin (Muruaga, 1999) (Fig. 2.3). Briefly, the major characteristics of each formation are as follows (Note: all formation thickness are from Muruaga (1999)):

Hualfín Formation (130 m):

This unit is composed of a distinctive red arkosic sandstone with minor intercalated conglomerate beds. The age of the base of the section is estimated at about 15 Ma (Allmendinger, 1986), but is not known with certainty. The basal sedimentary section overlying basement in the vicinity of the Sierra de Quilmes (about 40 km northeast of Sierra de Hualfín), a sedimentary section in the equivalent stratigraphic position as the Hualfín Formation, was dated to be ~10 Ma (Strecker et al., 1987). Muruaga (1999) has proposed

a possible correlation between the Hualfín Formation and the Saladillo Formation of Paleogene age (Bossi et al., 1997) in the Valle de Santa María.

Las Arcas Formation (226 m):

This unit lies unconformably over the Hualfín Formation and is composed of fine and medium-grained sandstones, brick red to brown-red in color (Muruaga, 1999).

Chiquimil Formation (940 m)

This formation is composed of three members:

Los Baños member (50 m) lies conformably on Las Arcas Formation and is distinguished from it by its beige-yellow color. This member has upward-fining sequences of sandstones with basal conglomerate lenses (Muruaga, 1999). Pelitic horizons at the top of the section contain rhizo-concretions and root traces (Muruaga, 1999) that would be indicative of a paleosol horizon.

El Aspero member (130 m) is composed of a cobble volcaniclastic conglomerate, green to gray in color. This unit decreases in thickness and pinches out to the south, about 8 km WNW of the village of Hualfín (Fig. 2.2). Mapping carried out for this study identified only one or two possible outcrops of this unit on the eastern flank of the range, towards the northern end. Provenance for this unit is from volcanic centers in the Puna (Muruaga, 1999). At the east side of the Sierra de Hualfín, where this member is not present, the distinction between the Los Baños member and the El Jarillal member is difficult to discern. These units are shown as undivided Chiquimil Formation and with a dashed line on the geologic map (Fig. 2.2).

El Jarillal member (760 m) defines an upward-fining sequence of fine-grained sandstones. It is beige to green-yellow in color (Muruaga, 1999). The upper section is characterized by abundant vertebrate fossils (Powell et al., 1998).

Andalhuala Formation (900 m)

The base of this unit is marked by a tuff located at the Puerta de Corral Quemado (Muruaga, 1999) and dated by Latorre et al. (1997) to be 7.14 Ma. This formation is in conformable depositional contact with the underlying El Jarillal member, is composed of beige to gray sandstones, and contains a distinct, eolian sandstone with large cross beds in the middle part of the section (Muruaga, 1999). In this study, this eolian sandstone unit was identified ~300 m from the 44°NW dipping thrust fault of the Cerro Negro (Fig. 2.2), suggesting that the overlying Corral Quemado Formation does not exist in its entirety in the NW region of the map.

Corral Quemado Formation (850 m)

This formation is characterized by a total predominance of conglomerate facies, clast supported and with sporadic lenses of medium-grained sandstone (Muruaga, 1999). The lower part of this section contains a tuff dated at 3.53 +/- 0.04 Ma (Marshall et al., 1979) and 3.66 +/- 0.04 Ma (Latorre et al., 1997).

The Tertiary section is unconformably overlain in places by the Punaschotter unit (Penck, 1920; Allmendinger, 1986; Muruaga, 1999), a boulder conglomerate of local origin (Muruaga, 1999) that mantles older terraces and small hills in the area. This unit has not been dated but is considered Quaternary in age (Allmendinger, 1986; Bossi et al., 1997; Muruaga, 1999). Other alluvial and colluvial Quaternary deposits occur on the east side of the Sierra de Hualfín, but these do not form part of the Punaschotter. These deposits are mainly composed of coarse alluvial fan deposits, including loosely consolidated boulder conglomerates, sandstones and gravels. They generally rest in angular, unconformable contact on top of the Tertiary formations.

2.2.4. Basement Unconformity

Exposures of the basement-cover interface, an unconformity, are well-preserved in the Sierra de Hualfín (Fig. 2.7a, b). The unconformity between Ordovician granitoid and Tertiary strata is a depositional unconformity, although in some locations there is evidence for shear within a meter below the interface that is likely related to Miocene to Recent folding and faulting. The unconformity is interpreted to be a regional surface identified in several other uplifts in the Sierras Pampeanas, and recognized in the Sierra de Hualfín by González Bonorino (1950). The surface was formed over 300–400 Ma, beginning in the Late Paleozoic (Jordan et al., 1989) and is presumed to have been nearly horizontal and subsequently buried by Tertiary strata (Jordan and Allmendinger, 1986; Jordan et al., 1989) before basement-cored deformation was initiated. Therefore, the unconformity surface can document rotation of basement fault-blocks along faults. Also, the original planar geometry of the basement unconformity provides a consistent structural datum for estimates of offset along faults and serves as a dependable surface for calculating structural relief. The exposure of the basement unconformity and preservation of cover sedimentary rocks at Sierra de Hualfín is valuable because it allows for the evaluation of basement deformation and of the range-scale structural form of the uplift. It is the unconformity that delineates the along-strike structural variations of the Sierra de Hualfín.

a)

b)

Figure 2.7. Excellent exposures of the basement unconformity on the west side of the uplift. Note the roughly planar nature of the surface and the prominent fracture sets visible. (a) Close up view of the unconformity, camera lens cap on the right for scale. (b) View SE of the unconformity in the foreground (Kirk Hofmann for scale). Top of the far cliffs in the background is also the basement unconformity (top basement).

2.3. STRUCTURAL DOMAINS AND TRANSITION ZONES

2.3.1. Structural Domains

In the Sierra de Hualfín, field mapping at a scale of 1:55,000 revealed abrupt, along-strike differences in the geometry of the basement unconformity. The variations in the geometry of the basement unconformity along trend of the Sierra de Hualfín can be divided into four principal domains: Southern (SD), West-Central (WCD), East-Central (ECD), and Northern (ND) (Figs. 2.4, 2.5). The structural variations along the uplift are expressed by the changes in the structural attitude and form of the basement unconformity. For example, the unconformity in the northwest (Fig. 2.8) dips gently west, whereas just to the south in the west-central area the unconformity is sharply folded. In turn, the structural form of the basement unconformity is directly related to the faulting that affects it. In some places it is not faulted, in other places it is folded, and in still other areas there are several subparallel reverse faults that displace the basement unconformity. Thus, variations in the structural form of the unconformity permit the identification of domains where varying combinations of faulting and folding are present and have affected the development of the uplift.

The following descriptions of the geology of each of these domains focus on the faulting and folding patterns in the basement and in cover, and how the geometry of cover strata may reflect basement faulting patterns.

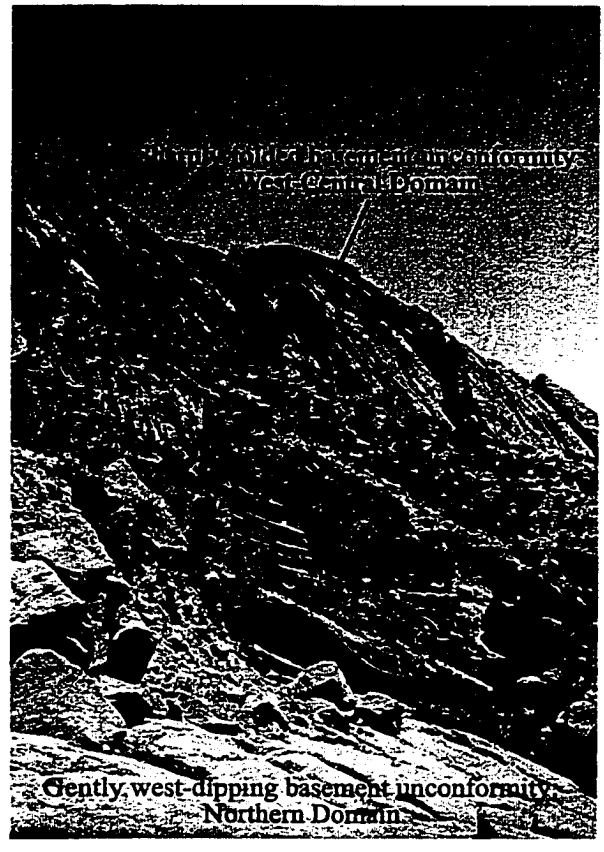

Figure 2.8. View south of gently dipping unconformity in the northern area of the uplift (surface in the foreground) and the folded unconformity in the West-Central Domain, just to the south.

2.3.1.a. Southern Domain (SD)

The SD (Figs. 2.4, 2.5) begins at the southern tip of the Sierra de Hualfín near the village of Hualfín, Catamarca Province. It extends north towards Termas de Nacimientos on the east, and approximately 2 km south of the confluence between the Río Aguas Calientes and the Río de las Zanjas on the west. Mapping in this area revealed the existence of a thin cover of the basal arkosic sandstone (Hualfin Fm.) above basement, occupying most of the southern portion of the range top (Figs. 2.4, 2.5). This part of the uplift had previously been mapped as Ordovician granitoid (González Bonorino, 1950; Allmendinger, 1986). The basement unconformity is clearly preserved in the southern end of the uplift. Thus, its position is known and constrains the geometry of the uplift.

The Sierra de Hualfín, in this domain, forms a faulted, asymmetric, southward-plunging anticlinal fold. The basement unconformity dips ~20°- 25°W on the west side of the uplift and is faulted on the east side. The large fault on the east side places Ordovician granitoid on deformed and apparently thinned red beds of the Tertiary Hualfín and Las Arcas Formations. This fault strikes NE to NNE and has fault surfaces that dip from ~23°W to ~54°W. The anticline plunge axis in the southern tip of the uplift is oriented 215°, 10° (Fig. 2.9). Northeast of the anticlinal plunge axis (Fig. 2.4), a network of normal faults oriented ~N40°W with steep NE dips, and ~N60°E with steep SE dips (Fig. 2.10) offset the basement unconformity by ~20 m to 50 m. The normal faults appear to terminate against a fault striking N50°W to N55°W and dipping north (Fig. 2.4), an orientation that is roughly perpendicular to the strike of the range. This faulting produces a NNE trending drainage which is along strike of the normal fault in Poso Verde just to the south (Fig. 2.4).

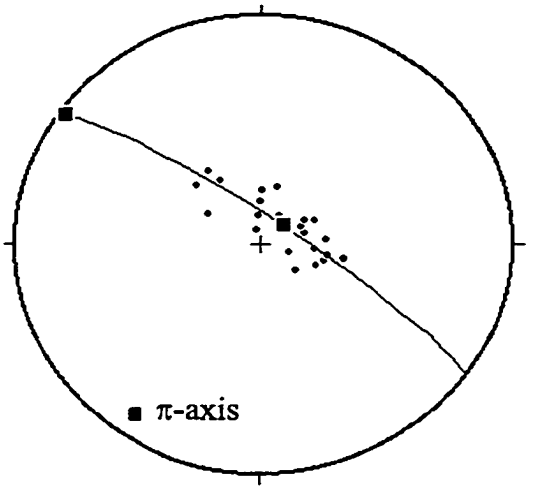

Figure 2.9. Stereonet of plunge axis calculation for the southern end of the Sierra de Hualfin. The fold axis trend and plunge is 215°, 10°.

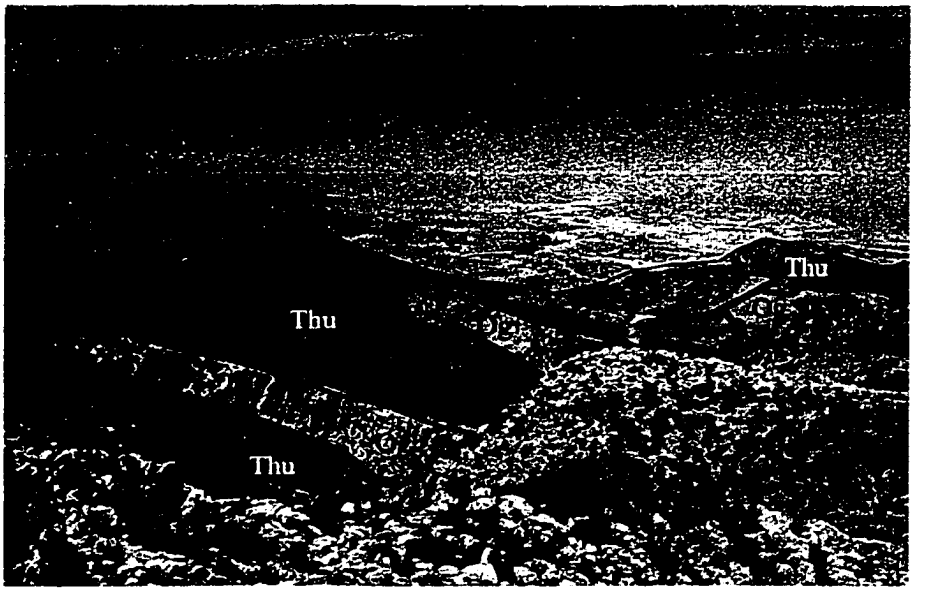

Figure 2.10. View south of normal faults on the southern ridge crest of Sierra de Hualfin. Offset on the faults is from ~15 m to 30 m. Thin lines represent lithologic contacts, thicker lines with ball-and-stick represent fault traces.

On the eastern side of the uplift near the village of Hualfín, a normal fault oriented ~N5°W to NS, located in the canyon Poso Colorado (Figs. 2.4, 2.5), offsets the basement unconformity approximately 40-60 m. The beds of the lower unit dip eastward here and define minor, monoclinal folds. These folds are characterized by changes in the dip of bedding from 5°SE to ~30°SE, over a 2 - 5 m distance. A π-diagram of bedding orientations in the Poso Colorado area (Fig. 2.11) shows that bedding consistently dips SSE and shows the trend and plunge of a fold axis calculated from this data (239°, 6°).

Nearer to the village of Nacimientos de Abajo, the range-front on the eastern side of Sierra de Hualfín typically is expressed by eastward dipping beds in the Tertiary section (Fig. 2.4). Bedrock exposures in the alluvial fan channels on the flank of the mountain show an increase in dip towards the range-front. Minor folds in these sedimentary units are oriented parallel to the range front, approximately N30°E, and are often visible in outcrop. These folds are similar to the monoclinal folds located in Poso Colorado described above, and in the area of Termas Nacimientos, described in the ECD.

2.3.1.b. West-Central Domain (WCD)

The WCD is characterized by a sharply folded basement unconformity (Fig. 2.6). The domain extends northward from the southern domain to the tear fault oriented ~N62°W, 71°N (Fig. 2.4).

From east to west, the basement unconformity increases in dip from ~20°W to 65°W to almost vertical within a 500 m to 800 m horizontal distance (Fig. 2.4). This increase in dip appears to be continuous with only minor faults (~.5 m - 2 m offset) to help accommodate the bending (Fig. 2.12). These faults appear in a cross-pattern on the surface

of the basement unconformity. In detail, the granite below the unconformity has a fracture foliation which is subparallel to the unconformity. In places, this foliation has slickenlines suggesting the observed folding was accommodated by slip along these fracture surfaces (García, 2000). The continuous fold geometry can be clearly seen in Figures 2.6b and 2.8. Mapping in this area defined a fold axis oriented N50°E to N65°E (Fig. 2.4).

2.3.1.c. East-Central Domain (ECD)

The ECD encompasses the area of Termas Nacimientos (Figs. 2.4, 2.5) where the basement unconformity is repeatedly faulted and superbly exposed (García, 1999). In this domain (Figs. 2.4, 2.5) there is a rapid change in the character of the range-front along strike. The originally planar basement unconformity is well exposed and dips northeastward (Fig. 2.13). A series of spaced subparallel reverse faults offsets the basement unconformity, producing an overall folded shape of the unconformity. Offset on these reverse faults results in folds in the overlying sedimentary rocks (Fig. 2.14) (García, 1999), similar to the minor, monoclinal folds in the SD. The folds in the SD, by analogy, may be caused by minor reverse faults in the underlying units. The ECD is also characterized by a range-scale fold in the Tertiary strata (Fig. 2.15). The axis of this fold is parallel to the trend of the uplift (44°, 15°), although in aerial view it appears that the sedimentary units thin to the southwest and to the northeast (Fig. 2.5), producing a concave eastward strike in the Tertiary strata (Fig. 2.2).

In the northern part of this domain, a reverse fault striking ~N60°W, dipping 65°NE places basement rocks from the north above the Tertiary strata and the basement unconformity to the south (Fig. 2.2). There is an associated footwall syncline parallel to the

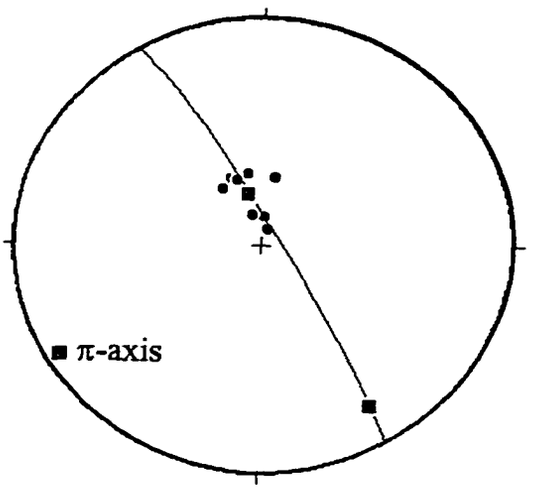

Figure 2.11. π-diagram of bedding near fold in Poso Colorado. The fold axis calculated for these bedding measurements is 239°, 6°.

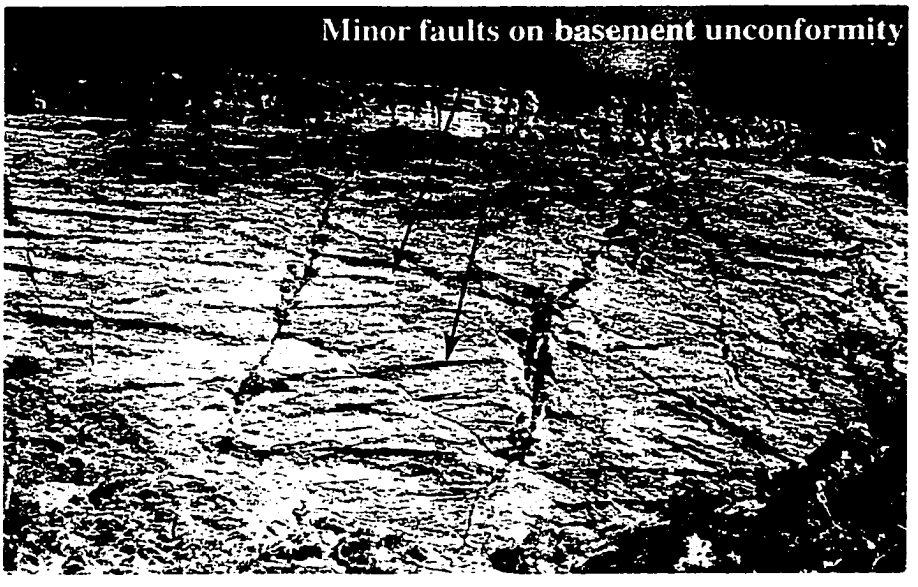

Figure 2.12. View to the east of the basement unconformity on the west side of the Sierra de Hualfín. Ledges and cross pattern of lineations are small-displacement faults. Note the cliffs of Hualfín Formation towards the top of the photograph.

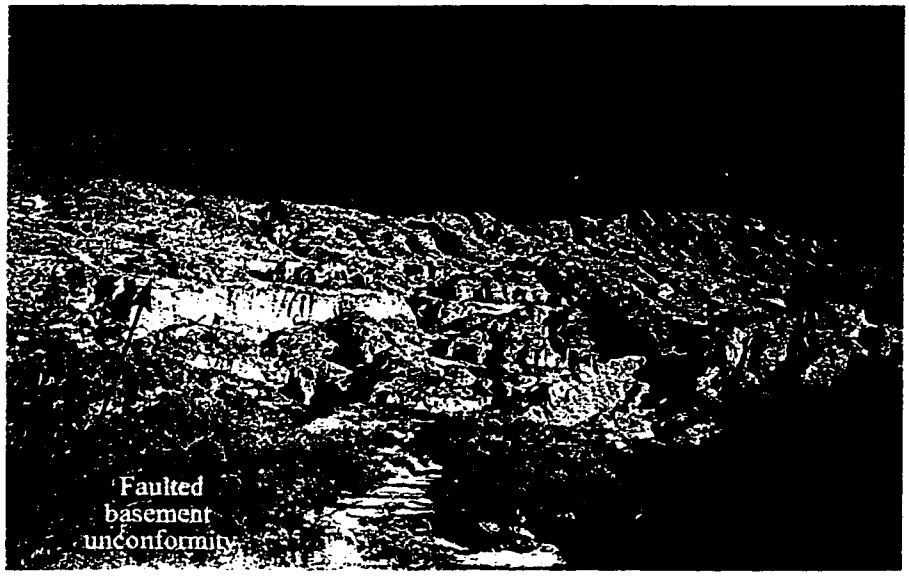

Figure 2.13. View to the west of the faulted, northeast-dipping basement unconformity at Termas de Nacimientos on the east side of the Sierra de Hualfín. Note faulted basement unconformity surface and overlying Tertiary strata.

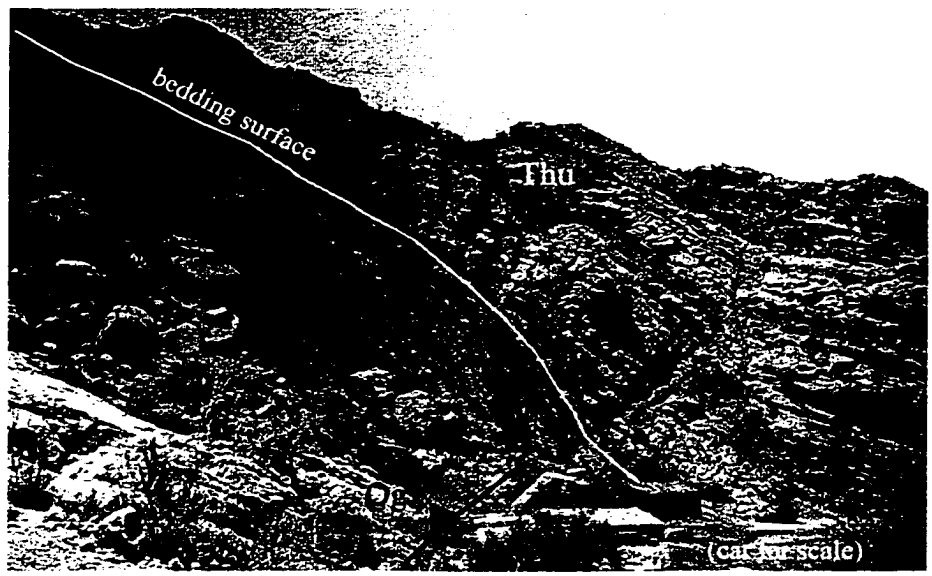

Figure 2.14. View NE along-strike of a fold in Tertiary Hualfín Formation directly above a fault in the basement (Og). Note car for scale in bottom right corner, and trace of bedding surface from upper left corner towards the center. Termas Nacimientos.

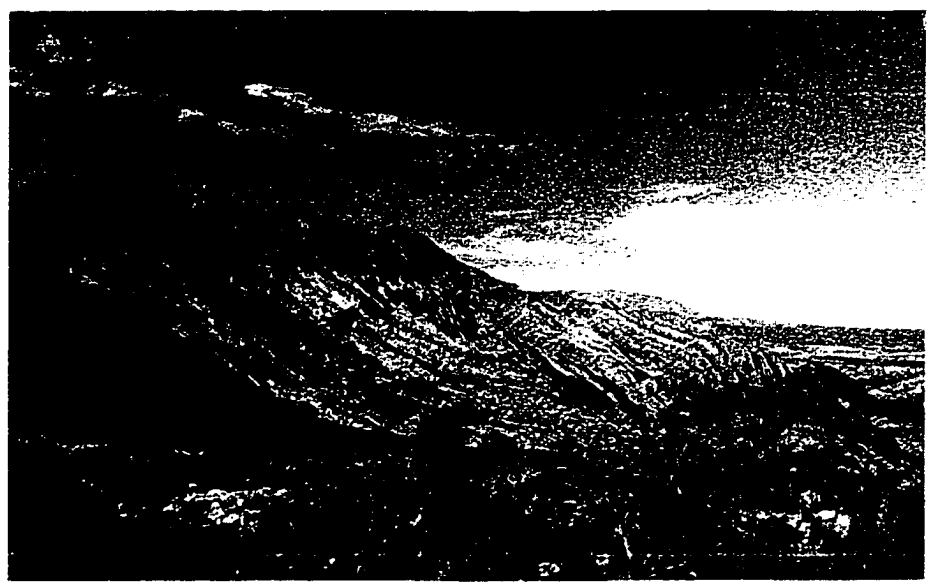

Figure 2.15. View NE along-strike of the uplift of the range-scale fold at Termas Nacimientos. Note the basement unconformity in the foreground is below the folded sedimentary units, while in the background, the basement unconformity would be at the top of the range.

reverse fault which is approximately perpendicular to the larger range-scale fold (Fig. 2.2). The intersection of these two folds causes an interference pattern in the cover rocks that reflects the interaction of several basement faults in this area (Fig. 2.16).

2.3.1.d. Northern Domain (ND)

The ND (Figs. 2.4, 2.5) includes the area of Sierra de Hualfín northeast of the ~N60°W 65°NE thrust fault on the east side of the uplift, and northeast of the ~N62°W 71°N tear fault on the west (both faults are described above). In the ND, the basement is faulted on the east, and the basement unconformity dips 20°W on the west, delineating the backlimb of the uplift (Figs. 2.4). The gently dipping backlimb can be seen in aerial view (Fig. 2.5) as a planar-looking surface that is highly fractured.

At the northern termination of the Sierra de Hualfín, there is another thick exposure of the Tertiary strata (Fig. 2.4). The strata overlie the south dipping basement unconformity of the next uplift to the north, the Sierra de las Cuevas. Basement rocks at the northern end of the Sierra de Hualfín are thrust over the Tertiary strata, overturning and folding the strata. This thrust is oriented ~N15°W, 40°S and intersects a normal fault towards the north. The normal fault trends generally northeasterly and is composed of several fault segments that are offset by north-striking faults (Figs. 2.4, 2.17). The north-striking faults offset the normal fault segments from 10 to 30 m in a right-lateral sense. Slickenlines measured on the normal fault segments (N65°W 60°S, N45°E 50°E) rake 70°NE and 65°N, respectively; slickenlines on the right-lateral fault planes (N10°E 60°E, N5°W 84°E) rake from 40°N to 62°S, respectively (Fig. 2.17). The interaction between these faults

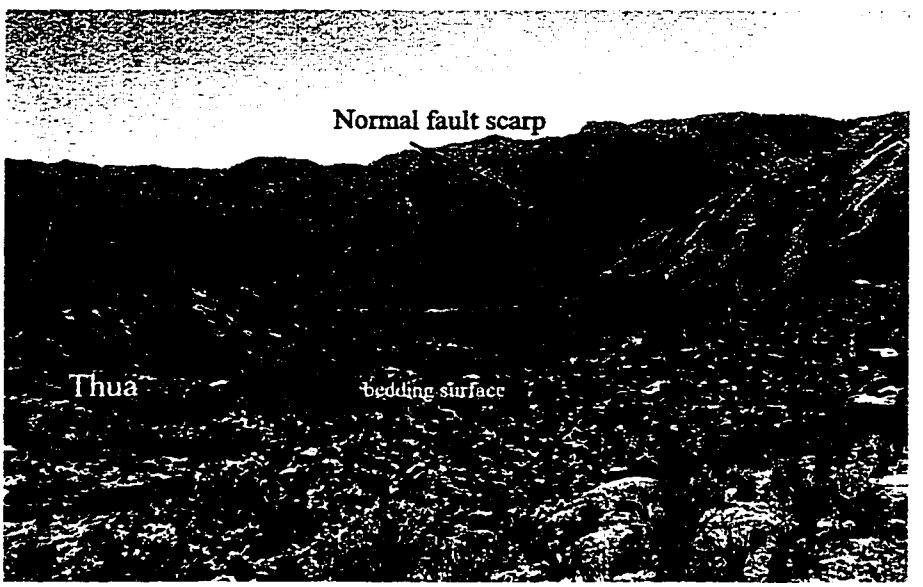

Figure 2.16. View west-northwest of the northern corner of East-Central Domain in the Sierra de Hualfín. Note the syncline next to the thrust that places Ordovician granitoid (Og) over the Tertiary Hualfín Formation (Thua). The line above the bedding surface trace separates the Tertiary rocks of the foreground from the granite cliffs in the back ground. The cliffs in the background are interpreted as a normal fault scarp (see text for more details).

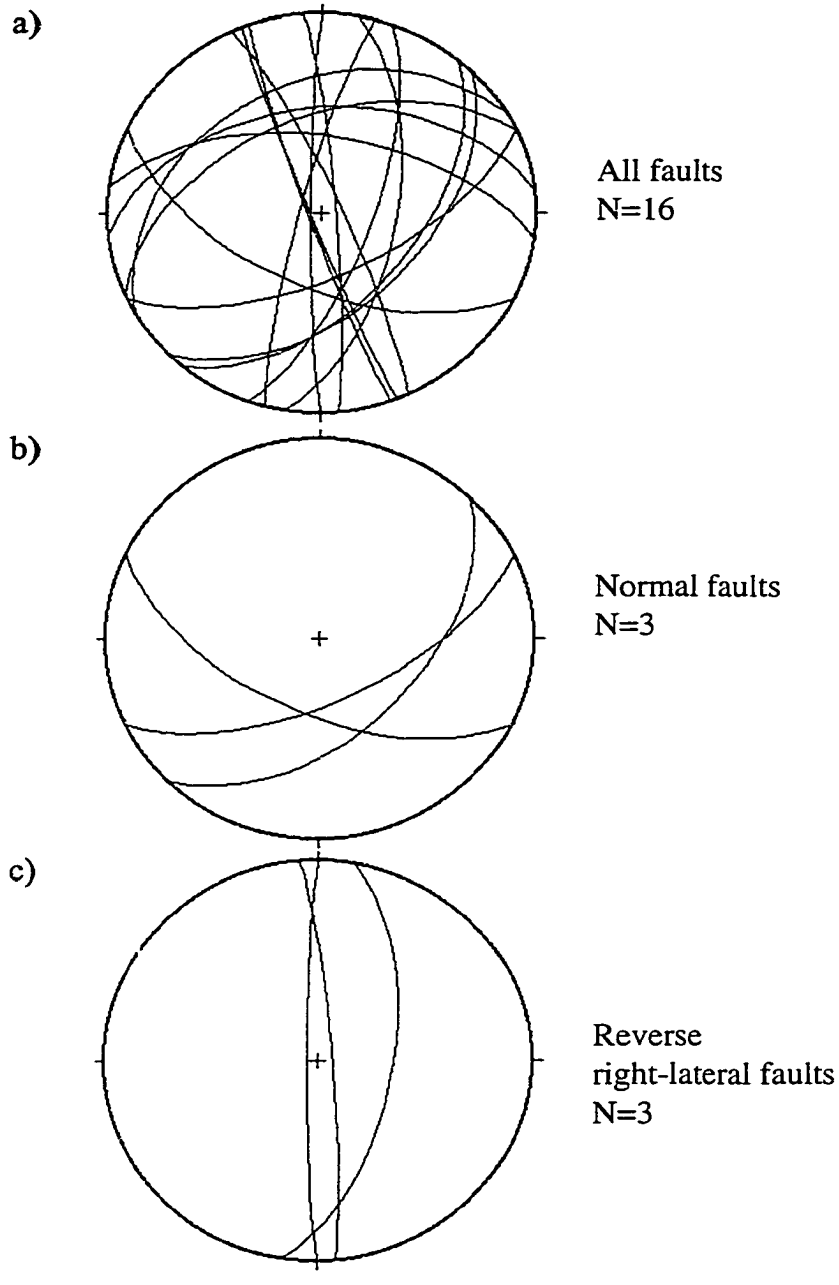

Figure 2.17. Stereonet representation of faults at Nacimientos de Arriba. (a) All faults (b) Normal faults (c) Reverse right-lateral faults.

(normal, thrust and strike-slip) produces a syncline trending ~N30°E, located to the south and along the strike of the normal fault.

2.3.2. Domain Transition Zones

The domain boundaries have been defined by faults that segment the Sierra de Hualfín into distinct basement blocks. Most of the transition zones are discrete and abrupt, often represented by a narrow fault zone. Only the transition between the SD and the WCD is a broader, diffuse zone composed of several faults.

2.3.2.a. Southern to East-Central Domain transition

The transition between the SD and ECD is denoted by a tear fault along which a steep-sided, deeply eroded canyon has been carved (Figs. 2.5, 2.18). The range-bounding fault just to the north of the canyon is oriented N40°E 46°W. In the canyon, there are several slickensided fault planes. The fault planes have strikes that vary from N75°E to N10°E to N39°W (Fig. 2.19).The NW fault set appears to offset the NNE fault set. The fault planes that best fit the orientation of the canyon and are likely related to the tear fault that separated the domains are shown in Figure 2.18. These fault planes strike WNW to NW, dip ~75°and have sub-horizontal slickenlines, suggesting a significant component of strike-slip motion on the fault. The location of these faults coincides with a change in the range-front fault orientation from ~N50°E in the south to N30°- 40°E in the north (Fig. 2.2). Map relations and field observations (Fig. 2.18) suggest that the ECD block moved down relative to the SD block (Fig. 2.20a). Sense of motion along the tear fault is interpreted from the presence of the basement unconformity on the ECD block at

progressively lower levels than the basement unconformity on the SD block (Fig. 2.20b). The tear fault has at least 550 m vertical displacement towards the southeast and tapers to zero towards the northwest. Horizontal displacement is more difficult to determine, but an estimate based on the exposed leading edges of the basement blocks in the hanging wall gives right-lateral displacement of at least 125 m and possibly up to 800 m.

2.3.2.b. East-Central to Northern Domain transition:

The transition from the ECD to the ND is marked by a thrust fault that dips ~ 65°N and varies in strike from N60°W to ~N35°W (Fig. 2.21a). This thrust has placed the basement block of the ND over the basement block of the ECD and has displaced the ECD basement block down and to the southeast relative to the ND basement block (Fig. 2.21b). Evidence for this displacement is the northward dip of the basement unconformity in the ECD, and the fact that the basement unconformity is topographically lower then the basement to the north, west, and south (Fig. 2.21b, 2.20b).

The ND is thrust only over the ECD and not over the WCD, thereby causing a steep normal fault to form in the northwest corner of the ECD (Fig. 2.4). An abrupt discontinuity in the basement unconformity, marked by a steeply east-dipping surface in the Ordovician granitiod can be seen (Fig. 2.16). The east-dipping surface is interpreted as the fault scarp expression of the normal fault.

2.3.2.c. Northern to West-Central Domain transition:

The transition from the ND to the WCD is also an abrupt transition defined by a tear fault that is oriented ~N62°W, dipping 71°N with slickenlines that rake 74°W (Fig. 2.18). The fault orientations, slickenline measurements and map relationships (Fig. 2.4) indicate

that the tear fault is a high-angle right-lateral reverse fault. The fault separates a gently-dipping basement unconformity in the ND, from a folded and steeply-dipping basement unconformity to the south in the WCD. Folding of the basement unconformity can be seen looking south from the location of the tear fault (Fig. 2.8). Although the tear fault marks the discrete transition from the ND to the WCD, the abrupt change from a gently west-dipping unconformity to a sharply folded unconformity may have caused significant deformation in the granite. The area from the location of the tear fault to the location of folded basement is marked by a lack of granite exposures in a region where granite is otherwise preserved (Fig. 2.5, just south of arrow pointing to tear fault).

2.3.2.d. West-Central to Southern Domain transition:

South of the ND on the west side of the uplift (Figs. 2.4, 2.22), the transition between the WCD, where the basement unconformity is folded, and the SD, where the unconformity can be seen again to dip gently westward, is a diffuse fault zone. Faults in this zone are evident in aerial photos (Figs. 2.5, 2.22). The faults in this 2-km wide zone trend approximately N52°W, N48°W and N46°W and are steeply dipping (Fig. 2.4, 2.22). South of the fault zone, the basement unconformity dips homoclinally ~ 20°-25° W.

2.3.2.e. East-Central to West-Central transition:

The transition between the ECD and the WCD is uncertain. The domains do not appear to be separated by faulting. The distinction between the ECD and the WCD is made simply on the fact that the basement is topographically lower in the ECD and more Tertiary strata are preserved on top of the basement unconformity to the south of the transition zone in the WCD than in the ECD (Figs. 2.4, 2.5).

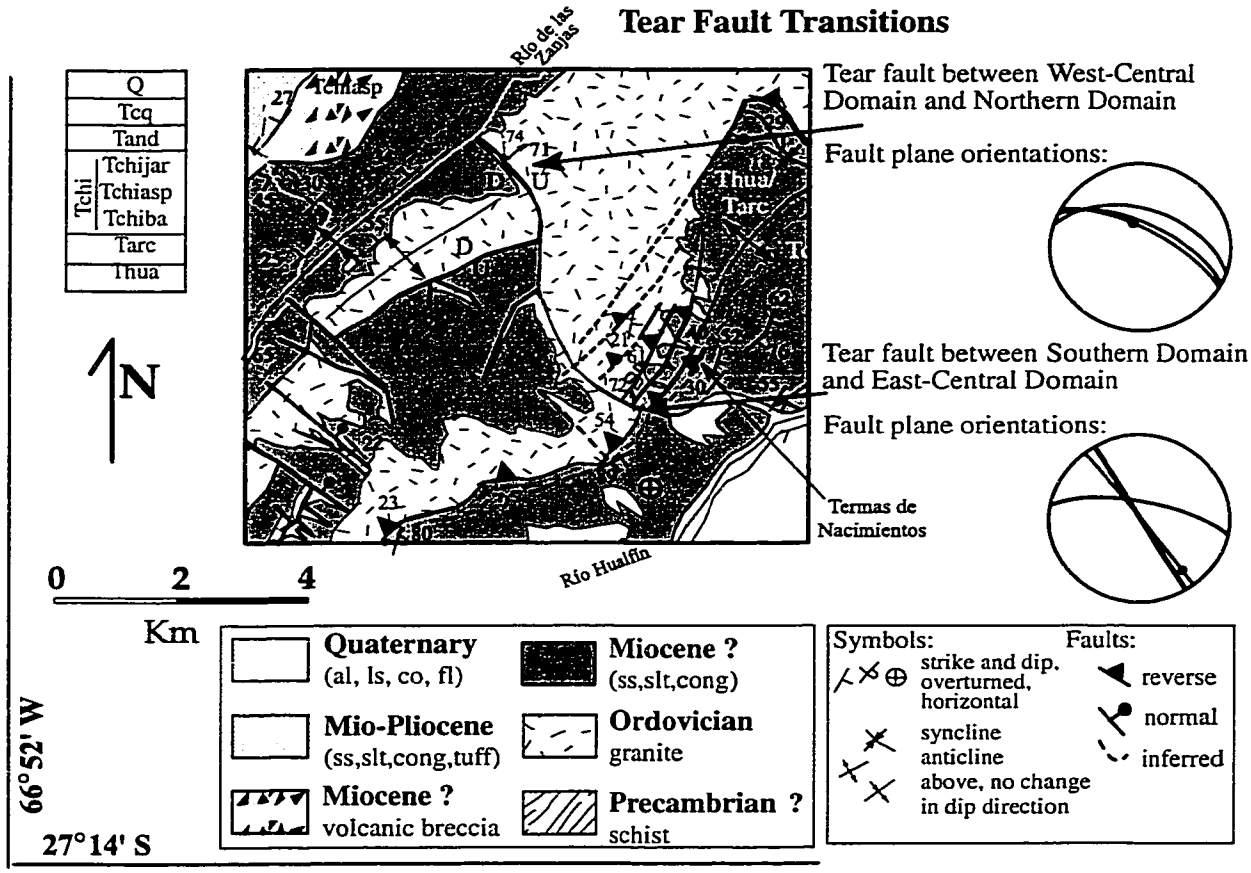

Figure 2.18. Details of the transition from the Southern Domain to East-Central Domain, and the transition between the West-Central Domain and Northern Domain.

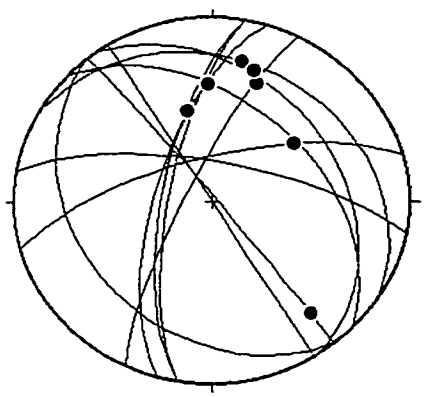

Figure 2.19. Stereonet of all fault planes with slickenlines measured in the canyon that separates the Southern Domain from the East-Central Domain (east-side tear fault).

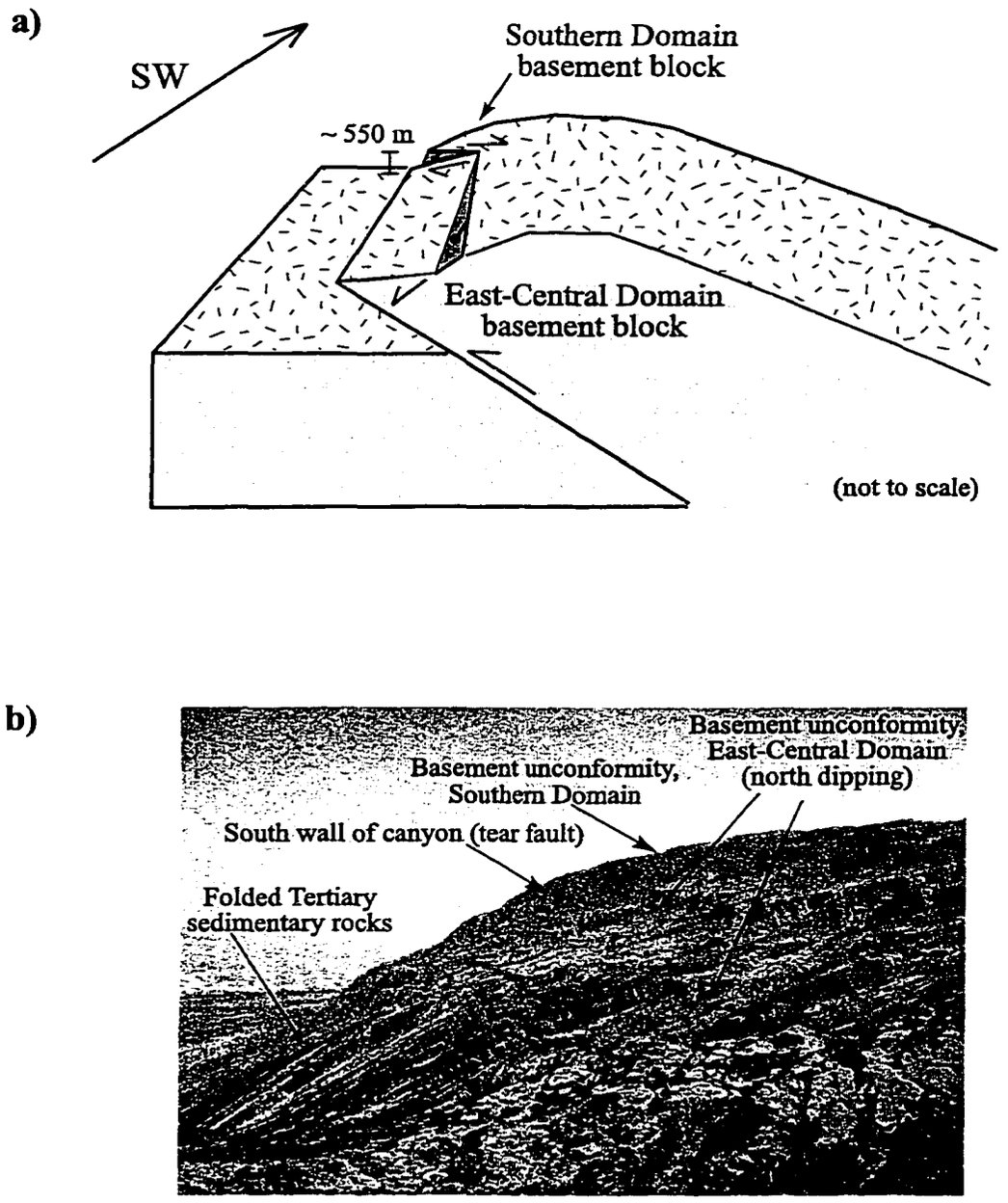

Figure 2.20. (a) Diagram showing movement of the East-Central Domain basement block relative to the Southern Domain basement block. View is to the southwest. (b) View southwest of the basement unconformity at the top of the Southern Domain (in the distant foreground) and the unconformity in the East-Central Domain dipping north and becoming lower in elevation towards the north.

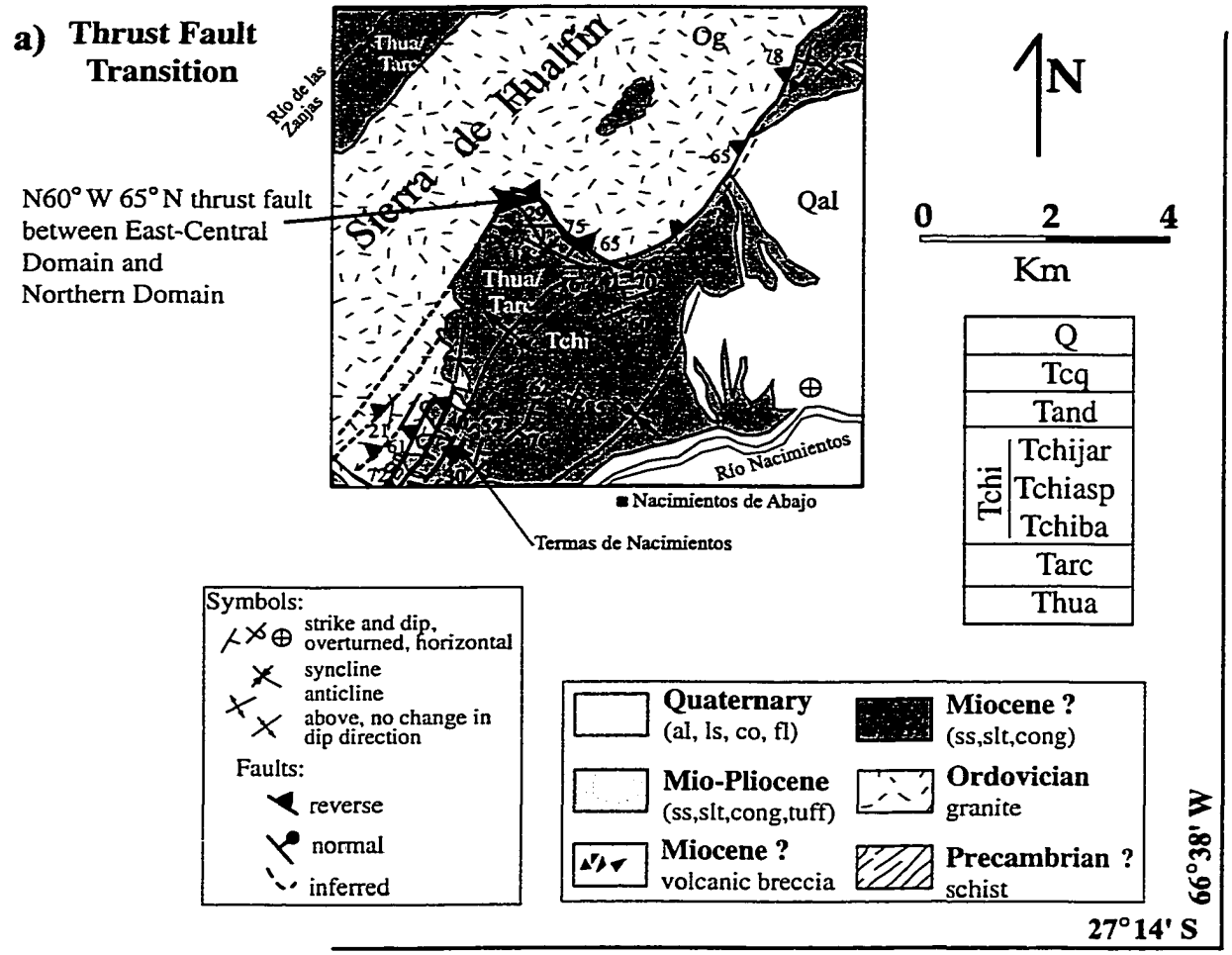

b)

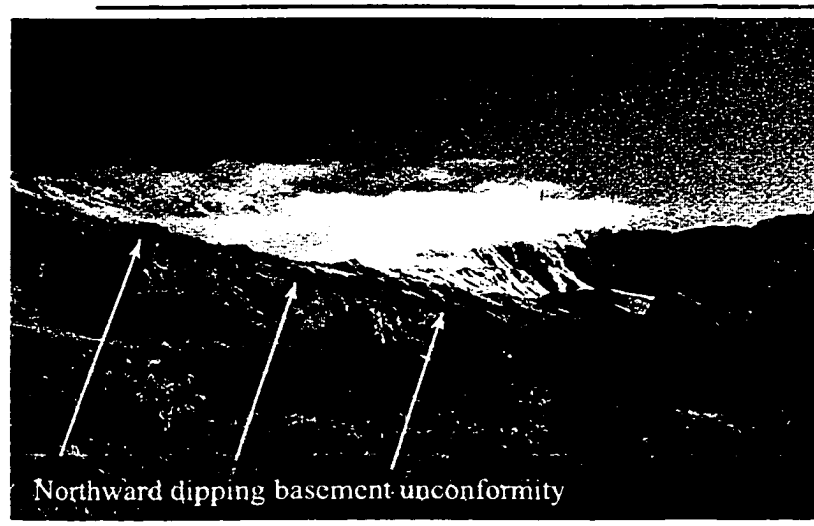

Figure 2.21. (a) Details of the thrust fault transition from the East-Central Domain to the Northern Domain. (b) View northwest of northerly dipping basement unconformity. Folded Tertiary strata are on the right (in the shadows). Note the topographically lower basement unconformity in the foreground relative to the north and the west.

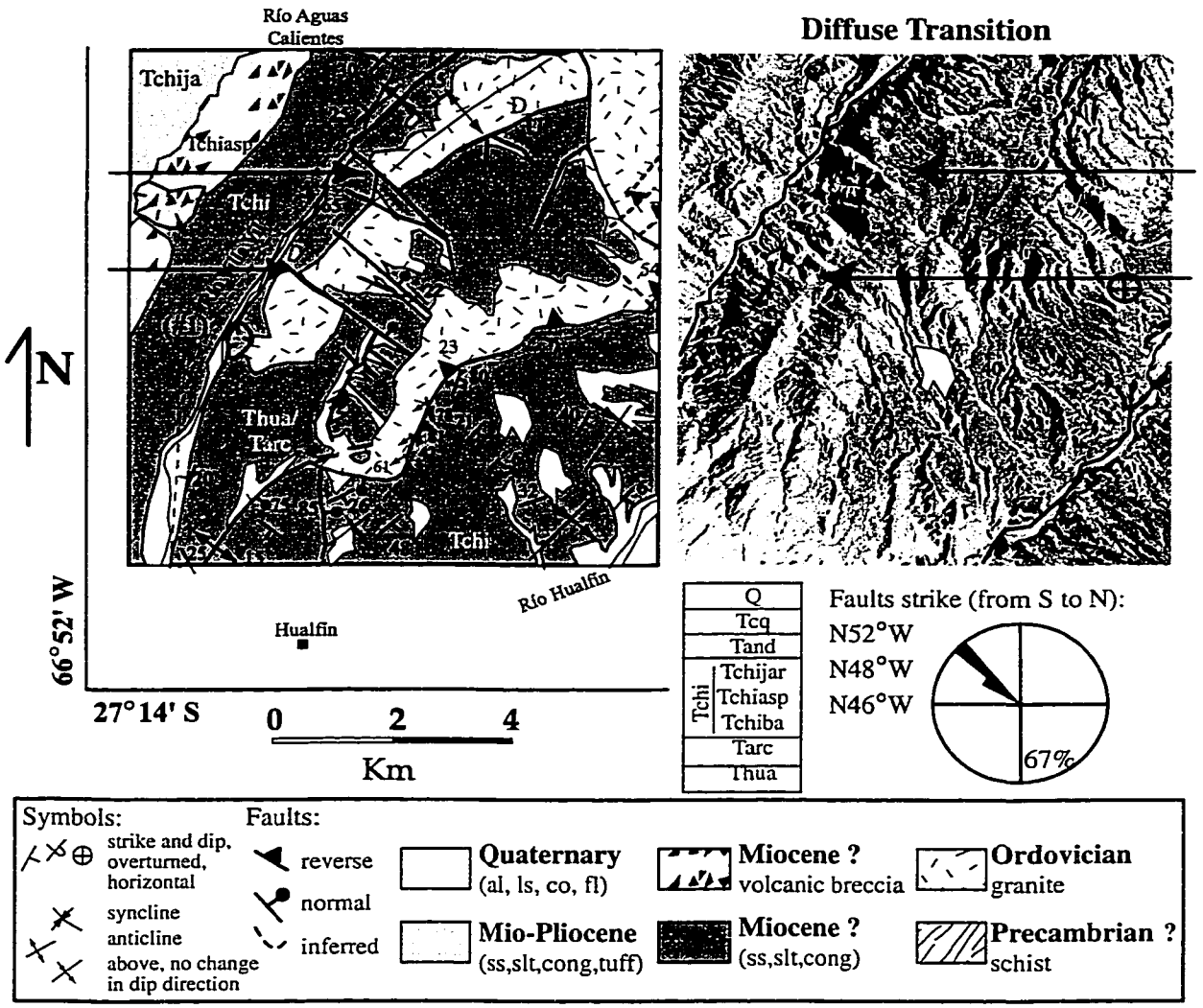

Figure 2.22. Details of the diffuse transition zone between the Southern Domain and the West-Central Domain. The 40° E dipping symbol is in the same approximate location in the geologic map and on the aerial photo.

2.4. CROSS SECTIONS AND THREE-DIMENSIONAL MODEL

2.4.1 Cross Sections

A series of six balanced cross sections across the Sierra de Hualfin (Fig. 2.23a-f) of show the structural form of the uplift across the four domains, and show interpretations of the faulting patterns related to the along-strike structural variations.

The cross sections were constructed perpendicular to an average of the trend of bedding and the trend of the main range-bounding fault. The trends of these features differs slightly along strike of the uplift, generally showing a change in orientation from ENE to NE towards the northern part of the range. Thus, the lines of section range from N54°W in the south (section line A-A', Fig. 2.23a) to N45°W (section line F-F', Fig. 2.23f). The cross sections show the uplift has an overall folded form in which the basement unconformity is folded to some degree. This interpretation is supported by field observations of folding of the originally planar basement unconformity and folding of sedimentary rock units above the basement unconformity (Fig. 2.6).

2.4.1.a. Regional basement elevations

The regional elevation of the top of the basement in the cross sections was determined from extrapolation of this surface from a seismic reflection profile line located ~26 km NE of the Sierra de Hualfin. The seismic reflection profile line 2545 was originally acquired by Yacimientos Petroleros Fiscal, and was reprocessed by Cristallini et al. (1998, 2001). Line 2545 is located on the west side of the east-verging Sierra de Quilmes.

Line 2545 (Cristallini et al., 1998) shows a thrust fault and an anticlinal fold structure in the western-most portion of the line. This structure is not visible at the surface, as is evident from the lack of topographic relief directly above the area of line 2545.

However, it is important to note the style of deformation that is produced by this thrusting. The fold shape is defined mostly by evenly spaced reflectors (e.g., reflectors at ~1.5 s and 1 s) which likely represent a constant thickness of bedding in the sedimentary rock units above the top basement. There is also some disturbance of bedding directly in front of the fold and thrust that appears to be low amplitude, longer wavelength folds. The presence of this thrust suggests there may be other blind structures underneath the basins in the Sierras Pampeanas, similar to blind basin structures in the Laramide province of the western U.S.

The velocity structure in this area is not know precisely. Average estimates for sandstone/sand, loosely consolidated (from surface exposures) range from 3 km/s to 4.5 km/s (Sheriff and Geldart, 1995). These velocities have been used elsewhere in the Sierras Pampeanas province (R. Allmendinger, personal communication, 2000) With surface elevations between 2200 m and 2250 m, and the above velocity values, the depth to basement could be between 0.8 km and 2.3 km below sea level. An average and median velocity of 3.8 km/s was used to place the basement at 1.6 km +/- 0.8 km below sea level in the footwall of the cross sections. These results are consistent with the interpretation of a 250 km regional cross section by Cristallini et al. (2001). Depth to the top of basement calculated from their regional cross section is 1.7 km +/- 0.5 km.

2.4.1.b. Methodology

The cross sections were constructed by fitting surface geology data to subsurface interpretations. The interpretations are constrained by calculations of depth to detachment, line length and area balance of the basement surface and the lower 1000 m of Tertiary strata, and restorability using flexural slip assumptions. All of the undeformed cross sections (Fig. 2.24a-f) are restored to the top of the basement surface elevation in the footwall. Since the top of the basement in the hanging wall is slightly higher in elevation

that in the footwall (higher than regional), the main thrust is interpreted to be dipping ~5°W under horizontal Tertiary strata in the hanging wall. The best control on the subsurface fault geometry is from the structural form of the basement unconformity. This originally planar surface deforms with the development of the uplift but is not subject to changes in thickness due to depositional factors (i.e. growth sedimentation). This, the cross sections focus on the basement unconformity, assuming that the geometry of the basement unconformity reflects the geometry of the underlying fault.

2.4.1.c. Cross section data

The six balanced cross sections are similar in their overall geometry, depicting an east-directed thrust fault with anticlinal and synclinal bends that reflect the geometry of the basement and cover rocks in the hanging wall. Shortening in the hanging wall of the six cross sections ranges from 6.9 km in the south to 9.0 km in the northern region.

Of the four domains identified in the Sierra de Hualfín, the ND and SD have the same geometry (steep range front on the east and gently dipping backlimb on the west). This geometry is represented in cross sections A-A', D-D', E-E', F-F' (Fig. 2.23a, d-f). The principal structural variations occur in the ECD and WCD, which separate the SD from the ND. In the WCD, the basement and basement unconformity is folded, and interpreted in cross section B-B' (Fig. 2.23b) as a result of movement along an east-dipping backthrust. In the ECD, illustrated by cross section C-C' (Fig. 2.23c), the basement unconformity on the east is preserved, dips NE, and attains a folded form by movement along a series of subparallel, spaced faults. Seven mapped reverse faults displace the eastward dipping basement unconformity in the ECD. These reverse faults vary in offset from 5 m to 36 m.

Figure 2.23. Cross sections are oriented NW-SE from left to right, with no vertical exaggeration and a topographic profile to the edge of the geologic map in Figures 2.2 and 2.4. The top and bottom of the bounding box are 7000 m and 5000 m elevation, respectively. The top of the basement in the footwall of the uplift is at ~1600 m below sea level, as calculated from seismic data 26 km NE of the Sierra de Hualfín published in Cristallini et al., (1998, 2001). The cross sections emphasize the basement unconformity and show only the lower 1000 m of Tertiary section (shaded gray). Dashed lines above basement in the hangingwall are approximate bedding orientations. Dip bars are shown in the footwall where data is available. Basement is depicted in a cross hatch pattern. Scale bar on the top left is 10 km. For cross section location, see Figure 2.4. (a) Cross section A-A' trends N54°W, and passes through the Southern Domain. (b) Cross section B-B' trends N55°W, and passes through the Southern and West-Central Domains. (c) Cross section C-C' trends N57°W, and passes through the East-Central and West-Central Domains. (d) Cross section D-D' trends N55°W, and passes through the East-Central and Northern Domains. (e) Cross section E-E' trends N50°W and (f) Cross section F-F' trends N45°W. Both (e) and (f) pass through the Northern Domain exclusively. See text for discussion.

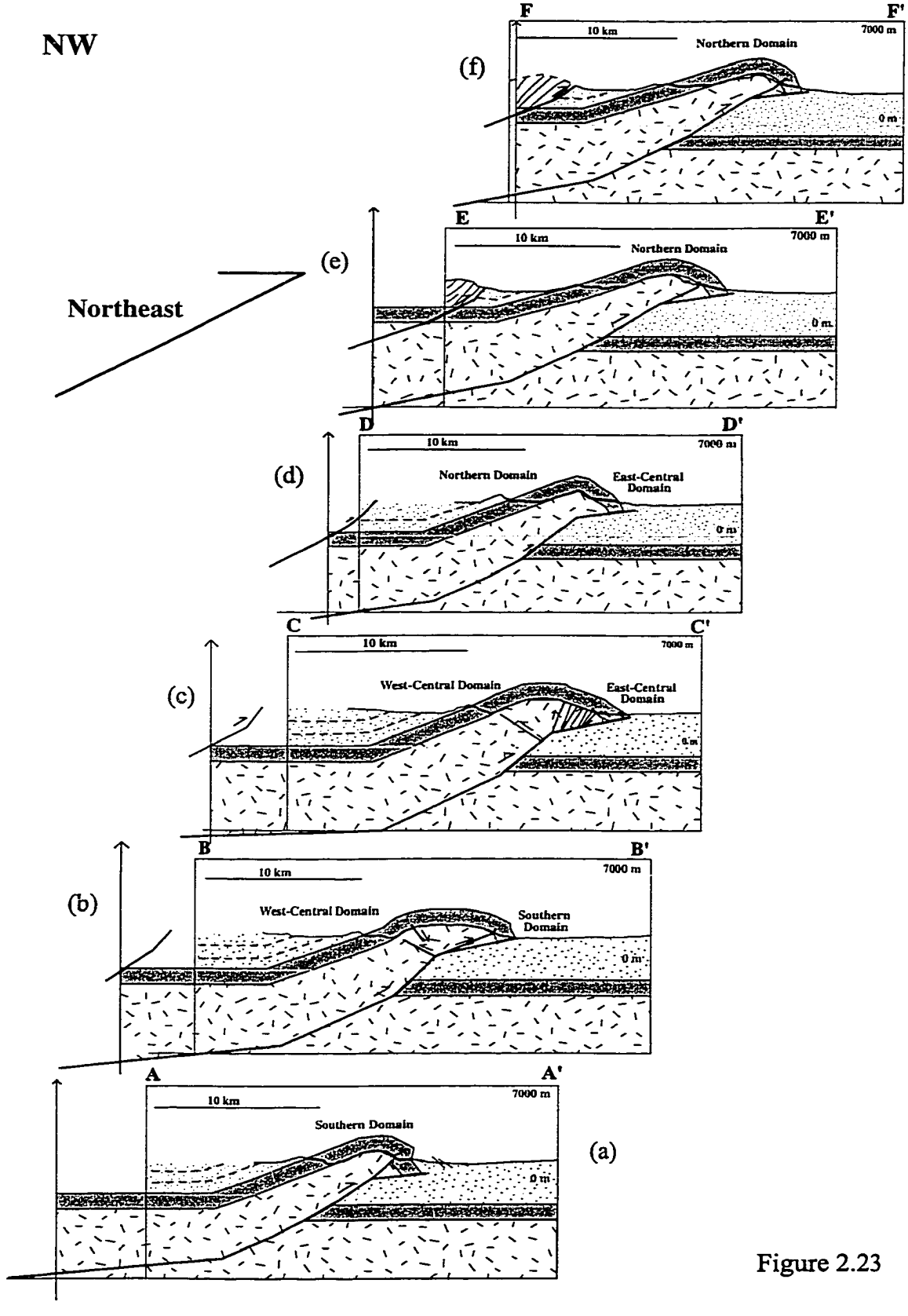
NW
SE
Northeast
F
F'
10 km
7000 m
Northern Domain
(f)
0 m
E
E'
10 km
7000 m
Northern Domain
(e)
0 m
D
D'
10 km
7000 m
Northern Domain
East-Central Domain
(d)
0 m
C
C'
10 km
7000 m
West-Central Domain
East-Central Domain
(c)
0 m
B
B'
10 km
7000 m
West-Central Domain
Southern Domain
(b)
0 m
A
A'
10 km
7000 m
Southern Domain
(a)
0 m

Figure 2.23

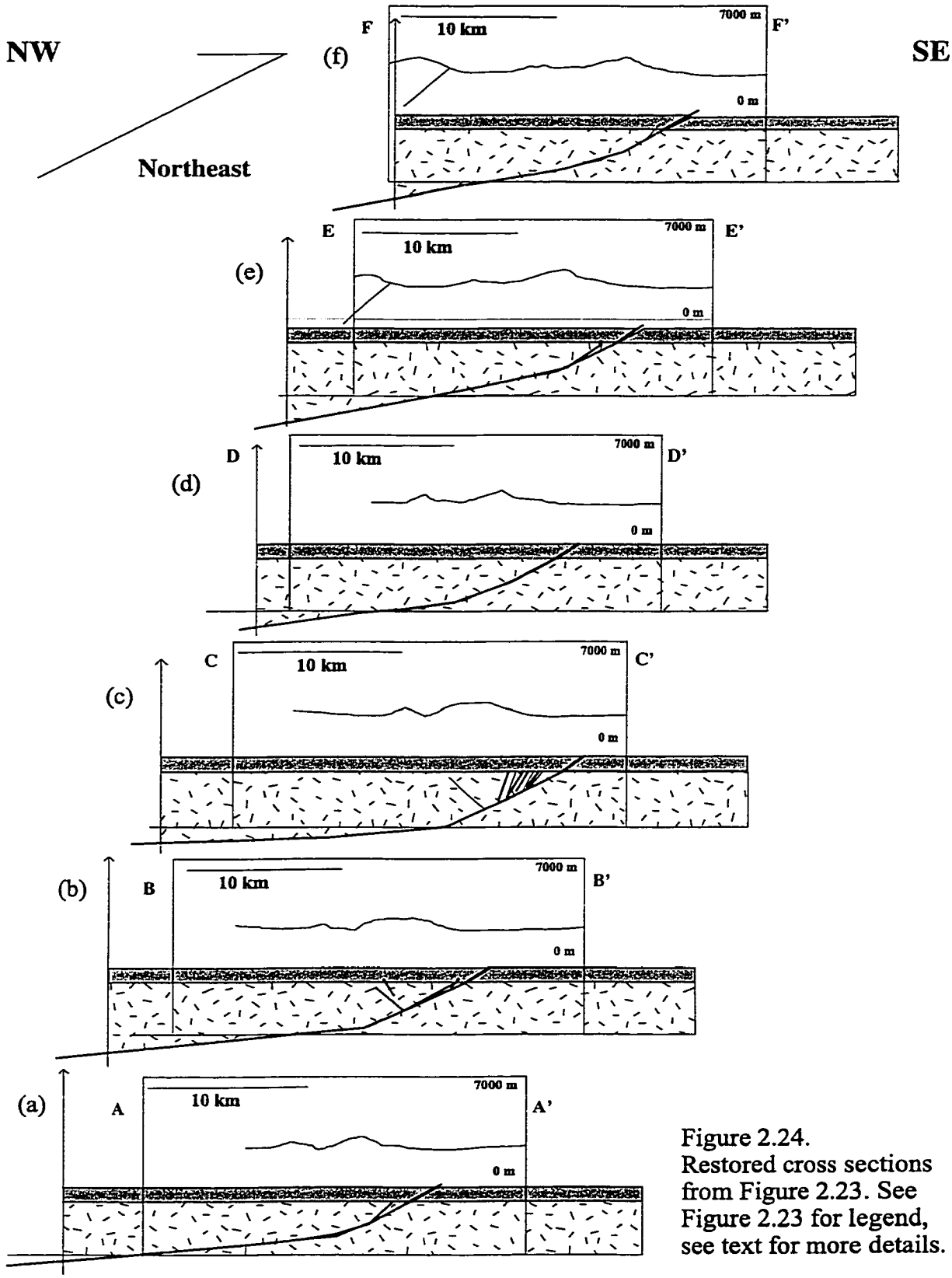

Figure 2.24. Restored cross sections from Figure 2.23. See Figure 2.23 for legend, see text for more details.

2.4.2. Three-Dimensional Model

In order to visualize the spatial relations between the cross sections and to better understand the observed domains, a three-dimensional computer model was constructed from the series of cross sections across the Sierra de Hualfín. The focus of the model was the main thrust plane of the Sierra de Hualfín (Fig. 2.25a, b).The model shows that, in the central part of the uplift at the location of cross section C-C', the main thrust plane protrudes southeastward ~ 1.5 km in front of the thrust plane in cross sections A-A', B-B', D-D', E-E', F-F'. This can be seen clearly in a plan view image of the model (Fig. 2.25a). At the same location of the SE protrusion of the thrust plane, there is also an abrupt kink in the thrust, which is visible in a view towards the NW (Fig. 2.25b). Tear faulting on the surface on the east side of the uplift correlates loosely with the location of the kink in the main fault plane.

2.5. DISCUSSION

Integrating the map relations, the cross sections and the three-dimensional model produces a more complete interpretation of the development of the Sierra de Hualfín, which has implications for the general formation of basement-cored uplifts. Mapping of the domains and the transition zones in the Sierra de Hualfín documents NW-SE trending tear faults that displace blocks of basement in a right-lateral sense of motion and/or in a NNE-NNW directed reverse motion. The balanced cross sections show that the uplift could have been formed by a gently-dipping east-directed thrust fault with anticlinal and synclinal bends, and with west-dipping fault splays and an east-dipping backthrust. The structural variations along strike of the Sierra de Hualfín are largely due to the effects of the backthrust in the west. The three-dimensional analysis of the main thrust of the uplift shows that there are more complexities in the subsurface expression of the main thrust than

the two-dimensional cross sections reveal or that mapping alone would suggest. The kink in the form of the main thrust plane observed in three-dimensional space may help explain the structural variations observed in the geometry of the basement unconformity, particularly on the east side.

Analysis of the tear faults (domain transition zones) and the domains suggests that there was NW-SE shortening followed by, or contemporaneous to, local NNE-SSW shortening. Shortening oriented NNE-SSW is marked by thrusting of the ND over the ECD and over the Sierra de las Cuevas. The thrusting of the ND basement block over the ECD caused the ECD basement block to move down relative to the ND and ~1-2 km SE, marked by the topographically lower, and northward-dipping basement unconformity. This interpretation would give the following order of events to the formation of the Sierra de Hualfín (Fig. 2.26):

1. Major faulting of the uplift, under NW-SE directed compression.

1a. Formation of the back thrust on the west.

2. Local NNE-SSW compression uplifts northern domain block.

2a. Thrusting of ND over ECD causes faulting/movement of ECD block.

The presence of NW-SE striking faults that displace blocks of basement in a right-lateral sense of motion and/or in a NNE-NNW directed reverse motion is consistent with regional kinematic interpretations that place the Sierra de Hualfín in the center of a dextral transpressional zone, the Tucumán Transfer Zone (Urreiztieta et al., 1996; Mon, 1976). The interpretation of the development of the Sierra de Hualfín (Fig. 2.26) is compatible with regional kinematic interpretations of two distinct shortening directions oriented E-W to WSW-ENE, and N-S (Allmendinger, 1986; Marrett et al., 1994; Urreiztieta et al., 1996).

a)

b)

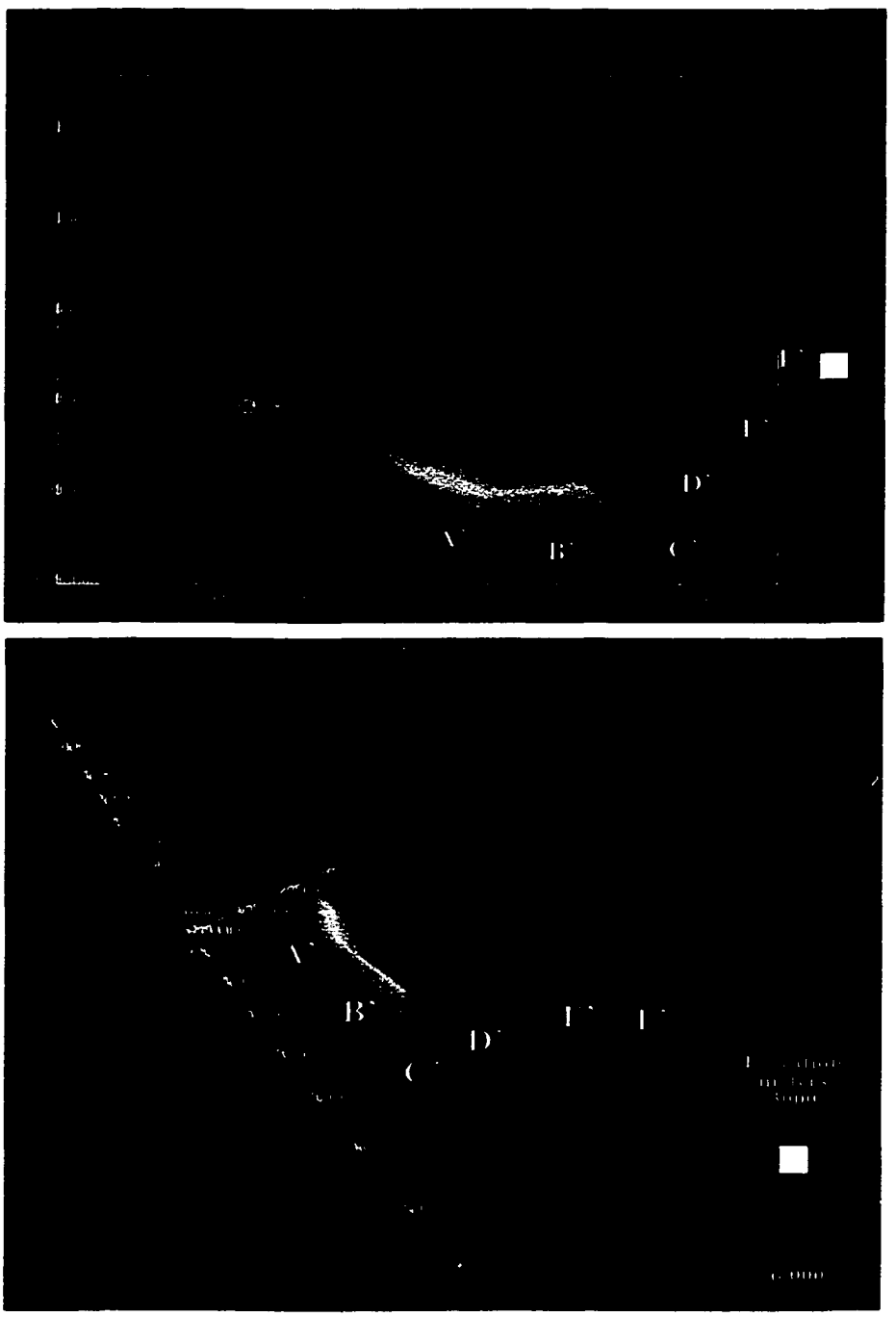

Figure 2.25. Three-dimensional computer model of the main thrust plane of Sierra de Hualfin. UTM grid shown for both figures. Surface is color contoured at 150 m (depth). Letters indicate the SE tips of the cross section lines. Artificial lighting is from the NE. (a) Plan view of the fault plane, with color bar denoting variations in the depth of the plane. The thrust deepens to the northwest. Note the protrusion of the thrust plane in the SE at the location of cross section C-C'. (b) View to the NW of the thrust plane showing the abrupt kink in the plane at the location of cross section C-C'.

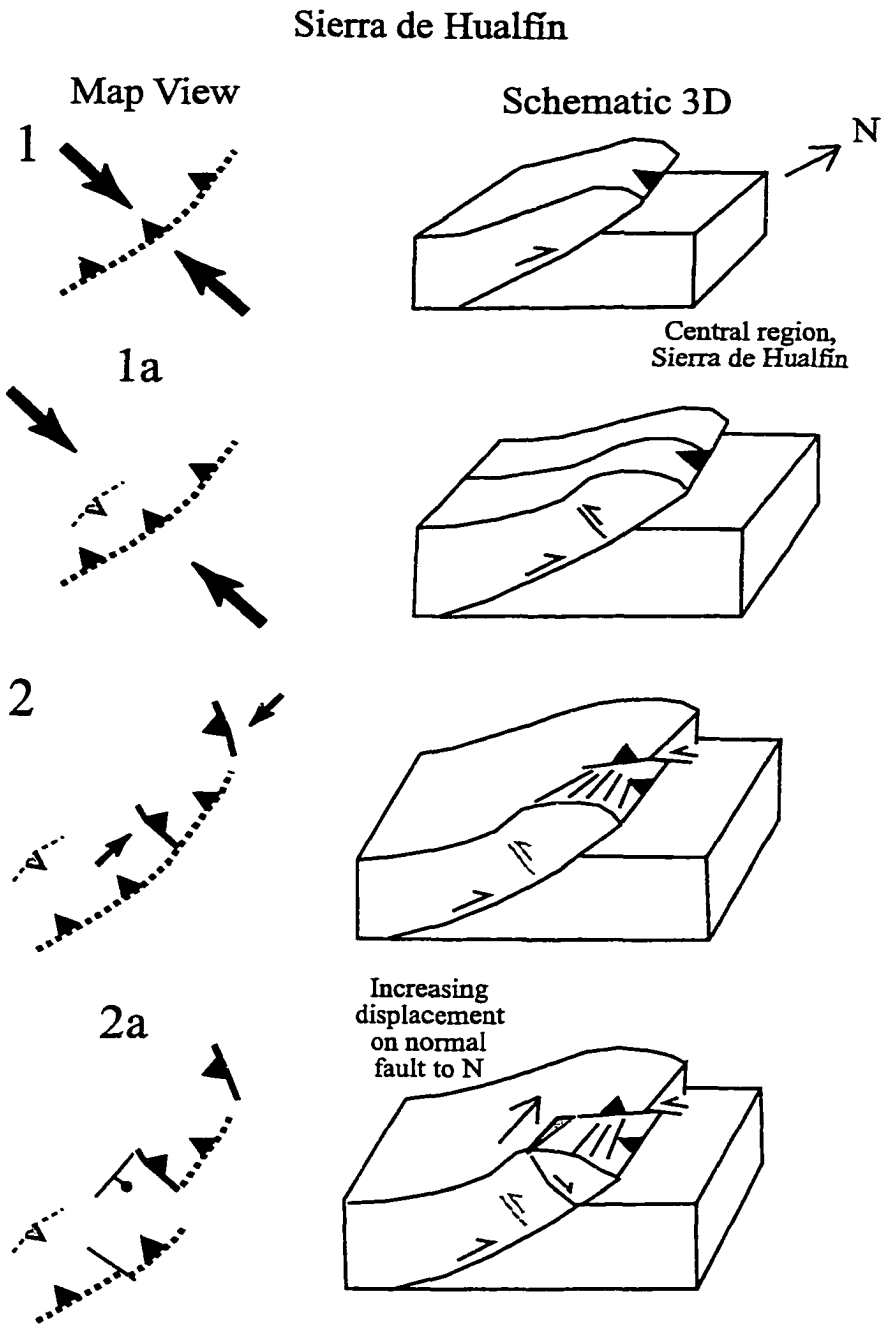

Figure 2.26. Block diagram of the central region of the Sierra de Hualfín northwards showing the development of the uplift.

2.6. CONCLUSIONS

The Sierra de Hualfín is marked by along-strike structural variations, largely due to backthrust formation and possibly to complexities in the main thrust plane. The uplift of the Sierra de Hualfín occurred along a thrust fault or several thrust fault segments that change in strike from ~N50°E in the south to ~N40°-35°E in the north. A three-dimensional model of the main thrust shows that the thrust appears to protrude southeastward in the central region of the uplift, coincident with a kink in the thrust surface. The basement core of the uplift is segmented by faults that trend ~N50°W, perpendicular to the strike of the uplift, and that displace blocks of basement in a right-lateral sense of motion and/or in a NNE-NNW directed reverse motion. The kinematics of the Sierra de Hualfín are consistent with the interpretations of the dextral-transpressional Tucumán Transfer Zone (Urreiztieta et al., 1996; Mon, 1976) in this region. Analysis of the compartmentalizing faults and the domains suggests that the Sierra de Hualfín was formed by (1) Major faulting of the uplift under NW-SE directed compression (1a) Development of the back thrust on the west (2) Uplift of the ND block by local NNE-SSW compression (2a) Movement of the ECD block due to thrusting of the ND over the ECD.

This study shows that a three-dimensional analysis approach is useful in examining complex areas of along-strike variations. In addition, cross section balancing shows that basement-cored uplifts can be formed by gently-dipping thrust faults whose geometry reflects the geometry of the overlying basement and cover rocks.

CHAPTER 3

MECHANISMS OF BASEMENT DEFORMATION AS REVEALED IN THE SIERRA DE HUALFIN BASEMENT-CORED UPLIFT, NW ARGENTINA

ABSTRACT

In the Sierra de Hualfín, a basement-cored uplift in NW Argentina, the excellently exposed basement unconformity delineates an overall folded form in granitic basement rocks. The Sierra de Hualfín, a 22-km long basement-cored uplift with ~ 66 km^2 area of exposure of the basement-cover interface, is composed of a core of Ordovician granite, overlain by and locally thrust over Tertiary sedimentary rocks. The geometry of the uplift is that of a faulted anticlinorium with a ~ 4 km amplitude fold. The uplift likely developed as a fault-propagation fold above a thrust fault tip initially located deep in the basement before it broke through. Standard models of basement-cored uplifts in the literature depict the fault tip exactly at the basement-cover interface. These models do not take into account the basement distortion that must take place in advance of the propagating fault tip when it is initially located below the basement-cover unconformity. Thus, these models cannot explain the folded shape of the Sierra de Hualfin and also the map patterns of some uplifts in the Rocky Mountain foreland.

An example of folded basement (above a fault tip located in basement) is the back limb of the uplift in the west-central area of the Sierra de Hualfín. Folding of the basement is accommodated by reactivation of joints as faults and mode I fissures, by fracturing and faulting near large displacement faults, and by flexural shear of the uppermost basement. These mechanisms are observed to deform the basement at shallow levels. Similar mechanisms were at work deeper in the basement to accommodate the fold geometry of the basement and basement-cover unconformity.

The form of the basement fold resulting from propagation of a fault tip initially in basement depends on the propagation to slip ratio of the fault. Kinematic modeling of such basement-cored uplifts using trishear demonstrates that a lower propagation to slip ratio promotes greater folding of the units involved, while a higher ratio (~ 2 and higher) will cause the fault to break through the units before folding can occur. In turn, the propagation to slip ratio is controlled by the "deformability" of the granite, i.e., by the extent to which the joints, microfractures, and fracture foliation are reactivated. Our findings at Sierra de Hualfín demonstrate the mechanisms by which granite basement can act as a deformable body to produce a folded basement-cover unconformity. Furthermore, our modeling suggests that a variety of the folded forms in granite are possible in other areas around the world.

3.1. INTRODUCTION

Basement deformation in basement-cored uplifts has been at the heart of debates about the structure and development of these low temperature, low-pressure tectonic elements. Most studies of basement-cored uplifts, particularly their structure, have been carried out in the Rocky Mountain foreland province in the western United States, a possible ancient counterpart for the Sierras Pampeanas. Where overlying cover sequences are seen to fold, comparable folding of the underlying basement unconformity and basement rocks is suggested. Folding of metamorphic basement rocks by flexural slip along foliation planes has been documented in the Rocky Mountain foreland (e.g. Schmidt and Garihan, 1983; Miller and Lageson, 1990; Schmidt et al., 1993). Foliation planes provide a planar anisotropy along which units of rock can slide past each other in a flexural manner, similar to bedding-plane slip in sedimentary rocks (Spang and Evans, 1988; Schmidt et al., 1993). However, folding of crystalline "isotropic" basement is not

understood (Spang and Evans, 1988), and even considered unlikely (Stearns 1975). In the absence of "folding" of granite there develops a challenging problem in modeling a structure compatible with folded cover and unfolded basement. Various configurations for the underlying basement, whether basement is exposed somewhat or not at all, have been proposed to account for the observed folding in cover. Geometries such as basement faulted by a single fault, by several faults, or containing a wedge of cataclastic material to help fold the cover have been proposed (e.g. Erslev, 1986; Spang and Evans, 1988; Narr and Suppe, 1984). These scenarios have different implications for the behavior of basement during deformation and for the kinematic development of an uplift. Thus, if basement deformation is better understood, kinematic models can be better constrained.

Sierra de Hualfín (Figs. 3.1, 3.2) is mostly composed of granitoid rocks, and in cross sectional representations it has a fold form with an amplitude of approximately 4 km (Fig. 3.2b). In addition, the basement unconformity on the west side of the uplift is smoothly folded over a horizontal distance of ~ 1 km (Figs. 3.2b, 3.3). We postulate that the folding of the unconformity is an example of basement folding above a fault tip within the basement, where fractures, reactivated joint planes, faults and a fracture foliation in the granitoid rocks document the distortion of the basement. Few opportunities exist to "observe" a fault tip beneath the basement-cover interface and the resulting basement response. Uplifts that formed by a fault tip initially deep in basement may only be postulated from map geometries and with much conjecture.

Basement-cored uplifts that form as a result of a fault that propagates to the basement-cover interface show minor deformation of the basement, and considerable deformation of the overlying sedimentary rocks (Fig. 3.4a). However, if the fault tip does not readily propagate to the basement-cover interface and remains in basement while slip is still fed into the fault, then the basement rocks above the fault tip deform in order to accommodate the slip (Fig. 3.4b). Numerical models of blind faults studied in the Los

Angeles basin show that slip on planar anisotropies (usually bedding planes) can take up significant coseismic deformation that would otherwise be taken up by propagation along the fault (Roering et al, 1998). The folded unconformity in the Sierra de Hualfín provides a glimpse of folded basement, frozen at a stage before possible continued propagation breaks through the basement-cover interface. The folded unconformity may be representative of an earlier time-step in the development of the entire uplift, and would help explain the overall folded shape of the basement.

Not all basement-cored uplifts have folded basement (e.g. Erslev and Rodgers, 1993; Schmidt et al., 1993). The circumstances under which basement actually folds are controlled by many factors, most important of all is the rheology of the basement during deformation. Whether basement folds or not is expressed kinematically in the propagation to slip ratio (P/S) demonstrated by trishear modeling. Modeling for this study shows that a lower propagation to slip ratio promotes greater folding of the units involved, while a higher ratio (~ 2 and higher) will cause the fault to break through the units before folding can occur. It is unclear at the moment what controls P/S, but application of trishear to the Sierra de Hualfín strongly suggests that it is greatly influenced by the material properties of the rocks undergoing deformation.

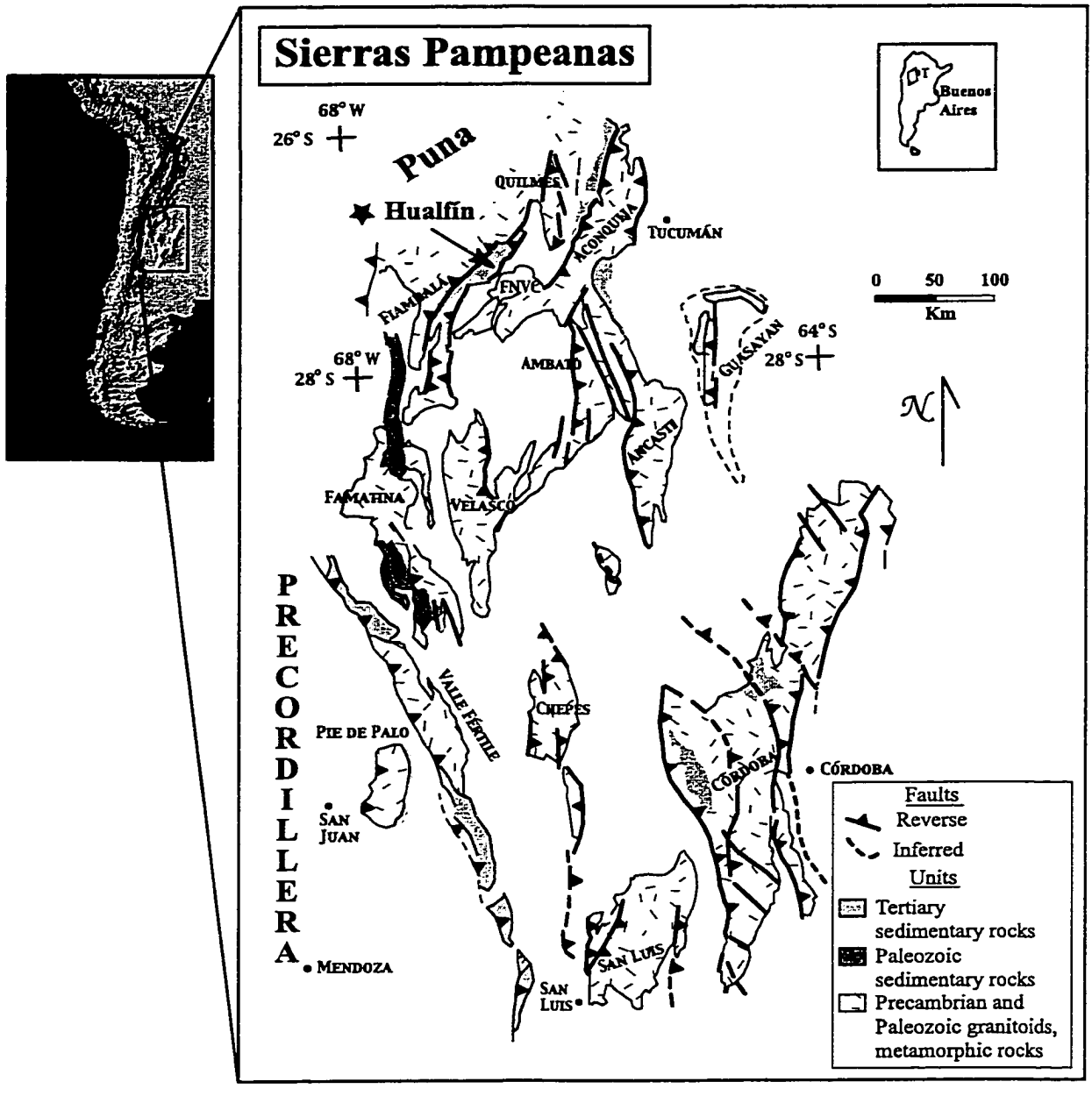

Figure 3.1. Shaded digital topographic image of the western margin of South America and simplified geologic map of the Sierras Pampeanas. Sierras Pampeanas are located in the black outline box. Adapted from Jordan and Allmendinger (1986) and the Geologic Map of Argentina (Achili et al., 1997) by the Servicio Geológico Argentino. Ranges are accompanied by their respective names. Sierra de Hualfín is located in the northern region.

Figure 3.2a. Geologic map of Sierra de Hualfín, with cross section locations and area names. Abbreviations used for units (where identifiable) are: **Og** (Ordovician granite), **Thua** (Hualfín Fm.), **Tarc** (Las Arcas Fm.), **Tchiq** (Chiquimil Fm., undifferentiated), **Tchiba** (Los Baños member, Chiquimil Fm.), **Tchias** (El Aspero member, Chiquimil Fm.), **Tchija** (El Jarillal member, Chiquimil Fm.), **Tand** (Andalhuala Fm.), **Tcq** (Corral Quemado Fm.), **Q**(al, ls, fl).

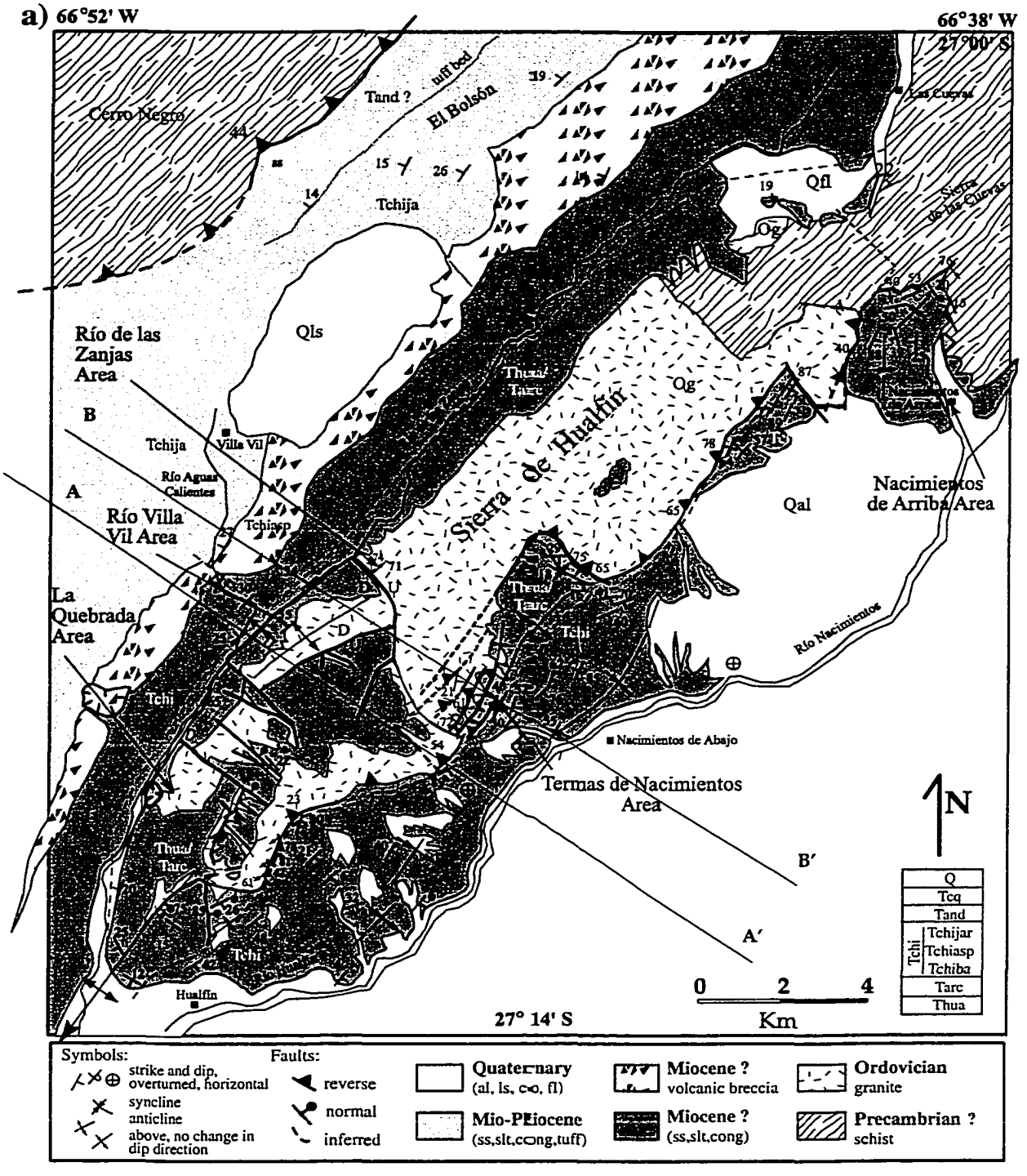
a)
66°52' W
66°38' W
27°00' S
27° 14' S
Cerro Negro
Tand ?
tuff bed
El Bolsón
Las Cuevas
Tchija
Qfl
Sierra de las Cuevas
Og
Qls
Río de las Zanjas Area
B
A
Villa Vil
Río Aguas Calientes
Río Villa Vil Area
Tchiasp
Thua/ Tarc
Sierra de Hualfín
Qal
Nacimientos de Arriba Area
La Quebrada Area
Tchi
Río Nacimientos
Nacimientos de Abajo
Termas de Nacimientos Area
B'
A'
Hualfín
N
0 2 4
Km
Q
Tcq
Tand
Tchi
Tchijar
Tchiasp
Tchiba
Tarc
Thua
Symbols:
strike and dip, overturned, horizontal
syncline
anticline
above, no change in dip direction
Faults:
reverse
normal
inferred
Quaternary (al, ls, c∞, fl)
Mio-Pliocene (ss,slt,cong,tuff)
Miocene ? volcanic breccia
Miocene ? (ss,slt,cong)
Ordovician granite
Precambrian ? schist

Figure 3.2a

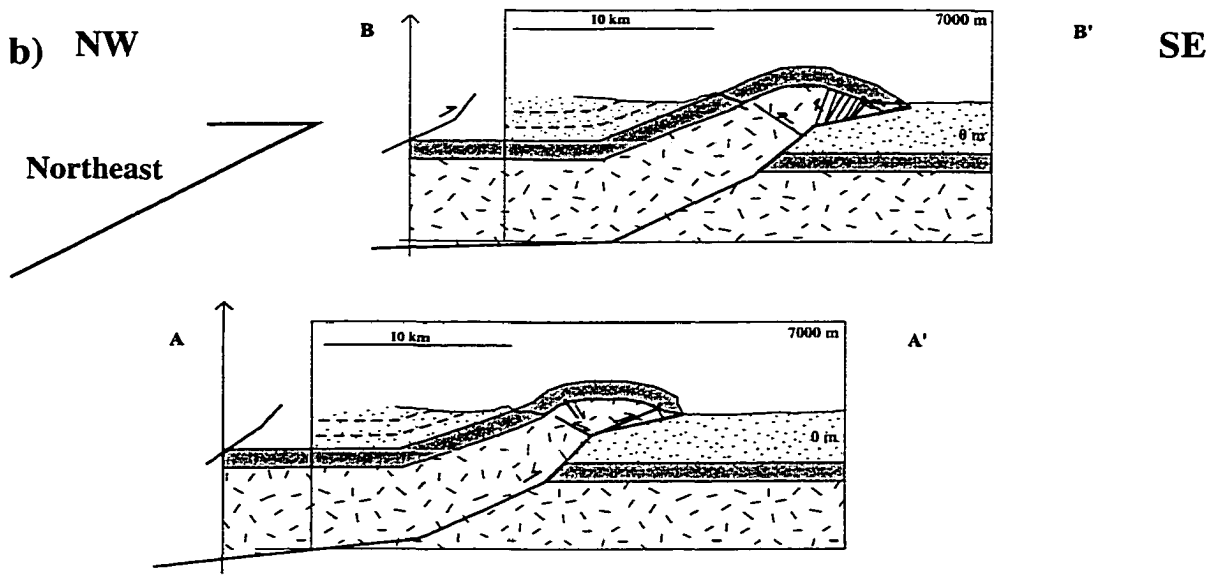

Figure 3.2b. Cross sections A-A' and B-B' through the central region of Sierra de Hualfín showing the western folded unconformity (Río Villa Vil area) and the eastern faulted unconformity (Termas Nacimientos area).

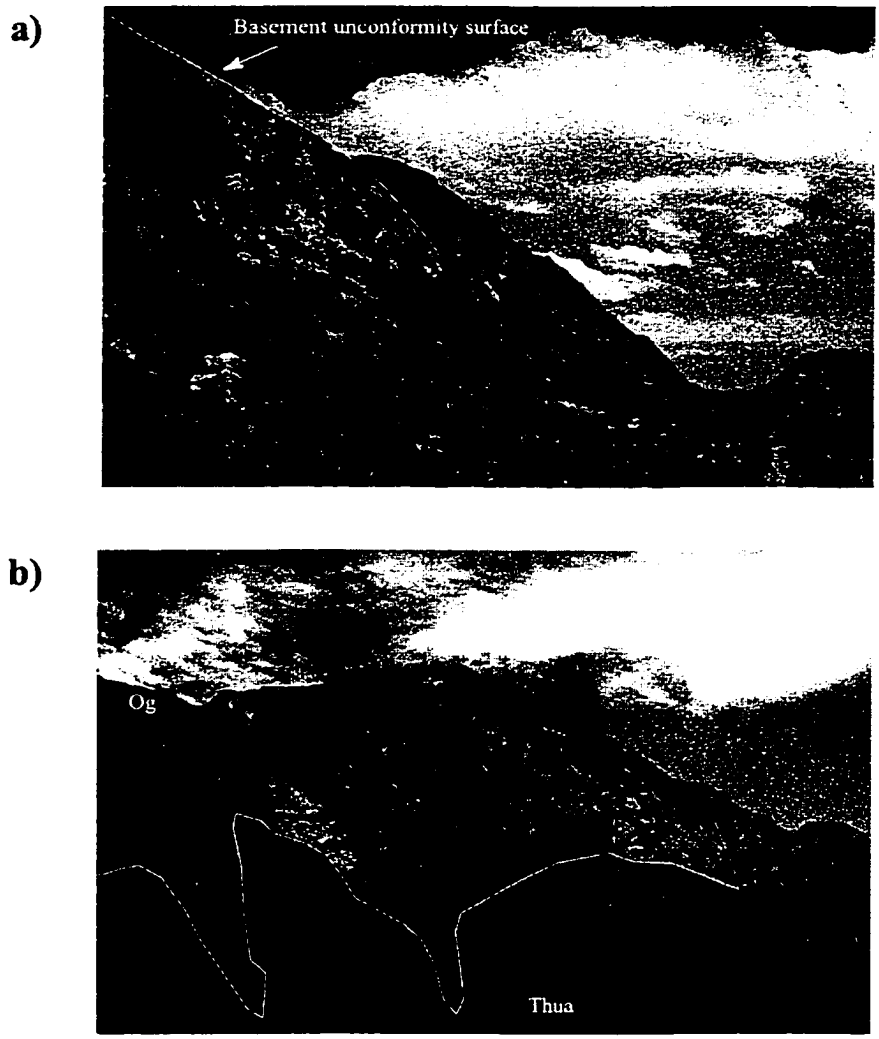

Figure 3.3. (a) View southeast from Río de las Zanjas area of smoothly folded basement unconformity in the Río Villa Vil area. (b) Closer view of the smoothly folded unconformity from the northwest. Basement granite is denoted by Og, the overlying basal sandstone of the Hualfín Formation is denoted by Thua.

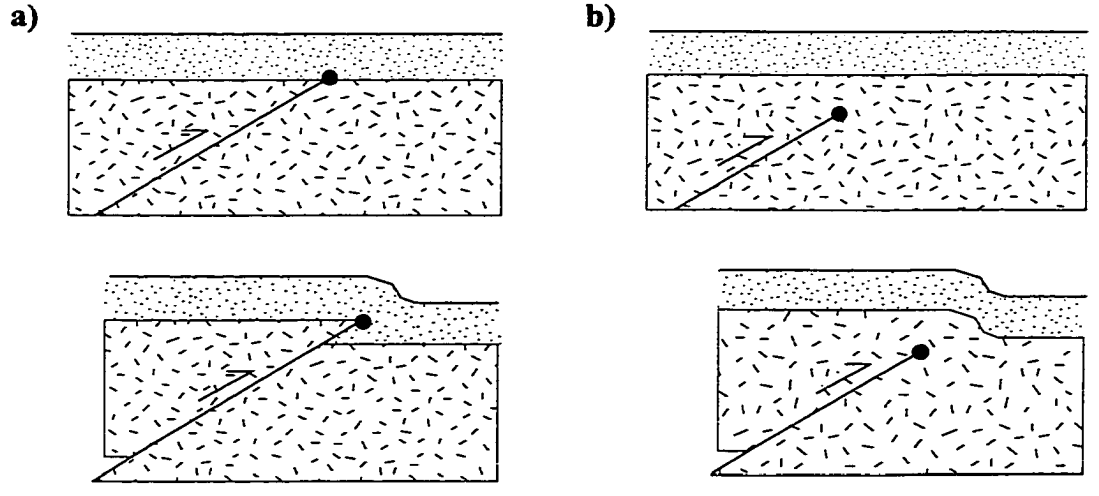

Figure 3.4. (a) Model of fault tip propagating from basement-cover interface into sedimentary cover rocks, resulting in deformation of cover rocks only.
(b) Model of fault tip propagating from within basement into shallower basement and sedimentary rocks, resulting in significant deformation of basement and cover rocks.

3.2. SIERRA DE HUALFIN

3.2.1 Setting and Background Geology

The Sierra de Hualfín is an ideal place for examining and analyzing basement deformation as it relates to uplift geometry because of the preservation of sedimentary cover rocks and the excellent exposure of the basement-cover unconformity (~ 66 km^2 in plan view, and some three-dimensional exposures). The Sierra de Hualfin is located in the northern Sierras Pampeanas and at the border with the Puna Plateau (Allmendinger, 1986). A west-dipping thrust fault places Ordovician granitoid rocks over Tertiary sedimentary rocks (Figs. 3.1, 3.2). The shape of the uplift is a broad fold, asymmetric to the east, with a steep range front on the east and a gently dipping backlimb on the west. Uplift of the range is estimated to have occurred between 10 Ma and 2 Ma (Jordan et al. 1983; Allmendinger, 1986; Coughlin et al., 1998; Muruaga, 1999). The range is small enough to be studied in its entirety (approximately 125 km^2), thus allowing for generation of a complete picture of a basement-cored uplift structure. Because the Sierras Pampeanas basement-cored uplift deformation is young (not older than ~ 10 Ma; e.g., Jordan et al. 1983, Coughlin et al., 1998) and is the last deformation event to affect the area, many of the features seen are clearly related to this Neogene deformation.

The basement rocks in the Sierra de Hualfín are mostly an Ordovician granitoid (Omarini, 1984), occurring as equigranular, coarse grained to aphanitic or very fine grained. Where it is coarse grained and equigranular, the granitoid is composed of quartz, potassium feldspar, and clumps of actinolite crystals that appear to radiate outward from common centers. Where finer grained, the granitoid is composed of quartz, potassium feldspar, some plagioclase and biotite. At the northern end of the uplift, the basement includes exposures of mylonitic schist (Precambrian ?).

Exposures of the basement occur mostly at the level of the basement-cover interface. Only in a few places do deep canyon cuts expose basement in cross-sectional view. In the area of La Quebrada, a three-dimensional view of the basement can be seen. Where basement is observed in canyon cuts (Rio Villa Vil exposure), the basement granite is jointed, sometimes with clastic material filling the joints.

3.2.2. Basement Unconformity

The unconformity between Ordovician granitoid and Tertiary sedimentary rocks is an originally-planar erosional surface. The unconformity is regionally extensive (González Bonorino, 1950; Allmendinger, 1986; Jordan et al., 1989) and its originally-planar nature is best seen on the gently-dipping backlimbs of uplifts throughout the Sierras Pampeanas. Thermochronology studies of the basement unconformity in the southeastern and north central area of the Sierras Pampeanas suggest that the surface formed from continuous and progressive unroofing of the basement over a 300-400 million year time period (Jordan et al, 1989). The surface is presumed to have been nearly horizontal prior to late Cenozoic uplift formation (Jordan and Allmendinger, 1986; Jordan et al., 1989). Therefore, the present day geometry of the unconformity documents rotation of basement fault-blocks along faults and other translations and deformations the basement may have undergone.

Comparison of the dip of the unconformity with the dip of sedimentary beds directly above (Fig. 3.5a), where both are homoclinally dipping, shows that the orientation of the basement erosional surface is generally concordant and that there is no preferred orientation of this surface prior to deposition of the overlying Tertiary sedimentary rocks (Fig. 3.5b). Thus, one can be used as a proxy for the other where one or the other is not present or not exposed.

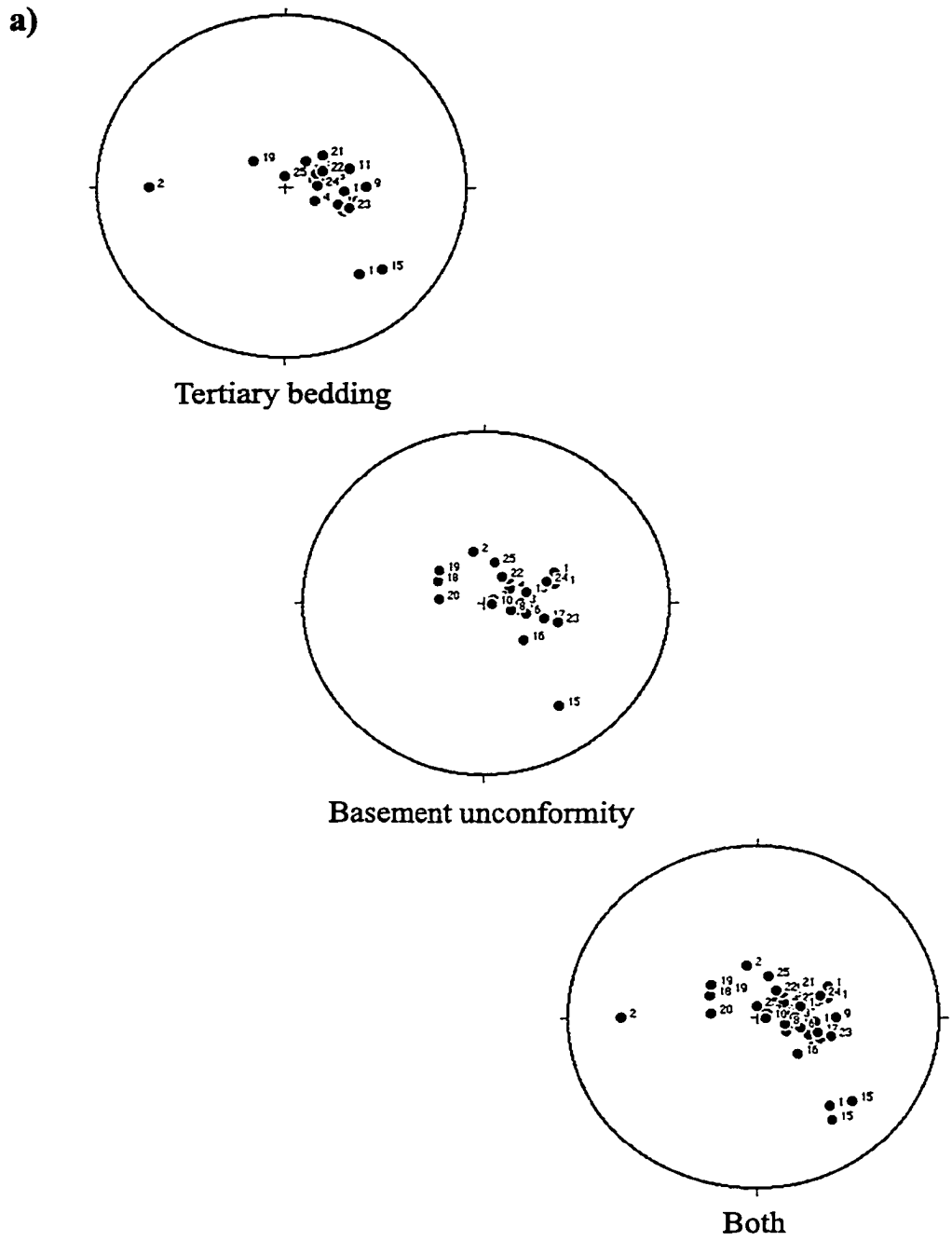

Figure 3.5. (a) Stereonet plot of bedding measurements of red sandstone at the base of the Tertiary section (black) and measurements of the basement unconformity surface (gray) at the same location as bedding measurements. N = 25 for both.

b)

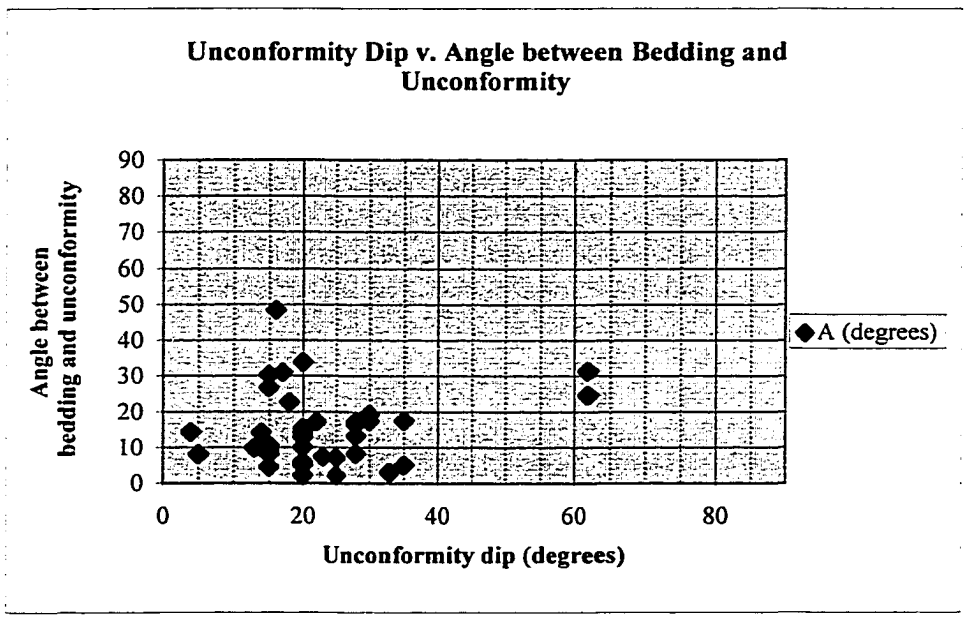

Figure 3.5. (b) Graph of dip of the unconformity vs. the angle between the unconformity and bedding.

The geometry of the basement unconformity delineates the geometry of the hanging wall of the uplift (Fig. 3.2b). The geometry of the hanging wall is critical to determining the kinematics of the uplift and to discriminating between different models of deformation. The basement unconformity in the central part of the Sierra de Hualfín delineates a broad fold, asymmetric to the east with a folded unconformity on the west and a faulted unconformity on the east (Figs. 3.2a, b). A balanced cross section, based on surface mapping, shows that the basement has a 4 km amplitude fold-shape, defined by the basement unconformity and the regional elevation (Fig. 3.2b). The location of the basement unconformity is well constrained at the surface because it is preserved almost entirely along the exposed uplift. The regional elevation is constrained by a seismic reflection profile 26 km NE of the Sierra de Hualfín (Cristallini et al., 1998) and by the thickness of the stratigraphic column in the area, which is between ~5000 m (estimate includes about 1000 m of Quaternary deposits, Allmendinger, 1986) and ~3000 m (measured section without Quaternary deposit thickness, Muruaga, 1999).

In many exposures of the basement-cover interface, the distinct Tertiary red sandstone of the Hualfín Formation that overlies the unconformity is partly composed of clasts of grus, produced from the weathering of the underlying granite (Fig. 3.6). The thickness of grus ranges from 0 m to 0.5 m to 0.05 m.. In turn, the granite directly below the basement unconformity is pervaded by clastic infilling along joints and fractures. The orientations of the fractures range from nearly vertical to subhorizontal. The infilling is mostly composed of silt particles, often with hematite and 1 - 2 millimeter quartz grains. The presence of grus in the overlying Tertiary sedimentary rocks, and of fractures and infilled fractures in the basement suggest an eroded and mechanically weak layer of basement around the unconformity.

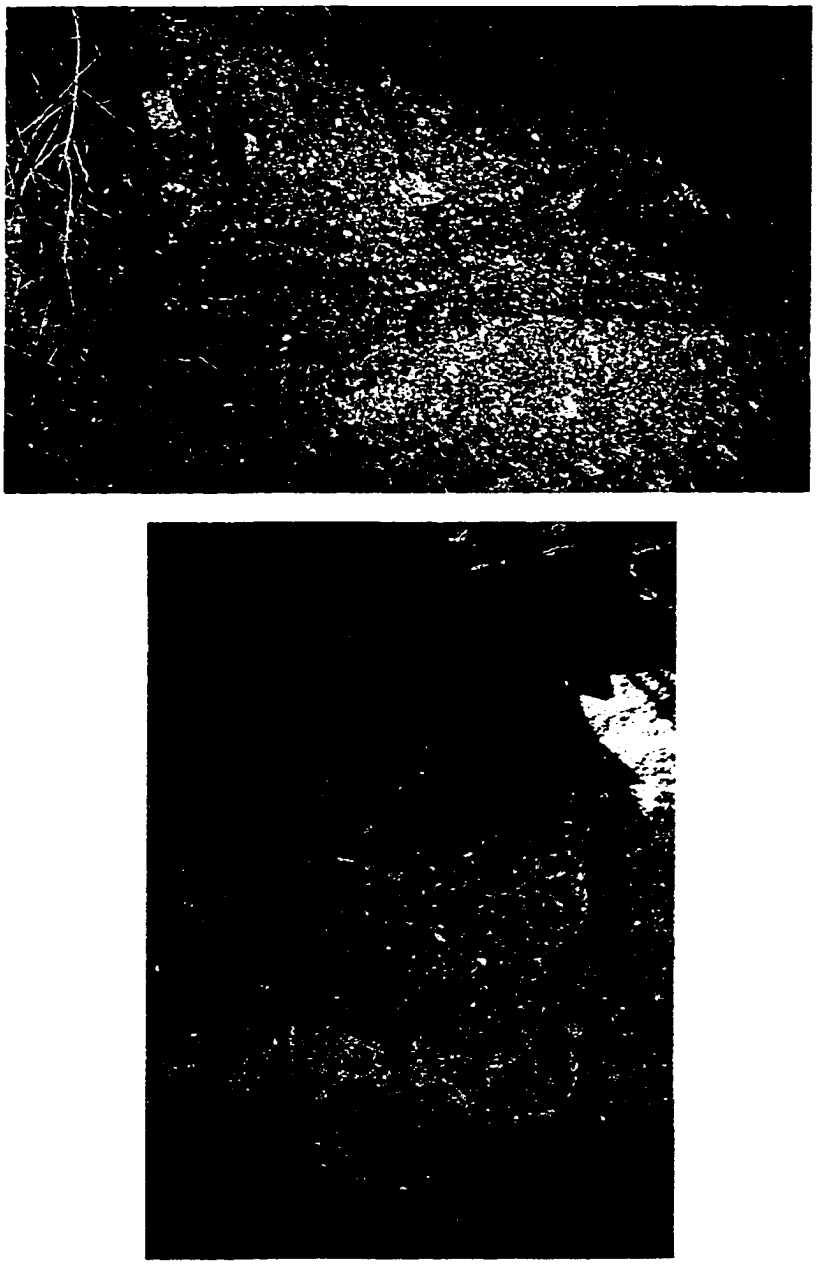

Figure 3.6. Photograph of the basement unconformity near the village of Nacimientos de Arriba and the village of Hualfín, showing abundant grus clasts in the overlying sandstone.

3.3. BASEMENT DEFORMATION

Basement deformation in the Sierra de Hualfín has been documented at the level of the basement unconformity and up to ~ 50 m below the unconformity. The principal deformation mechanisms are jointing (sometimes followed by dilation), faulting, and slip along subparallel, closely-spaced tensile fracture planes (which we refer to as a fracture foliation) oriented subparallel to the unconformity. Jointing, faulting and the development of a fracture foliation are documented throughout the uplift, both where the unconformity is homoclinally dipping east or west, and where it is folded. Slip along the fracture foliation planes appears only to have been active where the unconformity is folded. These features accommodated the distortion of the basement as necessary. There are four main locations where the characteristics of basement deformation are well exposed: Termas de Nacimientos area, La Quebrada area, Río Villa Vil area and Río de las Zanjas area (Fig. 3.2a).

3.3.1. Homoclinally Dipping Basement Unconformity: Jointing and Brittle Foliation in La Quebrada, Termas Nacimientos, Río de las Zanjas

3.3.1.a. Jointing

Areas of the exposed, gently dipping basement unconformity are notable for the pervasive fractures that cross-cut the surface (Fig. 3.7). Measurements of these spaced fractures revealed two to three distinct sets of similarly oriented mode I fractures, interpreted as joints. Joints were measured in five different locations, and in fine-grained and coarse-grained granite (Fig. 3.8). Two principal locations on the west side of the Sierra

Figure 3.7. View of a typical basement surface. Note the pervasive fracturing and alteration (dark bands symmetric about fracture planes) around many of the joints.

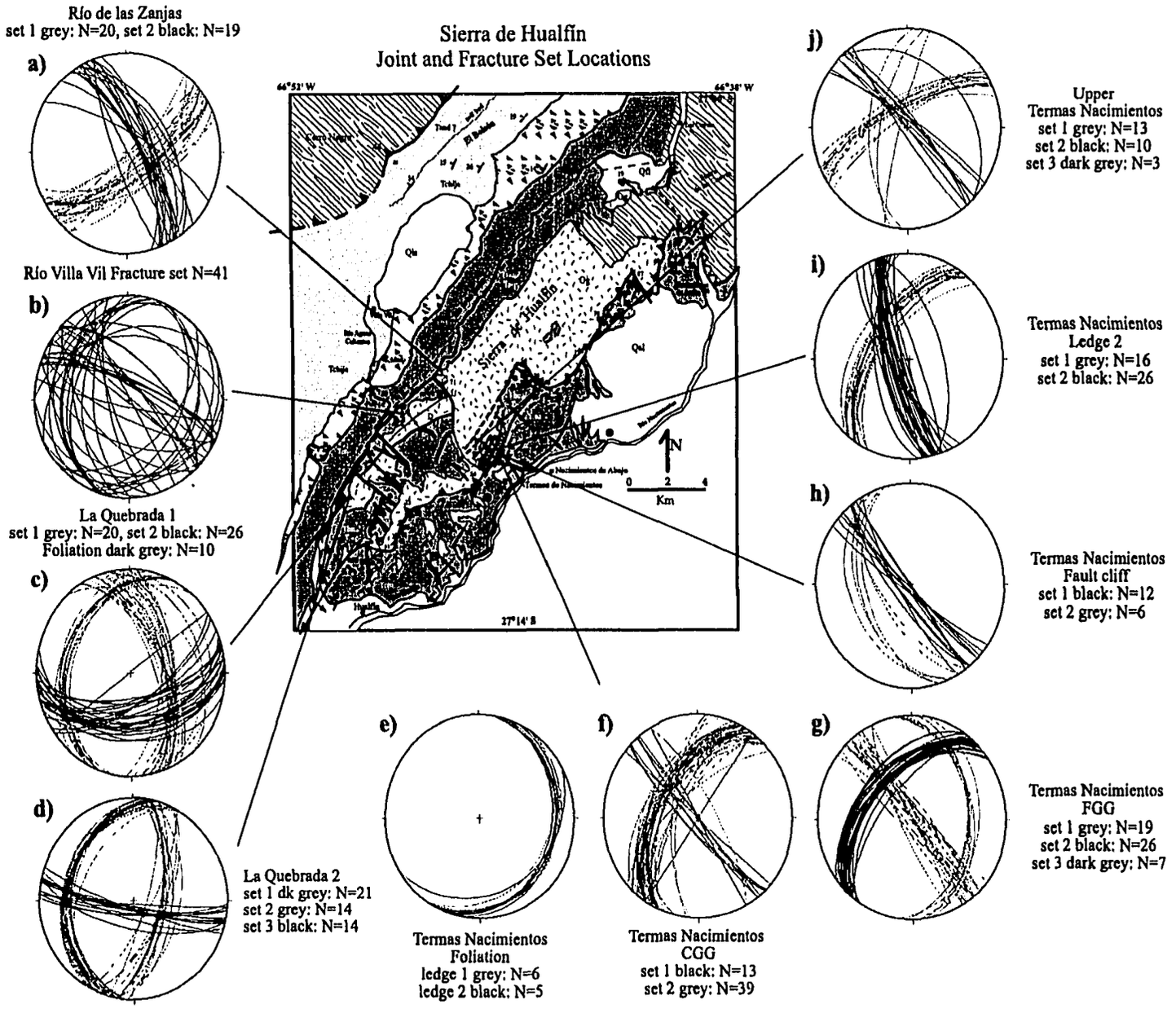

Figure 3.8. Stereonet plots of joint and fracture sets in basement and their locations around the uplift. See text for more details.

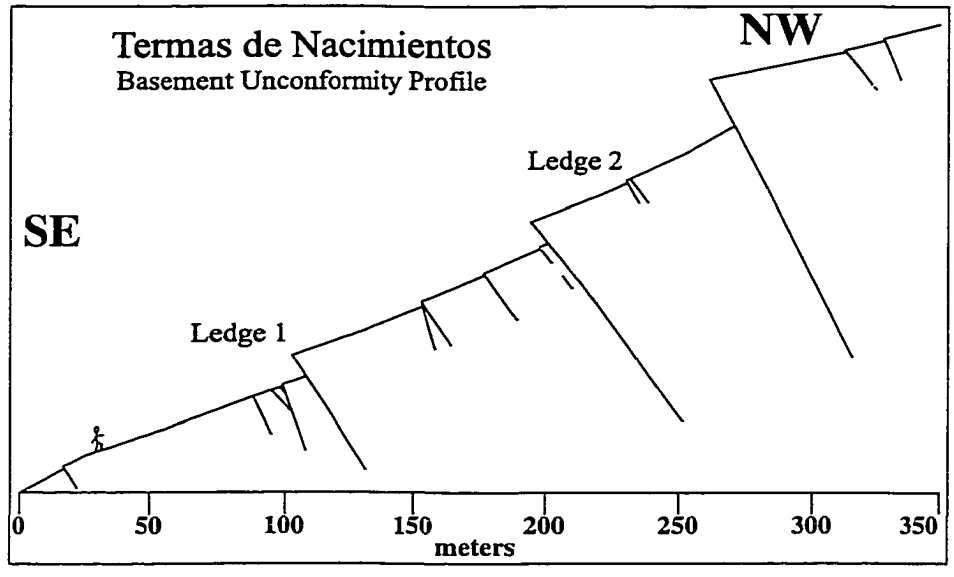

Figure 3.9. Profile of a 350-m transect across the basement unconformity at Termas Nacimientos showing the position of faults (reactivated joints) and their vertical offset. Note that the basement unconformity surface changes in dip from ~ 30°E at ledge 1 to ~23° at the uppermost ledges. Ledge 1 is the lower area at Termas Nacimientos. Stick figure not to scale.

de Hualfín are the Río de las Zanjas area and La Quebrada area, approximately 8 km apart. The other three are within the Termas de Nacimientos area on the east side of the uplift. Jointing in the basement is pervasive. The joints are systematic, regular features in the granite. Polished and slickenlined joint surfaces imply that movement was accommodated on these fractures, and that the fractures were reactivated as faults, some with significant offset. Also, infilling of joint fractures is evidence of dilation of the basement, most likely during deformation. The strike and dip of the average planes for separate joint sets, as well as average foliation planes, are noted in Table 3.1.

In the Río de las Zanjas location, the joint sets are in coarse-grained granite and are steeply dipping to the east (set 1) and to the north (set 2) (Fig. 3.8a). Average planes for these sets (Table 3.1) are virtually perpendicular, with an angle of 89° between the two average planes.

Joint fractures in two separate areas in the La Quebrada location were analyzed. In the first area, La Quebrada 1, two sets were measured in coarse-grained granite. One joint surface in set 1 is marked by red polish and slickenlines. The slickensides plunge 8° N24°E; offset could not be determined due to a lack of marker units or other distinguishable features. The second area, La Quebrada 2, affords a three-dimensional exposure of the basement granite where three sets of joint fractures were measured. The fracture sets occur in coarse-grained, fine-grained, and porphyritic granite. Set 1 is subparallel to the orientation of the basement unconformity in this area, which is N14°E 34°W. The foliation measurements at La Quebrada 1 are similar in orientation to fracture set 1 at La Quebrada 2 (Fig. 3.8c - black squares, 3.8d - white circles). Seventeen joint surfaces from the 3 sets combined are polished and have slickenlines raking steeply (70°)

to moderately (30°). Again, displacement could not be determined due to lack of offset markers.

On the east side of the Sierra de Hualfín, in the area of Termas de Nacimientos, several joint fracture sets were analyzed (Fig. 3.8e-j). The sets were measured in the lower area (first ledge), on a second ledge (Fig. 3.9) and in a higher elevation area to the west. In the first ledge, joints were measured in coarse-grained and fine-grained granite, and in an exposed fault-cliff face. Two sets were distinguished in the coarse-grained granite (Fig. 3.8f), and three sets were distinguished in the fine-grained granite (Fig. 3.8g) (Table 3.1). In an exposed fault cliff-wall, there also appeared to be two noticeable fracture sets, mostly in coarse-grained granite (Fig. 3.8h). Set 1 of all three sampling locations appears to be correlative (Table 3.1 - gray shaded boxes). Fracture foliation plane measurements in the coarse-grained granite (Fig. 3.8e) are similar to set 3 in the fine-grained granite (Table 3.1), with only a 21° angle between the two average planes. Six joints measured in the fine-grained and coarse-grained sets had measurable offset of the basement unconformity or of other markers (Fig. 3.10). The offsets measured range from 28 cm of right-lateral offset, 3-29 cm of vertical offset, and 1 cm right-lateral offset. Right-lateral reverse sense of motion on one joint fracture was determined from slickenline measurements, although the amount of offset was not discernible. Movement and offsets documented along these joint fractures demonstrates reactivation of joint surfaces as fault surfaces.

On the second ledge of the Termas Nacimientos area, joint measurements are similar but not the same as in the first ledge (Fig. 3.8i and Table 3.1) and the fracture foliation in the coarse-grained granite is the same as in the granite of the first ledge (Fig. 3.8e and Table 3.1). Finally, in the upper area of the Termas de Nacimientos (Fig. 3.8j), there appears to be three distinct joint sets in coarse-grained granite (Table 3.1). Four joints

Strike and dip of average joint planes								
				Nacimientos				
	Río de las Zanjas	La Quebrada 1	La Quebrada 2	Ledge 1 (CGG)	Ledge 1 (FGG)	Fault cliff	Ledge 2	Upper Nac.
Figure:	12a	12c	12d	12f	12e	12h	12i	12j
Set 1	N54E 73 SE	N17W 54 E	N15E 30 W	N41W 88 S	N39W 85 N	N24W 84 S	N35E 57 W	N61E 72 N
Set 2	N40W 73 NE	N79E 55 S	N14E 65 E	N31 E 57 W	N43E 50 N	N25W 51 S	N16W 76 SW	N44W 80 N
Set 3			N80W 80 S		N1W 37 E**			N9E 69 W
Foliation		N24E 31 W		N29E 22 E**			N26E 23 SE	
Basement unconformity			N14E 34W					
*gray shading denotes correlative sets			** 21 deg between average planes					

Table 3.1. Strike and dip of average joint planes for the stereonet plots in Figure 3.8.

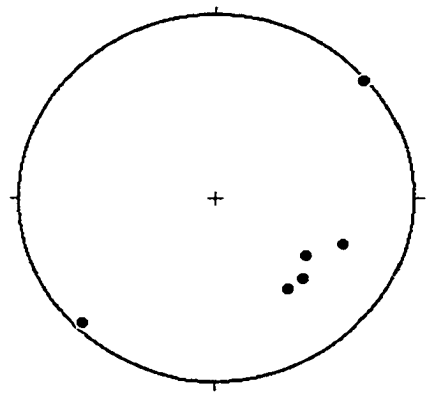

Termas Nacimientos
N=6

Figure 3.10. Stereonet plot of joints with measured offset at Termas Nacimientos.

from set 1 and set 2 combined have steeply raking slickenlines (66°-88°N), although offset was not measurable, and one joint in set 2 had 10 mm of right lateral offset of a joint fracture in set 1.

3.3.1.b. In-filled joint fractures

A large majority of the joint fractures in the Ordovician granitoid discussed above are infilled with clastic material. The amount of clastic infill material in the joints over the distance along the basement unconformity was recorded in order to determine the magnitude of dilation in the granite (Table 3.2). The average orientations of the joints and the direction of infilling (dilation) are shown in Figure 3.11.

Total infill material was calculated for five sites: La Quebrada 1, La Quebrada 2, Río de las Zanjas, Upper Termas Nacimientos and Termas Nacimientos. If the sampled areas are representative, the calculations (Table 3.2) show that there has been between 0.09 to 0.54% dilation in the granite that can be accounted for by infilling of veins with clastic material. The largest amount of infill material measured was 4.5 cm over a distance of 1336 cm (approximately perpendicular to joint strikes); the minimum measured was 0.5 cm over 538 cm. These measurements were made on infilled joints at the basement unconformity. However, infilled fractures are also present ~30 m stratigraphically below the unconformity. The distribution of these fractures was not as systematic and therefore difficult to determine a dilation amount in a given direction (Fig. 3.12). Also, it is not certain that these fractures are filled with clastic material; the infill material maybe cataclastic, as suggested by slickenlines associated with some of the infilled fractures.

Infilling of the joint fractures could have occurred at two different points in time. Joints could have formed and opened up during unroofing and exhumation of the granite and immediately would have filled with available material. Although exhumation of the

Joint Fracture Set	Perpendicular Orientation	Length (cm)	Total Vein filling (cm)	Type infill	Percent dilation
La Quebrada 1 CGG set#1	N73E	1336	4.5	clastic	0.34
La Quebrada 1 CCG set#2	N11W	1603	2.8	clastic	0.17
Area (cm^2)		2,140,807			
La Quebrada 2 set#1	N 75W	538	0.5	clastic	0.09
La Quebrada 2 set#2	N76W	887	0		0.00
La Quebrada 2 set#3	N10E	612	0.9	mainly qtz veins	0.15
Volume (cm^3)		292,050,072			
Rio Las Zanjas CGG set#1	N36W	982	1.5	clastic	0.15
Rio Las Zanjas CGG set#2	N60E	1162	1.3	mainly qtz veins	0.11
Area (cm^2)		1,140,503			
Upper T. Nac. CGG set#1	N29W	203	1.1	clastic	0.54
Upper T. Nac. CGG set#2	N46E	704	1.3	includes qtz.	0.18
Upper T. Nac. CGG set#3	N81W	373	0.5	clastic	0.13
Volume (cm^3)		53,174,880			
Termas Nac. FGG set#1	N51E	514	1.25	cataclastic?	0.24
Termas Nac. FGG set#2	N47W	678	2	clastic	0.29
Area (cm^2)		348,153			

Table 3.2. Amount of clastic material in-filling joint fractures.

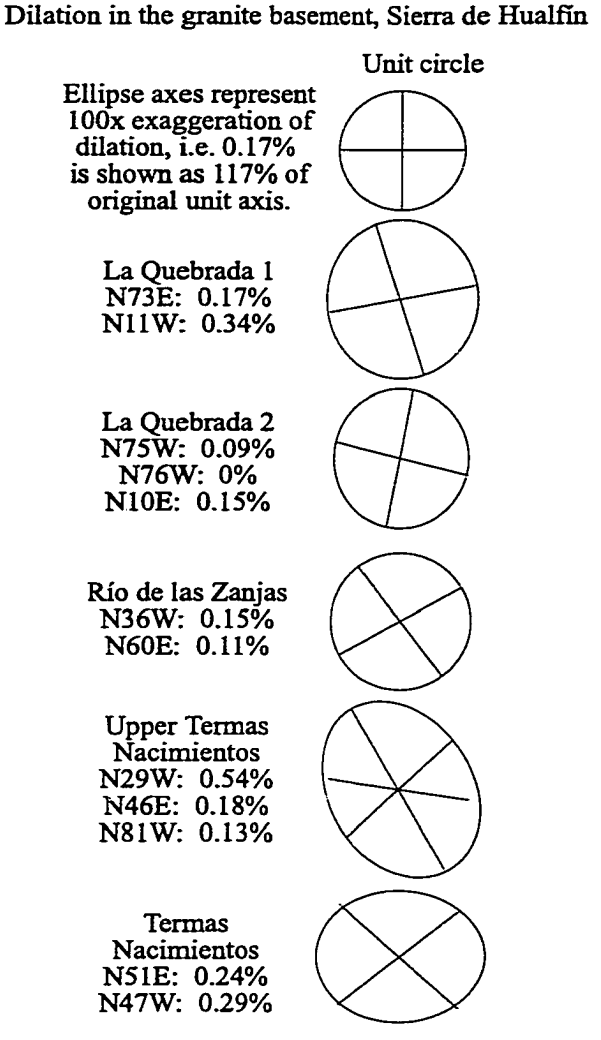

Figure 3.11. Map view representation of dilation in basement due to infilled joints at the basement unconformity. Unit circle shows a standard original length of lines. Ellipse axes correspond to percent lengthening of the original unit circle lines in the direction perpendicular to the average strike of the joint set for each area (calculations in Table 3.1).

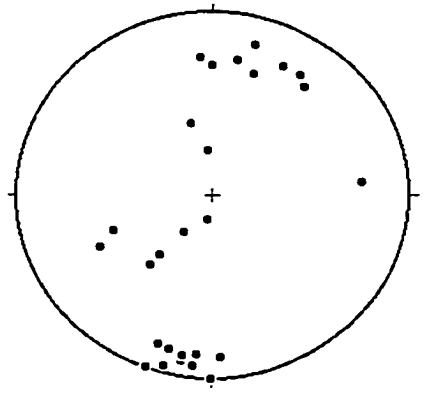

Río Villa Vil
Canyon cut, 25 m below
basement-cover interface
N=27

Figure 3.12. Stereonet plot of fractures in a canyon exposure near the Rio Villa Vil area. Specific fracture orientation with rake of slickenlines and/or cataclasitc material are as follows:
(1) EW 60° S, 55° W slicks, with 3-4 mm communated granite
(2) N50 °W 35° E, with 3 mm communated granite
(3) N75 °W 74° S, 54° W slicks, with ~1 mm of altered granite material
(4) N70 °W 90°, 64° W slicks, with 1 mm of altered granite material.

granite and the preserved peneplain surface would imply an erosion regime rather than depositional, material passing over open "fissures" would fall into open cracks and remain there. Alternatively, vein infilling may not have occurred until the basement surface subsided (in the Paleocene/Miocene - Muruaga, 1999) and was covered by the lower-most Tertiary sedimentary rocks of the Hualfín Formation. In this scenario, fluids (water) would have accompanied deposition of clastic material into the opened joint surface. Many of these joints show alteration concentrated 1-3 cm on both sides of the infilled joint. Also, there may have been a continuum of vein infilling from the time the basement granite was exposed to the time it became covered again. Similar infilled fractures have been found in basement rocks in the Appalachian mountains (G. Mitra, personal communication, 2001).

3.3.1.c. Fracture foliation

At three localities studied, Termas Nacimientos, Río Villa Vil, and La Quebrada, the upper ~ 0.5 m to 2 m of the basement granite displays closely-spaced, subparallel fractures that are often filled with silt particles, sometimes with hematite and larger grains of quartz (Fig. 3.13). The fractures are subparallel to the orientation of the basement unconformity (Figs. 3.14a, b) in all the locations where they were measured. These fractures separate domains of quartz and feldspar crystals in the granite. The fracture planes are anastomosing to subparallel, resulting in lenticular "microlithons" of quartz and feldspar and discontinuous planes. Spacing of the fractures is from 0.6 mm to 10 mm, and the thickness of the infill material in the fractures ranges from 0.1 mm to 3-4 mm (Table 3.3). Because of the close spacing of the fractures, and their planar and subparallel nature, we call this feature a fracture foliation. This fracture foliation decidedly imparts a mechanical anisotropy to the granite.

In thin section, the transgranular and tensile nature of the fractures is evident. The fractures cross individual grain boundaries, and often matching halves of grains can be

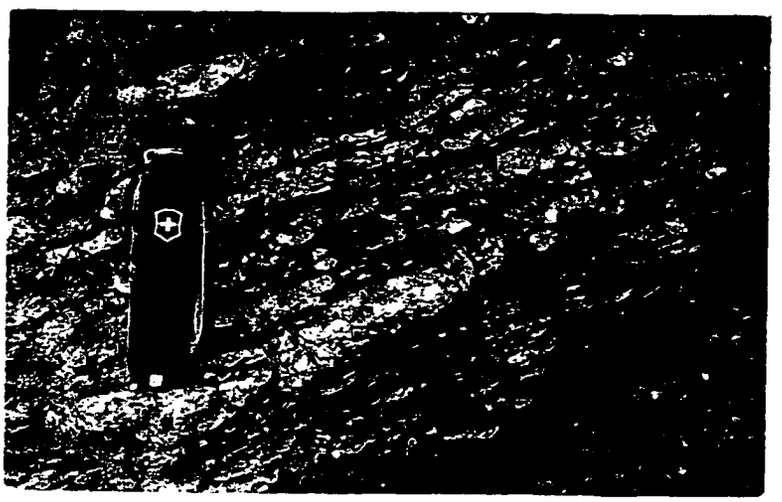

Figure 3.13. Close up photograph of the fracture foliation in granite, at and below the basement unconformity. Note that the fracture planes cut across grain boundaries and do not appear to follow any pre-existing feature. The fracture planes are often filled with fine-grained material, which shows up as the dark lines on the photograph.

Lower Río Villa Vil: La Quebrada

Foliation and basement unconformity are subparallel where unconformity is homoclinally dipping

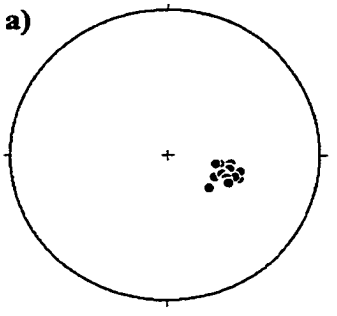

Termas de Nacimientos

Foliation and basement unconformity are subparallel where unconformity is offset by reverse faults

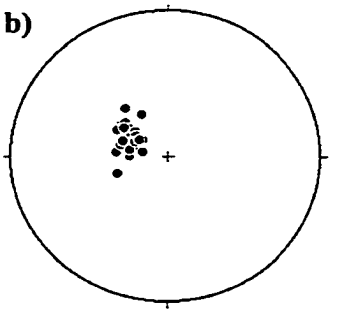

Upper Río Villa Vil: The Wall

Foliation and basement unconformity are subparallel where unconformity is folded

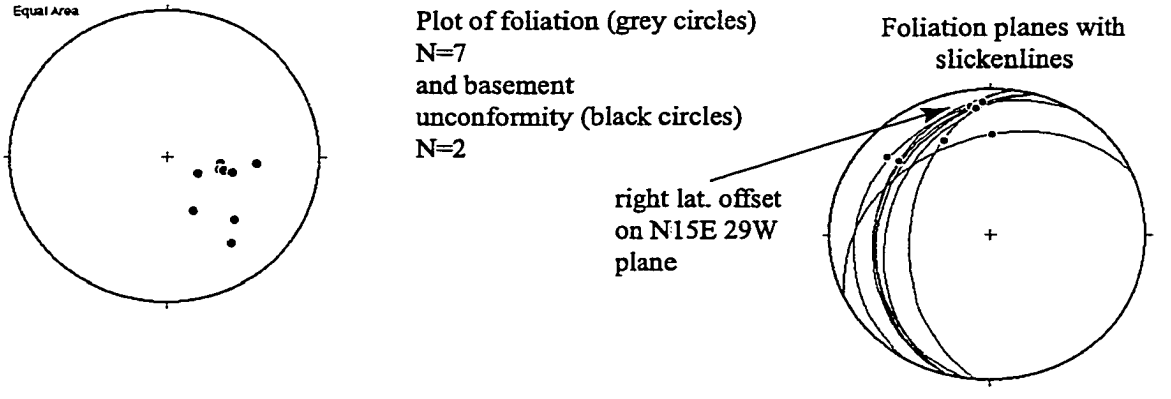

Figure 3.14. Stereonet plots of fracture foliation planes.(a) La Quebrada (b) Termas Nacimientos (c) Río Villa Vil.

Foliation Sample #:	Width fracture infilling* mm	Width microlithons mm
PG-98-13	0.25	4
	0.25	1
	0.25	2
	0.5	2
	0.25	4.50
	0.5	5
	0.25	3
	0.25	7
PG-TRV II	3.5	9
gr-ss rock	1.3	6
	1.25	4
	0.5	4
	0.5	6
	0.3	3
PG-98-46	0.5	3
granite	0.3	5.0-6.0
	0.3	5.0-3.0
	0.3	5.5-10
	0.1	3.5
	0.1	10
	0.1	6.5
PG-98-25	0.1	1.3-1.1
granite	0.1	1.1
	0.1	3
	0.1	3
	0.1	1.4
	0.1	1.4
	0.1	0.6

* width is estimated below 0.5 mm: 0.1 for hairline width, 0.25 and 0.3 are relative

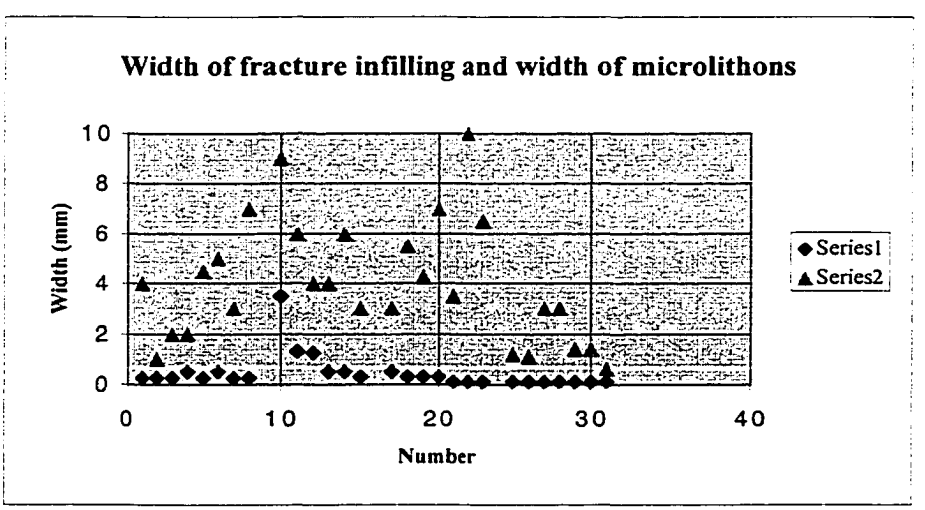

Table 3.3. Foliation spacing thickness.

seen across silt and/or hematite infilling (Figs. 3.15a, b). The infill material is mostly very fine-grained to fine-grained particles of quartz, altered potassium feldspar, and biotite. The material is sometimes extremely fine-grained, and some individual grains are visible but their grain boundaries are not clear. This is evidence that the material has been recrystallized at very low temperatures in the presence of fluids, or siderized (G. Mitra, personal communication, 2001). The grains in the fill material are subangular to subrounded, randomly oriented and poorly sorted. More rounded grains and allocthonous particles are evidence for cataclasis and fluid-assisted flow of material from other sources. Offset of other fractures and grains attest to movement of material along the boundaries of the infilled fractures and not just within the infill material. Not surprisingly, the sample with the greatest amount of infilled material, rounded grains and flow textures seen in thin section is PG-TRV11 (Fig. 3.15c), which is from the Río Villa Vil area where the basement-unconformity is folded.

The photomicrographs of the fracture foliation planes show a possible progression of deformation from a single, hematite-filled fracture cutting across a quartz grain (Fig. 3.15a), to hematite-filled fractures incorporating quartz clasts and developing around an altered feldspar grain (Fig. 3.15b) to a hematite-filled vein with many more particles of quartz and other minerals from the surrounding rock (Fig. 3.15c).

Figure 3.15. Series of photomicrograph of fracture foliation planes in thin section that show a possible progression of deformation from a single, hematite-filled fracture cutting across a quartz grain (a) to hematite-filled fractures incorporating quartz clasts and developing around an altered feldspar grain (b) to a hematite-filled vein with many more particles of quartz and other minerals from the surrounding rock. The photographs cover an area approximately 2.5 mm across; (a) and (c) are in polarized light, (b) is in plain light.

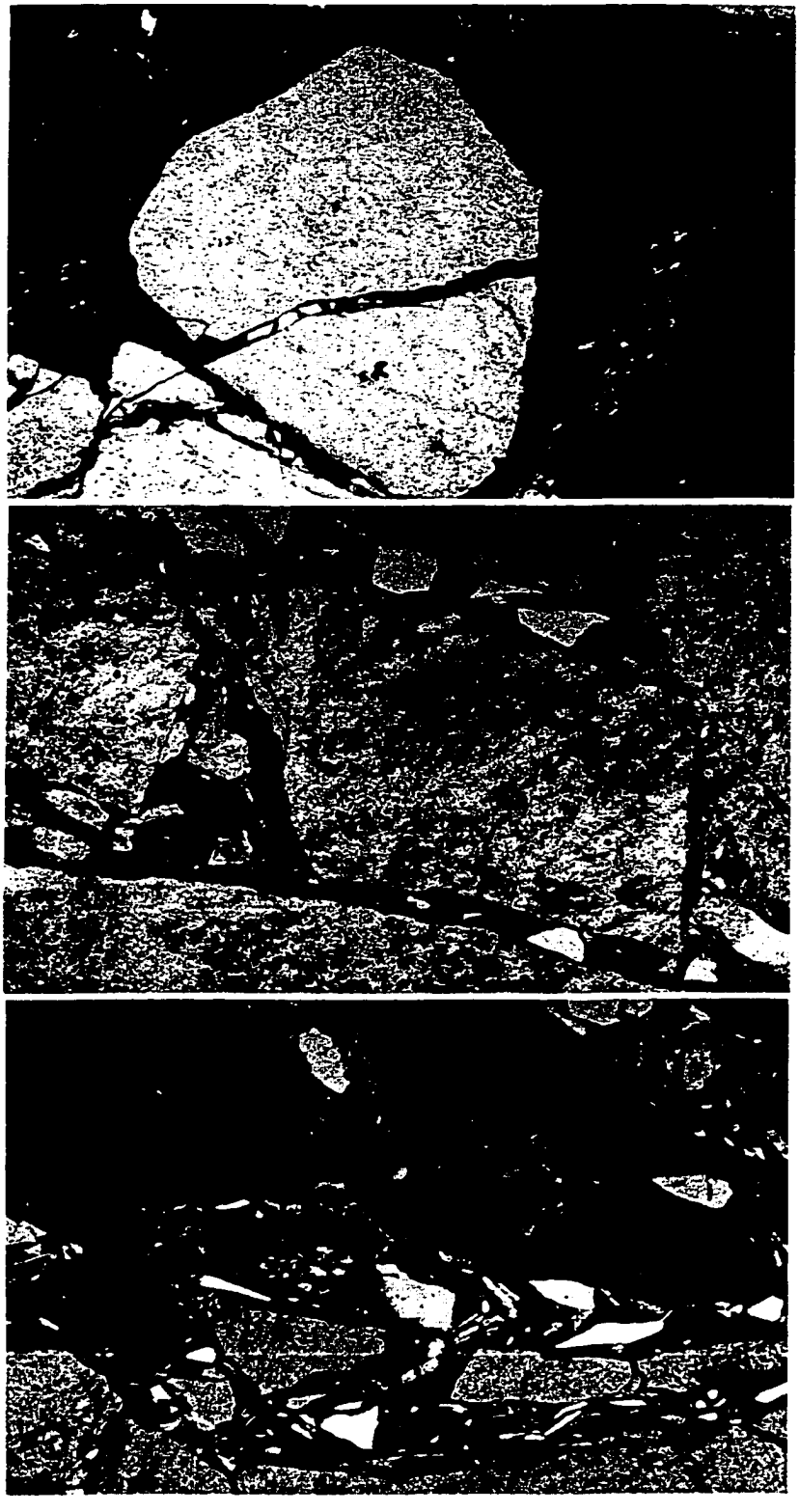

Figure 3.15

3.3.2. "Folding" of Basement by Faulting: Termas Nacimientos

In the vicinity of the Nacimientos area, coincident with a series of subparallel shear zones in the basement, there are cover rocks that have been deformed into a range-scale fold (Fig. 3.2a, 3.16). In order to evaluate the shape of the basement unconformity and the role of basement faulting in the folding of cover sedimentary rocks, we took measurements along a 350-m transect over bare exposures of the basement unconformity. The transect was oriented N60°W, roughly perpendicular to the strike of the range and to the strike of many of the reverse faults in this area (Fig. 3.2a, 3.16). Along the transect there are 14 measurable fault surfaces that accommodated a change in the dip of the originally-planar basement unconformity. The unconformity shallows from ~30°E in the east to ~20°E in the west, thus imparting an overall folded shape on the basement. This can be seen in both the profile of the transect (Fig. 3.9) and in a plot of distance from SE to NW versus dip of the basement unconformity surface (Fig. 3.17a). The plot and the profile show that the basement unconformity surface is not continuously folded, but that it achieves a folded shape via offsets on spaced faults bounding domains of homoclinal dip. Faults dip between 50° and 75° to the west, with the majority of faults dipping between 50° and 60°. However, there is no clear relationship of fault dip to distance traveled from E to W across strike of the range (Fig. 3.17b). The acute angles between the reverse faults and the bedding, which indicate how much bed lengths are being shortened or extended by the faults, are relatively large for all the faults and thus appear to be shortening bed lengths only slightly (Fig. 3.17c). The faults range in throw from 0.5 m to 23 m and accommodate about 43 m of shortening over the 350-m distance in the basement (12%).

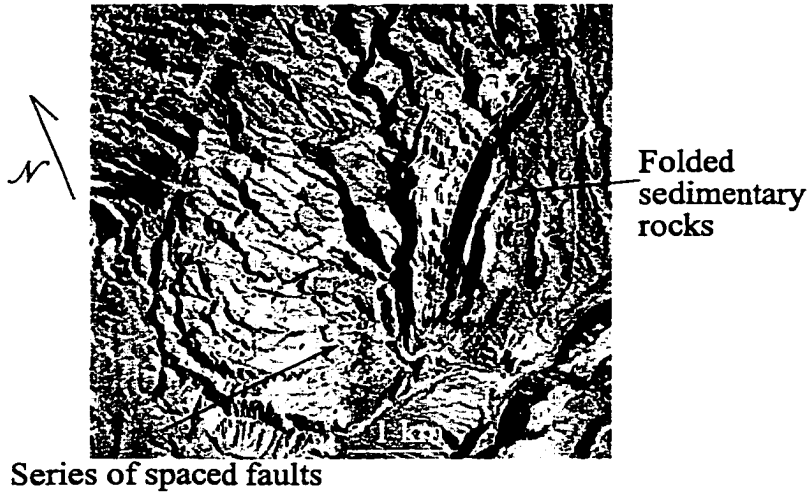

Figure 3.16. Aerial photo of the Termas Nacimientos area. Arrows point to the area of spaced faults in cross section B-B' (Fig. 3.2b) and Figure 3.9, and to the folded Tertiary strata.

a)

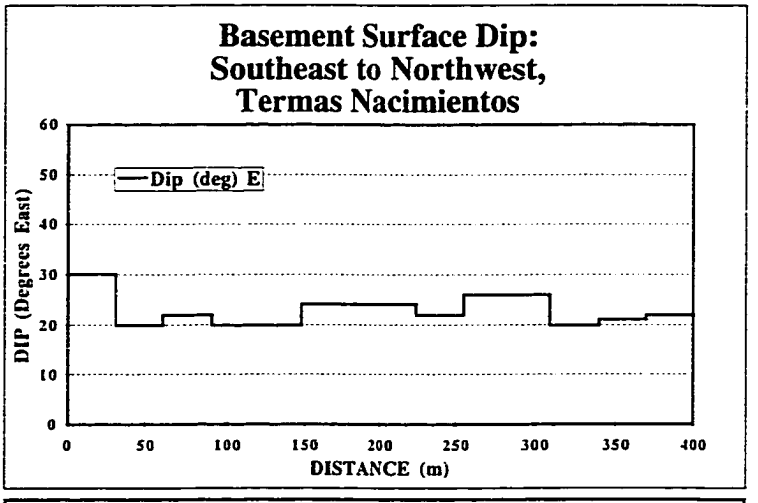

b)

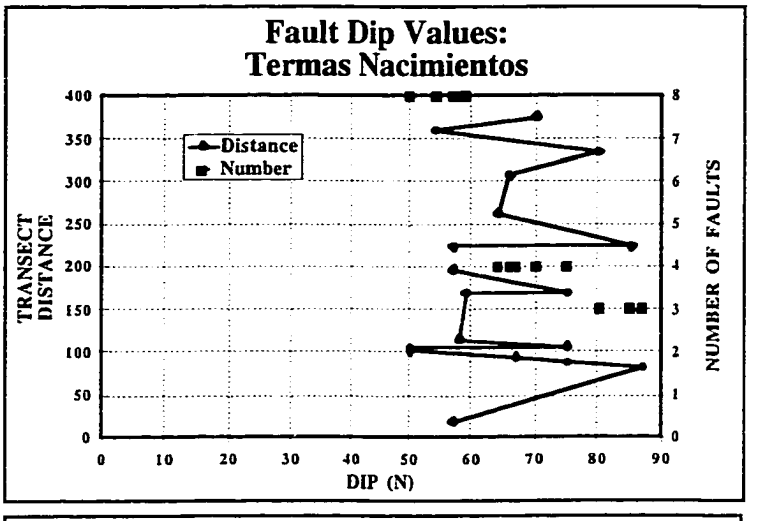

c)

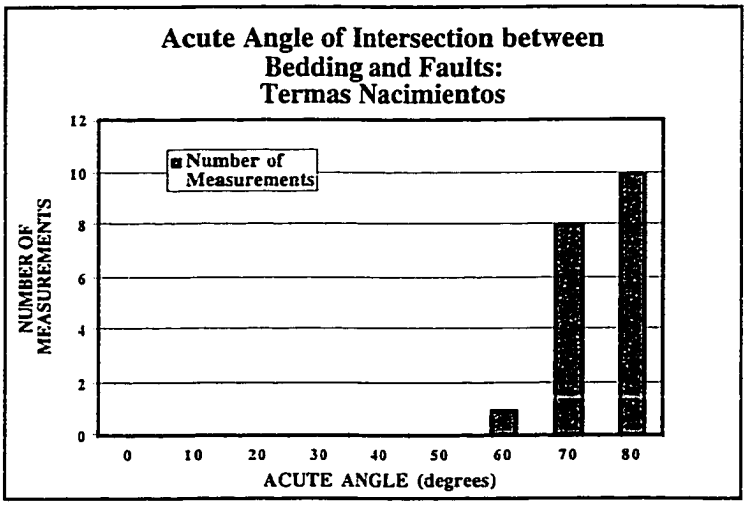

Figure 3.17. (a) Graph of dip of unconformity v. horizontal distance. (b) Graph of fault dip over horizontal distance. (c) Graph of acute angles.

Most striking are π-diagrams on equal-area stereonet plots for poles to bedding of the cover rocks and poles to strike and dip of the basement surface that show similar fold axes trends (Fig. 3.18). These fold axis trends are within the range of strike trends for the subparallel reverse faults that displace the basement unconformity, confirming the observation that these faults are participating in the folding of the cover rocks. The basement unconformity is clearly and discontinuously broken by faults with high cut-off angles, yet when viewed at greater distance, the basement unconformity may appear smoothly folded. Thus basement faults are not only allowing the cover to fold, but are permitting the basement to "fold" as well.

3.3.3. **Folded Basement Unconformity:** Río Villa Vil

The basement unconformity exposed on the west side of the Sierra de Hualfín is sharply folded (Fig. 3.3b). From east to west, the basement unconformity increases in dip from ~20°W to 65°W within a 500 m to 800 m horizontal distance (Fig. 3.2a). The (continuous) fold geometry can be clearly seen in cross section A-A' (Fig. 3.2b). A fold axis oriented N50°E to N65°E was determined from mapping.

3.3.3.a. Fracture foliation

At the location where the folded basement unconformity can be examined closely (Río Villa Vil area), the presence of a fracture foliation similar to the foliation described in other areas is notable (Fig. 3.19). The fracture planes can be seen as dark lines which are planes that project into and away from the plane of observation (Fig. 3.19a). Some of these fracture foliation planes were stripped of overlying layers, revealing slickenlined surfaces on red polish (Fig. 3.19b). Slickenlines on these planes were generally gently to shallowly

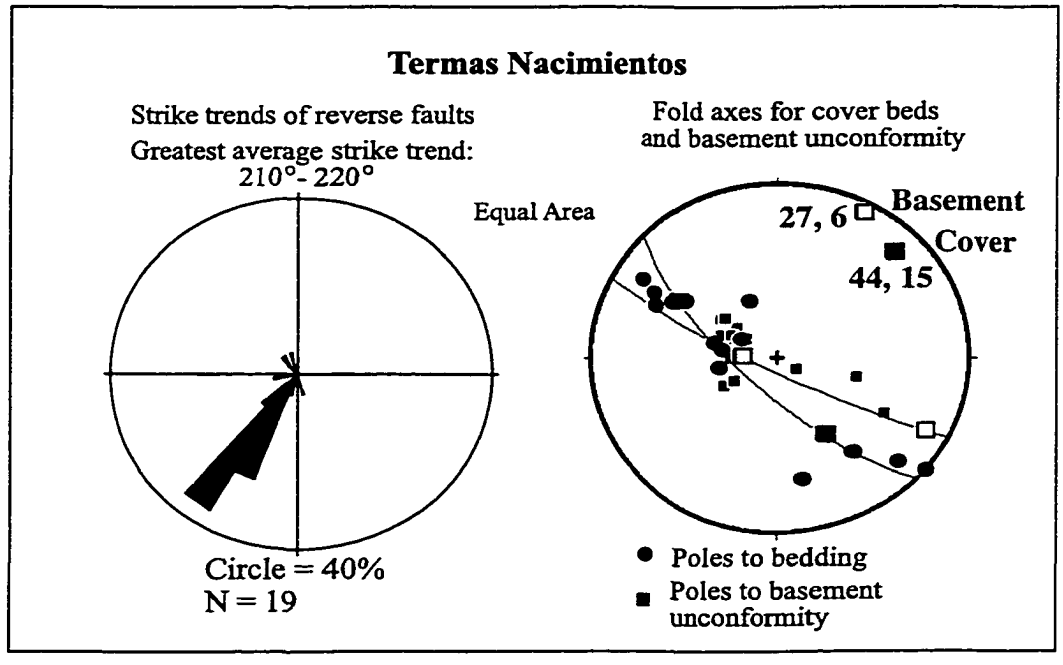

Figure 3.18. Rose diagram of the strike trends of reverse faults and a π-diagram of bedding of sedimentary rocks and dip of the basement unconformity in the Termas Nacimientos area. The plots show that the trends of the reverse faults coincide with the π-axis of the folded strata.

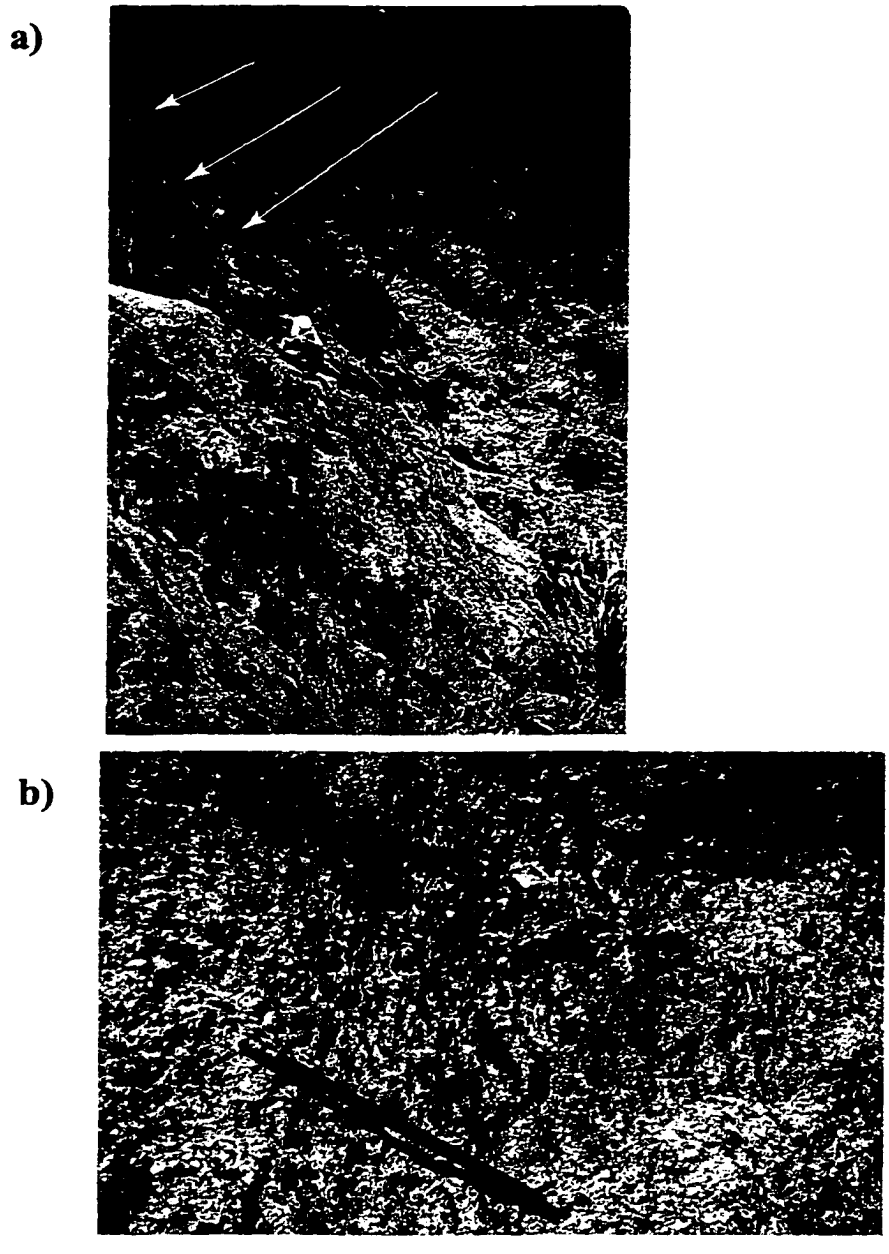

Figure 3.19. Fracture foliation at the folded unconformity in the Río Villa Vil area. (a) Dark lines on surface are fracture foliation planes. (b) Slickenlined surface of a fracture foliation plane suggesting slip has been accommodated along these planes.

raking (Fig. 3.20a), and one plane showed right-lateral sense of motion. The orientation of the fracture foliation planes (average N22°E 32°W) and the orientation of the basement unconformity (N50°E 57°W) in this area do not coincide as closely as the orientations of these features in the other two areas described previously (angle between average orientation planes is 31°) (Fig. 3.14c). The basement unconformity in this area appears to have a much greater component of hematite-stained silt material compared to other sites. Hand sample PG-TRVII collected at this location shows a greater thickness of infill material from 0.3 mm to 4 mm, in comparison to fracture filling in other samples from Termas Nacimientos and La Quebrada (Table 3.3) which show a maximum thickness of 0.5 mm. Because the exposure at Río Villa Vil is parallel to the plane of foliation, the depth of the fracture foliation in the granite cannot be observed here.

3.3.3.b. Faults and joints

The increase in dip of the unconformity from east to west appears to be continuous. Up close, though, the surface of the basement is riddled with fractures (Fig. 3.19a). Some fractures are faults with minor measurable offset (~.5 m - 2 m offset). Prominent fractures appear in a cross pattern on the surface of the basement unconformity. A stereographic plot of all the fractures measured on this surface shows that there are almost all orientations and dips of faults (NS to EW strikes and 15° to 89 °dips), though there is a cluster of about eleven fractures that dip steeply and trend WNW (Fig. 3.8b). Among these fractures, six faults with measurable offset (Fig. 3.20b) displace the basement unconformity surface in reverse and normal right-lateral sense. These faults range in length from ~ 40 cm to 10 m and larger (out of the view of outcrop) (Table 3.4). Five faults have reverse sense of motion, with offsets measuring from 0.05 m to at least 3 m. A normal right-lateral fault

measured has 0.17 m right lateral offset. Four of the six faults, when rotated back to horizontal 65° about an axis oriented 043°, remain reverse faults (Fig. 3.20c); one reverse fault (#8) becomes a normal fault (Fig. 3.20c, Table 3.4), and the right-lateral normal fault remains a normal fault. A comparison of the angle between the basement unconformity surface and the present day fault surfaces confirms that four out of six faults are shortening the basement unconformity (at variable degrees), one fault is extending the unconformity, and another fault is at 90° to the unconformity, thus neither shortening or extending the surface (Table 3.4). A stereonet of these faults in combination with this analysis shows that there is approximately NW-SE shortening and N-S extension of the surface. This is similar to the regional strain field that uplifted the Sierra de Hualfín.

3.3.4. Small Scale Fault-to-Fold Examples

In the areas of Termas Nacimientos, La Quebrada and Nacimientos de Arriba, the basement unconformity is dipping homoclinally and appears to be displaced by reactivated joints that have between 0.04 m and 20 m of vertical offset. In all of these examples, the fault tip is at the basement-cover interface because many (if not all) of the faults are reactivated joint fractures in the basement (Fig. 3.10 - Termas Nacimientos). The transfer of displacement from the basement fault to the sedimentary cover can be observed where there are sedimentary rocks overlying these basement faults. Faulting in the basement causes displacement of the sedimentary rocks immediately overlying the basement by various fractures that often emanate from the fault tip (Fig. 3.21a, b). Fracturing in the sedimentary unit displaces the upper bedding "boundary" into a fold shape and promotes folding of the units farther upsection, depending on the amount of initial displacement.

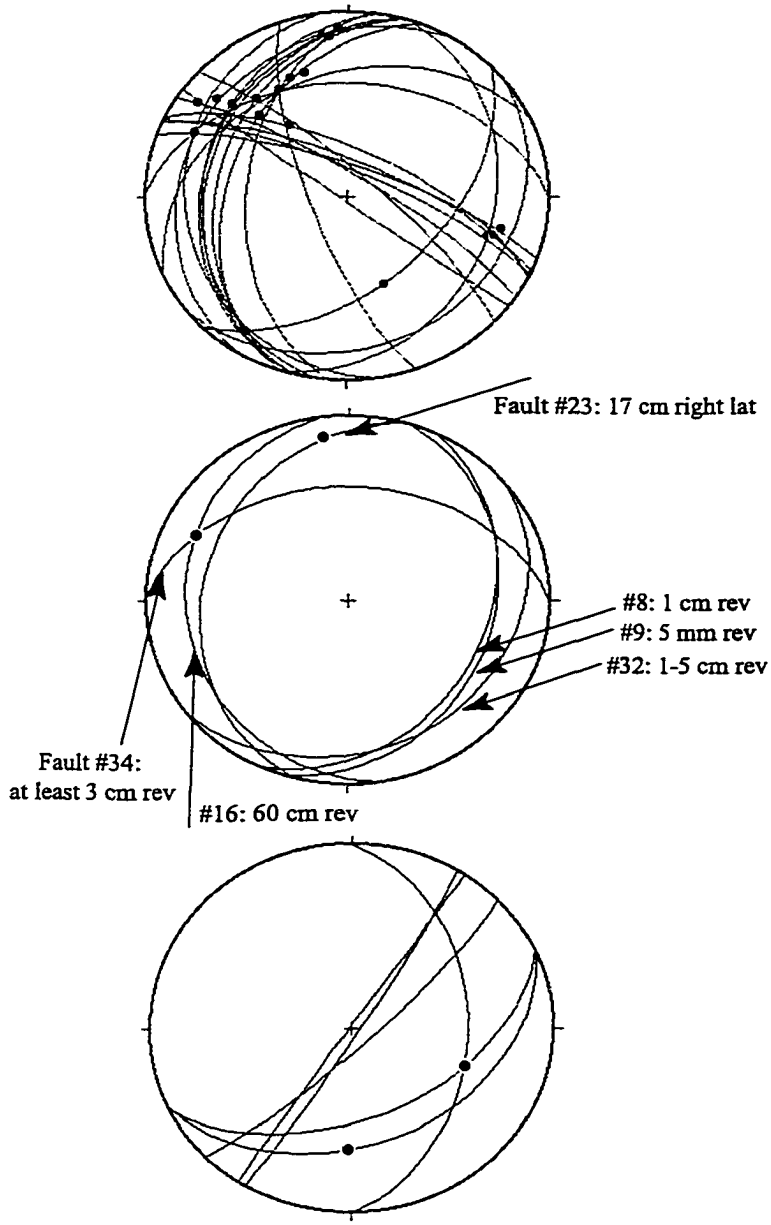

Rio Villa Vil Faults
(fracture measurements
with slickenlines and/or offset)
N = 21

Río Villa Vil Faults with offset

Río Villa Vil Faults with offset:
rotated 61 deg. about N43E axis

Figure 3.20. Analysis of faults in the Río Villa Vil area (a) stereonet with fault/fracture planes and slickenlines (black circles) (b) faults with offset (c) rotation of (b) 65°about a 043°axis.

Set #1												
		Strike			Dip		Rake		Slicks	Comments	Slicks	
"The Wall" AVG orientation: N60E 62W											trend	plunge
sed	8	N	25	E	31	E				protrudes 1cm from surface		
sed	9	N	18	E	28	E				Fault: 5mm reverse displacement, 39 cm long		
basement	16	N	9	W	21	W				Fault: ~60 cm offset base/sed contact, 10 m long		
base/sed	23	N	15	E	29	W	26	N	slicks	Fault: 17 cm right lat. offset, 2-3 mm red cat.mat., 180cm long	N8W	12
base/sed	32	N	52	E	21	E				Fault: rev. offset 1-5 cm, has same orientation as big fault	N65W	18
basement	34	N	89	W	38	E	28	N	grooves	Fault: at least 3m rev. offset, ph. 16 &17		
Bedding		N	43	E	61	W				best bedding		
measurements rotated about axis 43, 61 degrees (best bedding)												
			Strike		**Dip**		**Rake**		**Slicks**			
sed	8		214		89							
sed	9		32		87							
basement	16		65		50							
base/sed	23		65		37		187	48	slicks			
base/sed	32		46		82							
basement	34		360		42		2	77	grooves			
Angle between faults and N43E 61W bedding										Angle between faults and N55E 62W unconformity		
			223		61				235			
			Strike		**Dip**		**Angle**		**Angle**			
sed	8		25		31		91		90	neutral		
sed	9		18		28		87		85	shortening/neutral		
basement	16		171		21		50		55	shortening		
base/sed	23		195		29		37		42	shortening		
base/sed	32		52		21		82		83	extending/neutral		
basement	34		271		38		42		36	shortening		

Table 3.4. Orientations of faults and slickenlines at Río Villa Vil, along with calculations of the angle between faults and bedding or the basement unconformity at the same location.

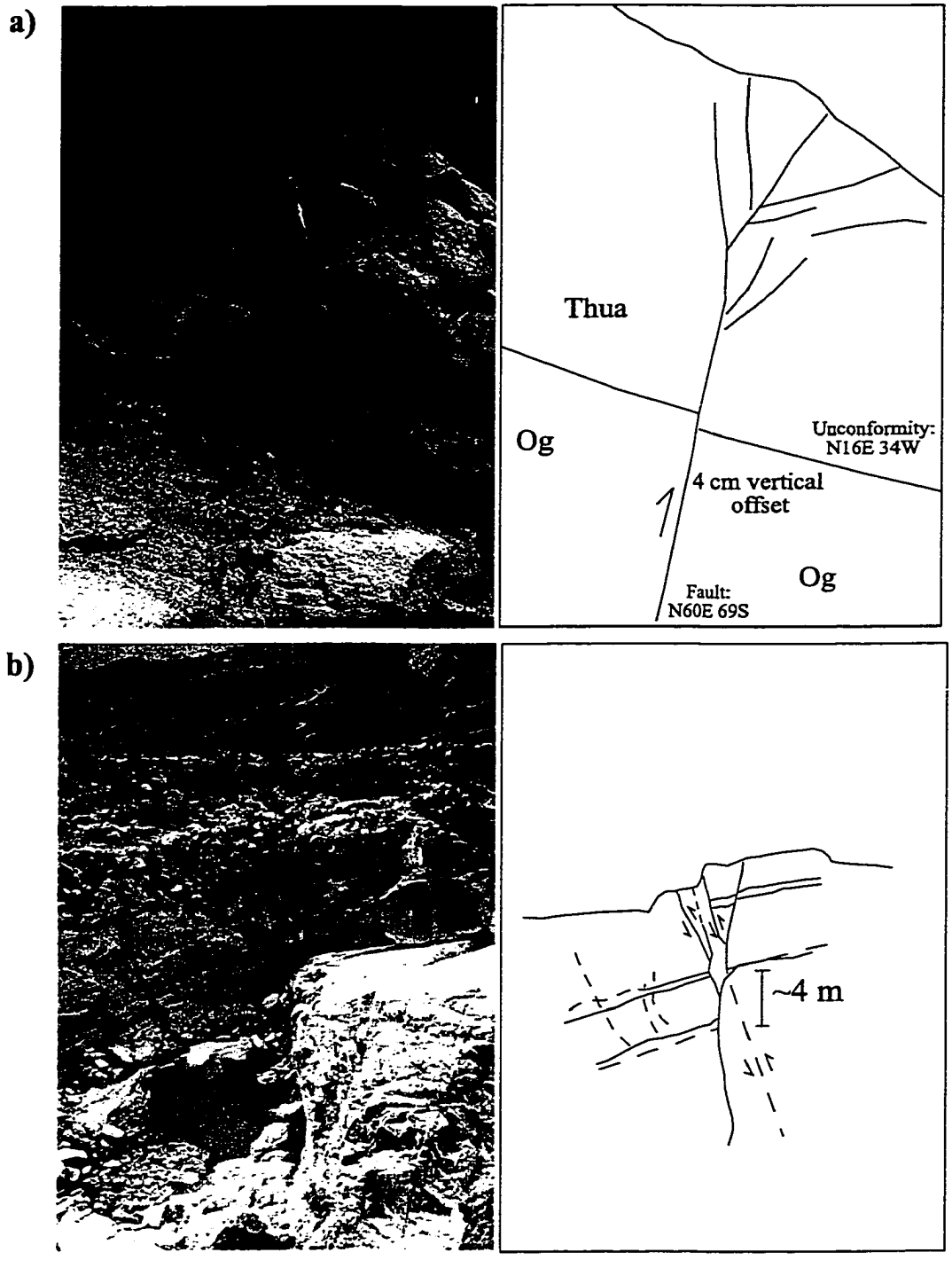

Figure 3.21. Photos and corresponding sketches of faults in basement propagating into overlying sedimentary rocks. The fault in basement generates fracturing and an overall fold shape in the sedimentary rocks. (a) La Quebrada area (b) Nacimientos de Arriba area.

These outcrops show a mechanism for folding of rocks due to fault-propagation that is not entirely by flexural slip, especially in the units closest to the tip of the propagating fault. One outcrop in La Quebrada is a fault with 12 cm of vertical offset that shows a pattern of fractures fanning from the main fault plane in basement (Fig. 3.22a). Displacement on the basement fault causes a triangular zone of distortion in the (thin) sedimentary rocks above the fault (Fig. 3.22b). If these small scale fault-to-fold examples can be representative or indicative of processes active at a larger scale, then their existence supports the idea of fault-propagation folding as a mechanism active in the Sierra de Hualfín, and possibly in other basement-cored uplifts. The geometry of the exposures in the rocks is also very similar to descriptions of the effects of trishear and would argue for the relevance of trishear in this system.

3.3.5. Mechanical stratigraphy

The pattern of deformation in the Sierra de Hualfín suggests that a macro-mechanical stratigraphy exists in the rocks (Fig. 3.23), similar to the structural lithic units described by McConnell and Wilson (1993) in the Rocky Mountain foreland province of the United States. McConnell and Wilson (1993) used the concept of structural lithic units to describe the different deformation mechanisms by which sedimentary rocks accommodate folding above basement faults in the Rocky Mountain foreland. In the Sierra de Hualfín, we propose a mechanical stratigraphy composed of stiff granite basement, a semi-stiff intermediate zone of basement and cover (a transition zone), and a soft, clastic-dominated cover sedimentary sequence (Fig. 3.23). The basement undergoes translation and rotation with some faulting and jointing. The transition zone deforms by cataclasis, folding, faulting, and jointing. The cover deforms by flexural slip folding, jointing, fracturing, and some faulting, which includes some of the same mechanisms described for

the Rocky Mountain foreland (Spang and Evans, 1988). McConnell and Wilson (1993) also noted that sedimentary rocks that are low-ductility units deform by faulting, whereas high-ductility units deform by other mechanisms, such as cataclastic flow. This analysis can be applied to basement as well as cover rocks. Where rocks are "ductile" they will deform by more distributed deformation because of the presence of pervasive fractures. At low temperatures and pressures, ductile behavior can be visualized as flow via movements along grains, where the grains are separate sand grains in a sandstone, or are blocks of granite separated by joints and fractures. For example, a highly fractured and faulted layer of basement above a fault might exhibit a pseudo-ductile bulk behavior. Where rocks are very stiff and low in ductility, they will simply break.

The mechanical stratigraphy is clearly a function of the rheology of the materials. The semi-stiff nature of the intermediate transition zone is due to the fracturing of the top portion of the basement and penetration of silt and clay material into the granite through those fractures, which impart a lubricated fracture foliation to the top of the basement. This foliation is only present in coarse-grained granite, even when fine-grained sills rest stratigraphically above coarse-grained granite (Fig. 3.24). The pervasive fractures and joints, and the fracture foliation allow the transition zone to deform almost incrementally along these fractures surfaces, effectively flowing, much like sedimentary rocks flow along grain boundaries, but less continuously or smoothly because the "grains" in this zone are blocks of granite, ranging from 1-10 mm in thickness (microlithon thickness - Table 3.3) to tens of centimeters or more (defined by the spacing of joints). This fundamental property allows the basement unconformity on the west side of Sierra de Hualfín to assume a smoothly folded appearance from a relatively close distance (~ 100 m). However, the folded shape of the Sierra de Hualfín extends deeper than the ~ 2 meters that the foliation has been observed to exist. Thus, movement on faults, joints and fractures deeper in the basement must be accommodating the folded form of the entire uplift.

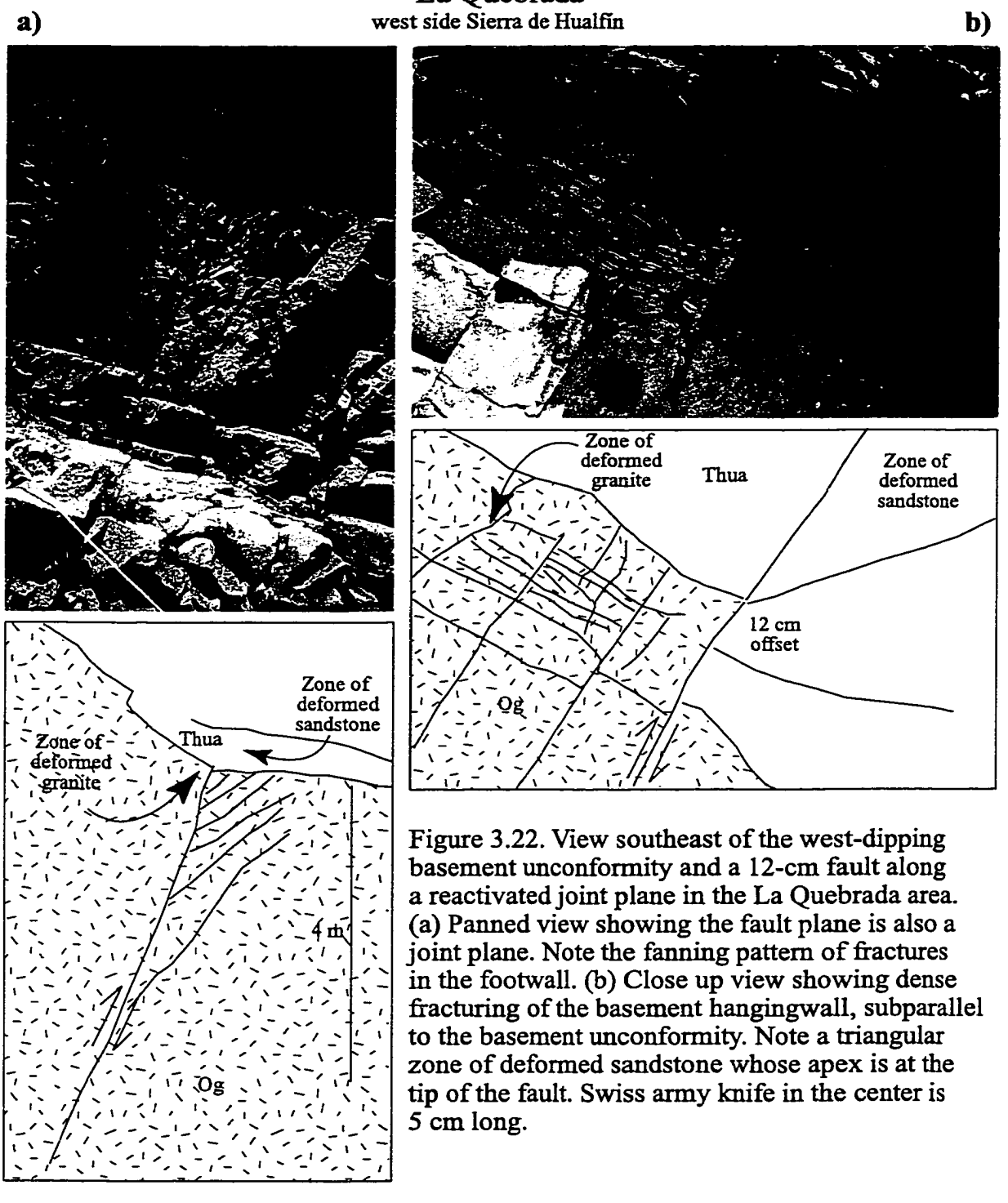

Figure 3.22. View southeast of the west-dipping basement unconformity and a 12-cm fault along a reactivated joint plane in the La Quebrada area. (a) Panned view showing the fault plane is also a joint plane. Note the fanning pattern of fractures in the footwall. (b) Close up view showing dense fracturing of the basement hangingwall, subparallel to the basement unconformity. Note a triangular zone of deformed sandstone whose apex is at the tip of the fault. Swiss army knife in the center is 5 cm long.

Stratigraphy	Mechanical Stratigraphy	Outcrop-scale Deformation Mechanisms
Tertiary sedimentary rocks	Mechanical cover	Flexural-slip folding, jointing, minor fracturing, faulting, layer parallel shortening and extension
	"Transition" zone	Cataclasis, flexural-slip folding, internally faulted, jointed
Ordovician granite	Mechanical basement	Rigid translation and rotation, jointing

Figure 3.23. Diagram showing the macro-mechanical stratigraphy seen in the Sierra de Hualfín, as related to the stratigraphy and the outcrop-scale deformation mechanisms. The width of the transition zone can be variable, but has to extend at least to the depth of the amplitude of the overall fold in basement.

Figure 3.24. Photograph of a fine-grained granite sill over coarse-grained granite. Note that the fine-grained sill is fractured but does not develop the closely-spaced, subparallel fracture foliation that is seen in the coarse-grained granite, despite the sill occurring at the basement unconformity level. The basement unconformity is just above the sill in the photograph.

3.4. DISCUSSION

3.4.1. Folded basement in the Sierra de Hualfín

The data presented from Sierra de Hualfín show how basement has deformed into a fold shape with a ~ 4 km amplitude fold. Deformation mechanisms at shallow levels seen on the west side of the uplift where the basement unconformity is continuously folded are suggestive of deformation mechanisms at work deeper in the basement, where these are presently not observable.

The basic structure of Sierra de Hualfín is a fault-propagation-fold breached by a through-going fault. Fault-propagation folding is cited and accepted as a mechanism for the development of basement-cored uplifts (DeCelles et al., 1991; Erslev and Rodgers, 1993; Allmendinger, 1998). Fault-propagation folding has been mostly used to describe the distortion of sedimentary rocks above a fault in the same units or in basement, while basement was seen to behave mostly rigidly with little internal deformation. However, there are numerous studies that document internal deformation in the hanging wall of basement-cored uplifts, away from the main fault zone. For example, in the hanging wall of the Wind River Mountains there are significant fault and fracture zones throughout the range (Mitra and Frost, 1981; Mitra and others, 1988). In the Washakie range, there is small-scale faulting within the range, and broad zones of faulting at the front (Evans, 1985 and 1986). The presence of closely spaced faults in the hanging wall of the Madison Range, Montana, has been noted by Spang and Evans (1988).

How do the granitic basement rocks assume a bent folded shape? Studies in the Rocky Mountain province show the dominant mechanisms in crystalline basement that accommodate deformation and "folding" are fracture and faulting. In Coad Mountain in southeast Wyoming, Barnes and Houston (1969) suggested that basement folded passively along microfractures that parallel vertical joints formed during the uplifting event (Fig.

3.25a). From deformed experimental rock models by Friedman et al. (1986), Cook (1988) postulated that cataclastic flow near the basement-cover interface and directly above a master fault create the appearance of folding (Fig. 3.25b), a theory that was subsequently applied to Rattlesnake Mountain and to Sage Creek anticline structures in Wyoming (Cook; 1988). In the Teton Mountains, Wyoming, folding of basement appears to have occurred by movement on minor normal and reverse faults in the hanging wall (Erslev and Rodgers, 1993). Slip along closely spaced fractures can also produce an overall folded form in rocks (Spang et al, 1985; Spang and Evans, 1988; García, 1999), and backthrust faulting and cataclastic flow observed in deformed rock model experiments have also been proposed as mechanisms for "folding" (Chester et al., 1988).

Opponents of folded basement cite that isotropic basement, similar to a brick, would not fold but break under compression because of a lack of planar and other anisotropies by which folding could take place (Stearns, 1975). Isotropic basement would be difficult, if not impossible, to fold; however, basement is typically pervaded with pre-existing faults, fractures (including joints, a regular and often regional system of fractures) and fabrics that have an affect on the final basement-cored uplift shape. These pre-existing structures (fractures and fabrics) have been recognized as a way to impart anisotropy to the basement and help effect observed distortions (Blackstone, 1983). Thus, it is these ubiquitous and pervasive discontinuities that allow basement to attain a folded form.

At shallow basement levels in the Sierra de Hualfín, the basement unconformity assume a smoothly folded shape via movements on joints, minor faults and brittle foliation. Faulting along spaced reactivated joints in the Termas Nacimientos area has also imparted an overall fold shape on the basement. Deeper in the basement, the combination of joint fractures that define blocks (as seen in La Quebrada 3D exposure), and faults move granite blocks and distorts the basement into a fold shape. A simple analogy for this would be the behavior of several rows of wooden blocks lying above a faulted block when one part of

the block moves up (or down). A real, small-scale analogy mainly folding sedimentary rocks would be the fault-to-fold exposures in La Quebrada and Nacimientos (Figs. 3.21, 3.22).

3.4.2. Influence of propagation to slip ratio on form of folded basement

The trishear kinematic model is a helpful tool to visualize the propagation of a fault tip into the overlying medium and to visualize how the ratio of propagation to slip affects the fold shape that occurs in the basement rocks. Figure 3.26 shows a chart created in Trishear v. 2.9.4 (Allmendinger, 1999) with varying fault angles and varying P/S that help describe the deformation in the Sierra de Hualfín. A direct inversion or forward model of the Sierra de Hualfín cannot be carried out in the Trishear program, if one assumes that the main fault uplifting the Sierra de Hualfín is listric or has several bends (R. Allmendinger, 1999, personal communication). However, it is still useful to compare simpler trishear models to the cross section of Sierra de Hualfín.

Clearly, a high propagation to slip ratio (> 2) does not fold rocks very much (Fig. 3.25), and this may be the case for basement-cored uplifts such as Rattlesnake Mountain, and the Uncompaghre uplift where the fault tip from which folding occurs appears to be at the basement unconformity. In other uplifts, where folding of basement has been documented (Coad Mt., Sheephead Mt., Elk Mt. - Barnes and Houston, 1969; Blackstone, 1983; Schmidt et al. 1993), a smaller propagation to slip ratio would be more relevant (< 2). It is also likely that P/S changed during the development of an uplift, thus having a larger ratio in the basement (less folding) and a smaller ratio in the cover (more folding). In summary, structures that are folded will have been formed by trishear with a smaller P/S than a structure that is purely faulted.

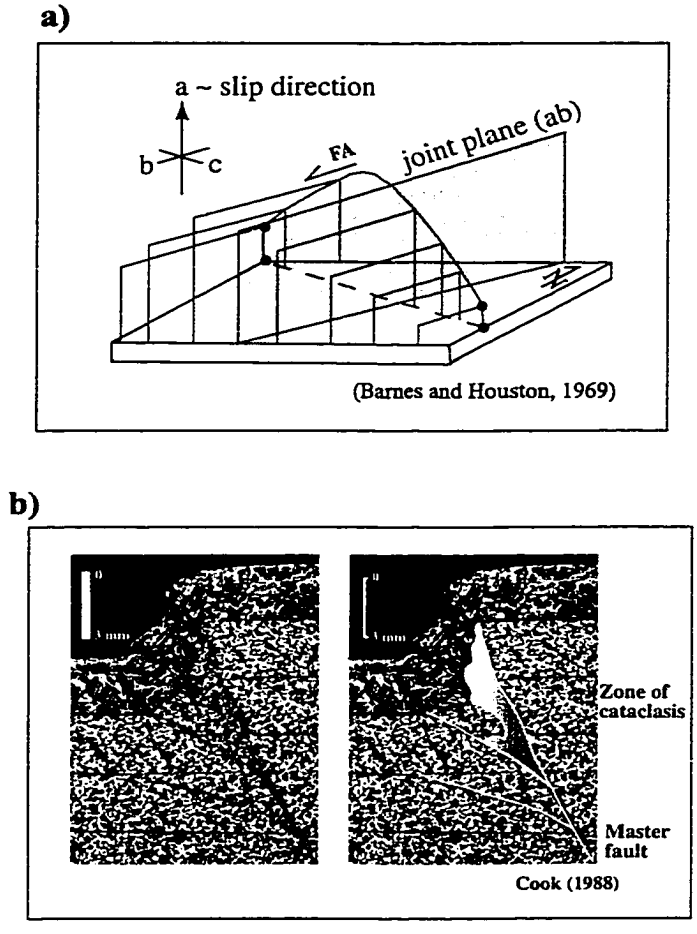

Figure 3.25. Mechanisms of folding basement proposed by other authors:
(a) Barnes and Houston (1969): Basement surface folds passively by variable m ovement along joints and/or microfractures.
(b) Cook (1988): Pseudo-folding of the basement-unconformity surface achieved by cataclastic flow of granite along the basement-cover interface.

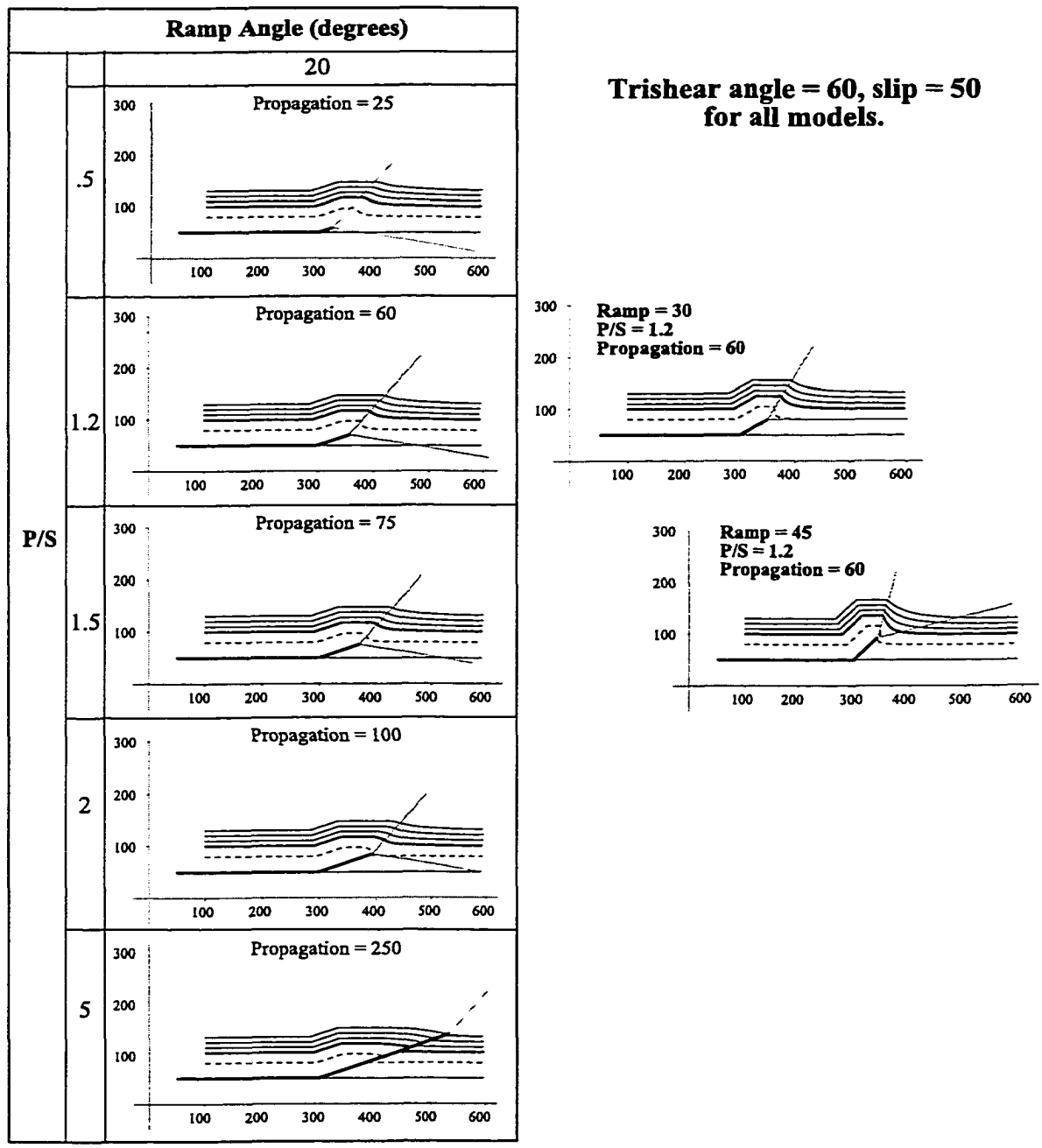

Figure 3.26. Models of folds using Trishear (Allmendinger, 1999). All models have a trishear angle of 60 and a slip of 100 units. The P/S varies along the vertical axis for a ramp angle of 20° (best fit to the orientation of the backlimb of Sierra de Hualfín). Two models on the right show the effects of using higher ramp angles (30° and 45°) for a P/S of 1.2.

3.5. CONCLUSIONS

In the Sierra de Hualfín, the critical exposure of the folded basement unconformity on the west side of the uplift, as well as the faulting at Termas Nacimientos, has allowed us to develop a model of basement deformation that can explain how basement folds (Fig. 3.27). The basement unconformity is variously deformed by reactivated and infilled joints, faults and a fracture foliation. These features imply similar mechanisms at work deeper in the basement in order to produce the 4-km amplitude fold that occurs in the hanging wall of the Sierra de Hualfín uplift.

In order for basement to fold or assume a folded shape via various deformation mechanisms (such as the ones discussed here), conditions have to be such that the tip of the fault propagating through the basement lies within the basement while slip is accumulating, causing folding and distortion of the basement rocks above it. This implies that the propagation to slip ration (P/S) as seen in trishear modeling, must be low enough to induce folding in the basement while the fault tip is still in the basement. The factors that influence the position of the propagating fault tip are unknown at this time but undoubtedly are related to the mechanical properties of the medium through which the fault is propagating.

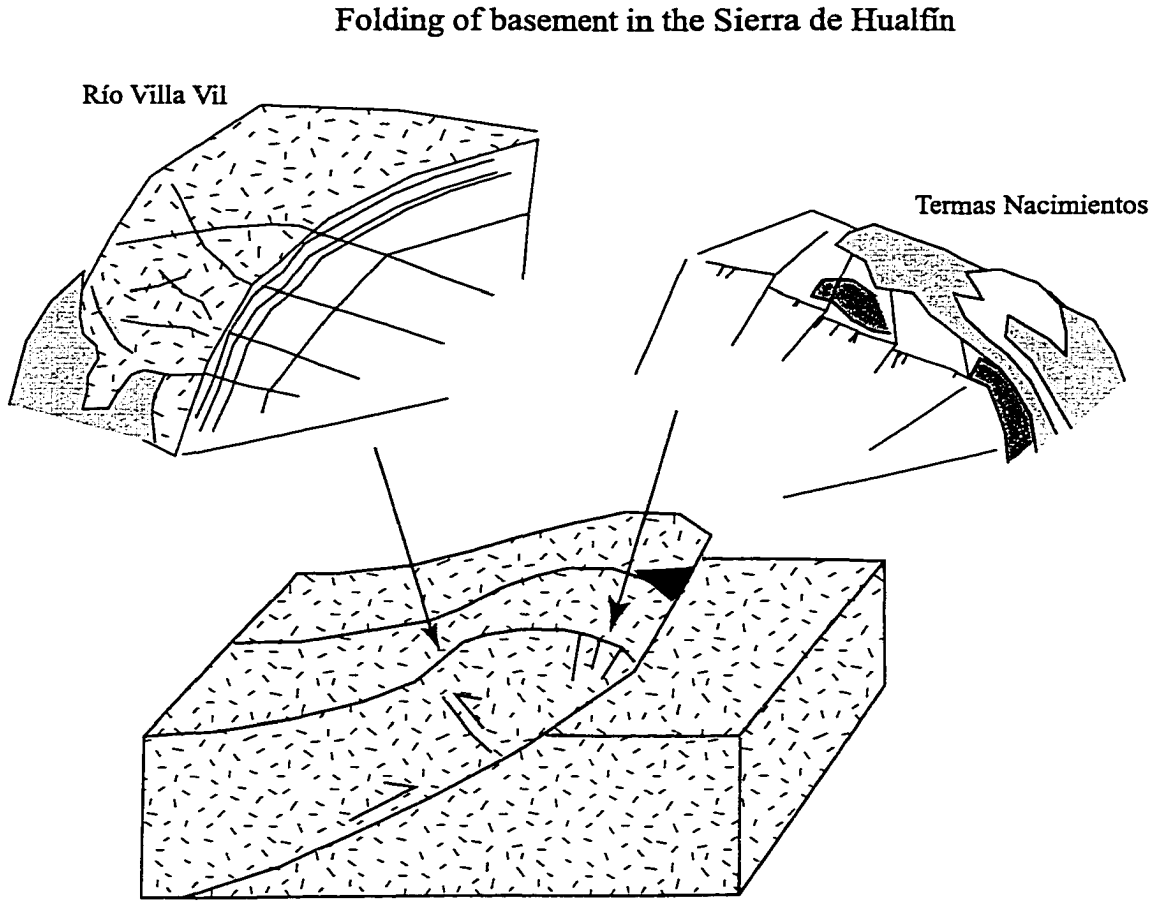

Figure 3.27. Illustration of folding of basement in the Sierra de Hualfín, showing the two type areas, Río Villa Vil and Termas Nacimientos. At Río Villa Vil, the basement unconformity has a smoothly folded form, the result of movement along joints, fractures and fracture foliation planes. At Termas Nacimientos, the basement attains a folded shape via offsets on spaced, reactivated joint surfaces. Shaded areas represent overlying cover strata.

CHAPTER 4

THE NORTHERN SIERRAS PAMPEANAS AND THEIR RELATION TO THE ADJACENT PUNA PLATEAU AND EASTERN CORDILLERA-SANTA BARBARA SYSTEM

ABSTRACT

The northern Sierras Pampeanas are an ideal place to study the relation of basement-cored uplifts and proximal fold-thrust structures. Located at the southeastern edge of the Puna Plateau and the southern end of the Eastern Cordillera and Santa Barbara System, the northern Sierras Pampeanas constitute a transition zone between flat and steep subduction of the Nazca Plate, and between lesser and greater thickness of Paleozoic and Mesozoic sedimentary strata. Relating structures across these along-strike changes and across transitions between provinces remains an important and understudied subject.

Two balanced cross sections (along a 260-km transect at ~ 27° 30'S) were constructed in order to investigate the structural relationships between the northern Sierras Pampeanas and the eastern edge of the Puna Plateau. Individual basement-cored uplifts in the northeastern cross section are products of both east- and west-directed fault systems, separated by intervening basins. Basement-cored uplifts in the southwestern cross section are more closely spaced and are separated by relatively narrow and shallow basins. In the westernmost region, where there is almost twice the thickness of sedimentary strata, deformation includes normal faulting, as well as compressional basement-involved structures. Despite the surficial presence of normal faults, the elevated regional top of basement from ~3 km below sea level in the east to 1.5 km above sea level in the west

indicates that there are younger thrust faults in the subsurface, increasing the thickness of basement and raising the top of basement in the western region.

This study presents a comparison of decollement levels, and structural geometries of the northern Sierras Pampeanas, the Eastern Cordillera-Santa Barbara System, and the Puna Plateau as an initial step towards producing a three-dimensional picture of how these different foreland thrust systems of the Andes are evolving. Thrust structures are more closely spaced in the Eastern Cordillera and Santa Barbara System (EC-SBS) than in the northern Sierras Pampeanas, and have shallower decollement levels (19 km to 12 -11 km in the EC-SBS, versus 16 km and 27 km below sea level, calculated for the northern Sierras Pampeanas in this study). Previous studies of Puna and northern Sierras Pampeanas kinematics show a continuum and an eastward progression of timing of deformation and consistent kinematics between provinces. These kinematics suggest there is a link between the thrust structures of the Puna and those of the northern Sierras Pampeanas. In the regional cross sections presented, thrust faults at the eastern edge of the Puna are interpreted to join and interact with faults and structures of the northern Sierras Pampeanas, soling into similar detachment levels as basement-cored uplift faults and forming a consistent system.

4.1. INTRODUCTION

Along-strike variations of the structure of the Andean Cordillera have been noted and discussed mostly in relation to the development of the Central Andes (e.g. Isacks, 1988; Whitman et al., 1996; Kley and Monaldi, 1998, 1999a). These variations and the transitions between them are some of the most intriguing parts of the Cordillera and can tell us a great deal about orogenic processes, specifically, the differential responses of the crust

(and lithosphere) to compressive forces. The northern Sierras Pampeanas from 26°30' S to 28° S (Fig. 4.1) are a key transition area in the Andean foreland. Thicker sedimentary strata and a 30° dipping segment of the Nazca Plate occur to the north, and much thinner sedimentary strata and a more shallowly subducting segment of the Nazca Plate occur to the south. The Eastern Cordillera and the Santa Barbara System lie to the north of the Sierras Pampeanas, the Puna Plateau is to the west and northwest, and the Precordillera fold and thrust belt, although not contiguous with the northern Sierras Pampeanas, lies to the southwest (Fig. 4.1). Whereas each of the provinces of the central Andes are well understood, relating structures across the transition between provinces remains an important and understudied subject (Allmendinger and Gubbels, 1996; Grier et al., 1991; Kley and Monaldi, 1999b). This study focuses on the structure of the northern Sierras Pampeanas and their relationship to the adjacent Eastern Cordillera-Santa Barbara System and the Puna Plateau, specifically looking at the possible depth to detachment of major thrusts.

Two balanced cross sections were constructed in order to examine the relation of the northern Sierras Pampeanas to the adjacent provinces. The combined section lines extend 260 km from the foreland to the eastern edge of the Puna Plateau at 27°30'S and 27°42'S (Figs. 4.1, 4.2). In the eastern region of the cross sections, there are individual basement-cored uplifts, products of both east- and west-directed fault systems, separated by intervening basins. In the southwestern cross section, basement-cored uplifts are more closely spaced and are separated by relatively narrow and shallow basins. In the westernmost area of the southern cross section there is almost twice the thickness of sedimentary strata due to the addition of Ordovician, Permian and Carboniferous deposits.

Figure 4.1. Location map of the northern Sierras Pampeanas region showing the Sierras Pampeanas, the Precordillera fold-thrust belt, the Puna Plateau, the Santa Barbara system and the Eastern Cordillera. Black outline box on shaded digital relief image of the western coast of South America shows location of larger map. Location of cross sections in Figures 4.2a and 4.2b are shown as A-A', B-B'. Outline box on map bounds the study area.

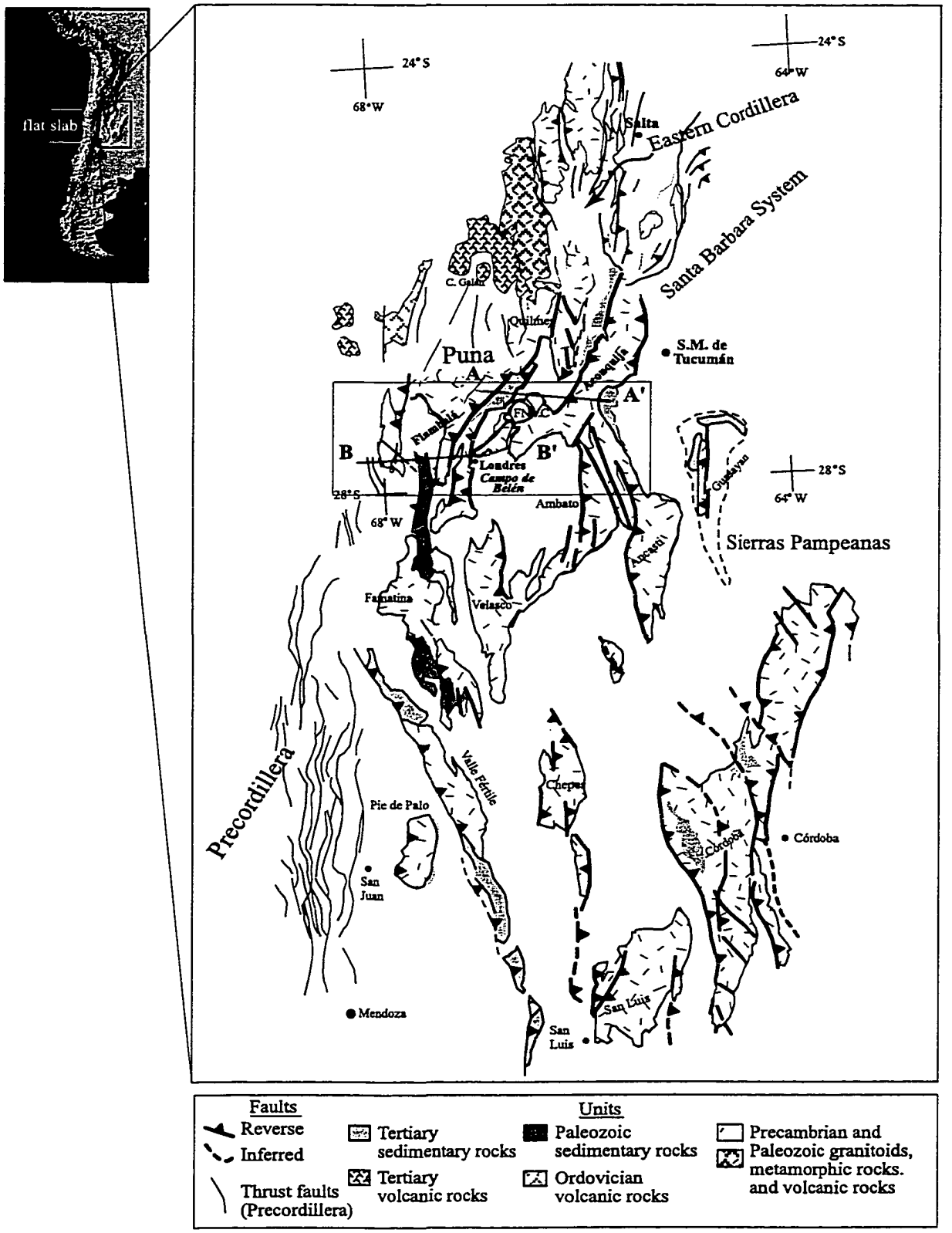
flat slab
24°S
68°W
24°S
64°W
Salta
Eastern Cordillera
Santa Barbara System
C. Galán
Quilmes
Puna
A
A'
S.M. de Tucumán
Aconquija
Fiambalá
Fiambalá
B
B'
Londres
Campo de Belén
28°S
68°W
Ambato
28°S
64°W
Guayaya
Sierras Pampeanas
Aconquija
Famatina
Velasco
Precordillera
Valle Fértil
Pie de Palo
Chepes
Córdoba
Córdoba
San Juan
Mendoza
San Luis
San Luis
Faults
Reverse
Inferred
Thrust faults (Precordillera)
Units
Tertiary sedimentary rocks
Tertiary volcanic rocks
Paleozoic sedimentary rocks
Ordovician volcanic rocks
Precambrian and Paleozoic granitoids, metamorphic rocks. and volcanic rocks

Figure 4.1

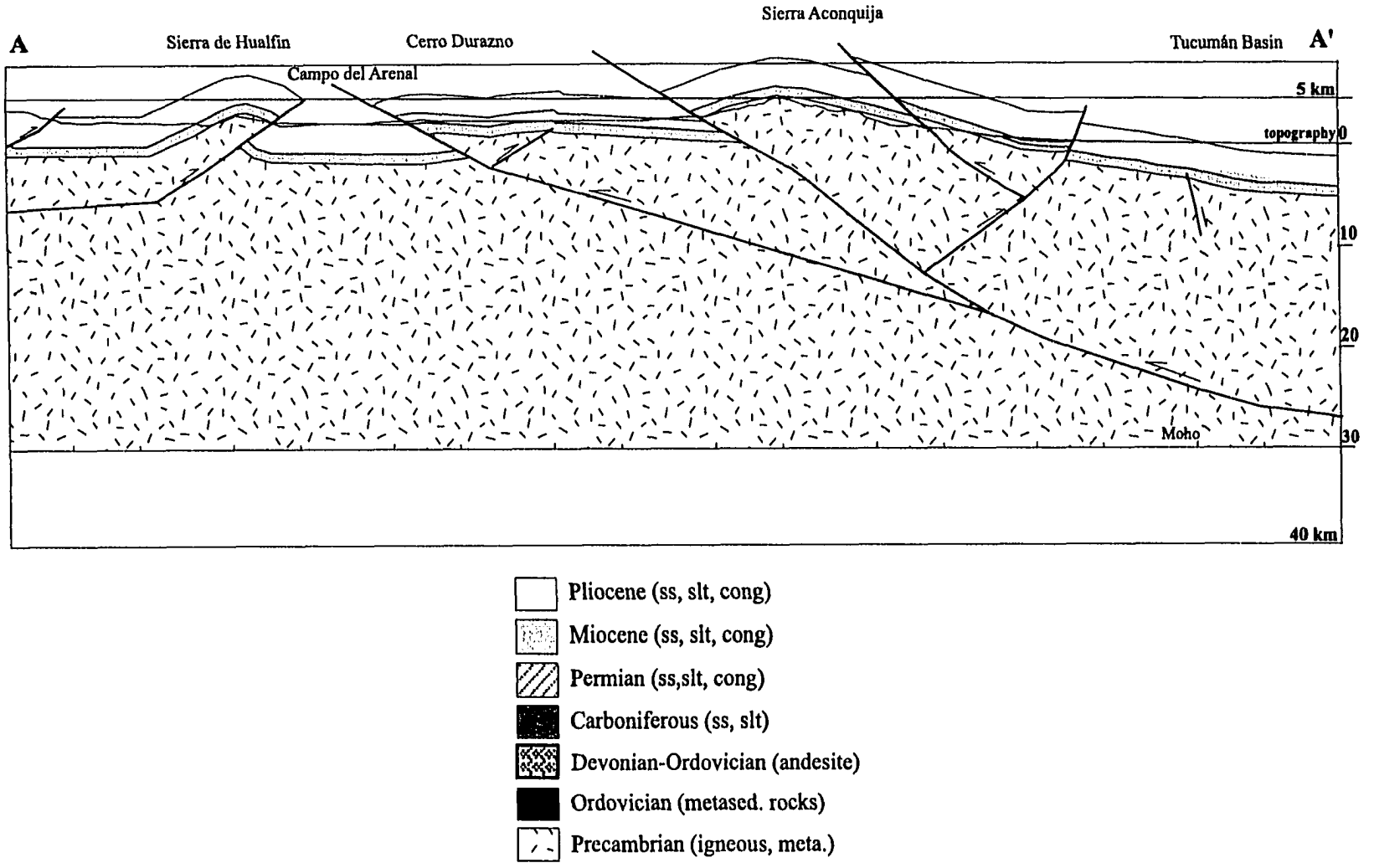

Figure 4.2. (a) Northeastern cross section A-A'

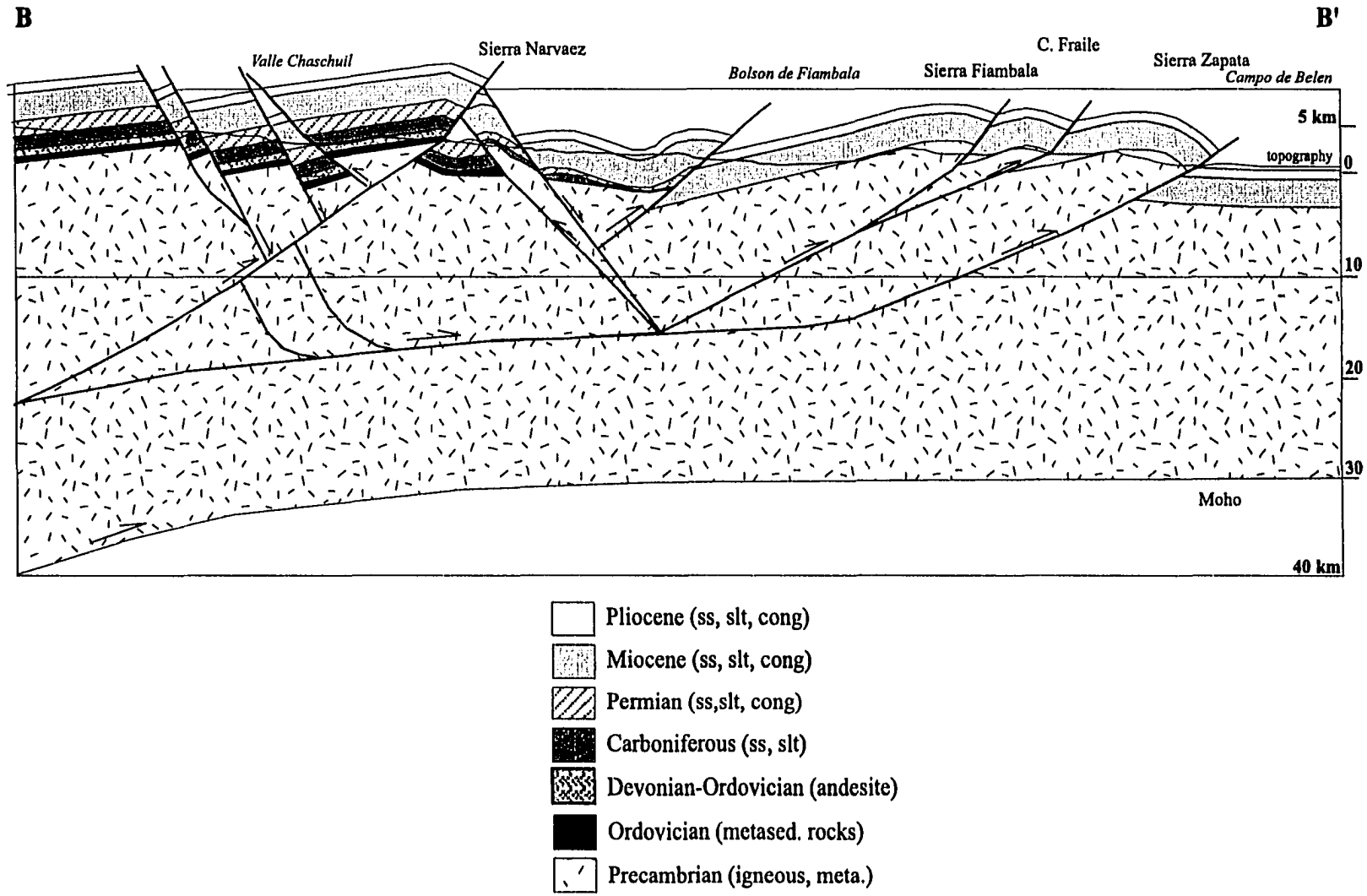

Figure 4.2. (b) Southwestern cross section B-B.'(Note: Only basement-cored uplifts are balanced)

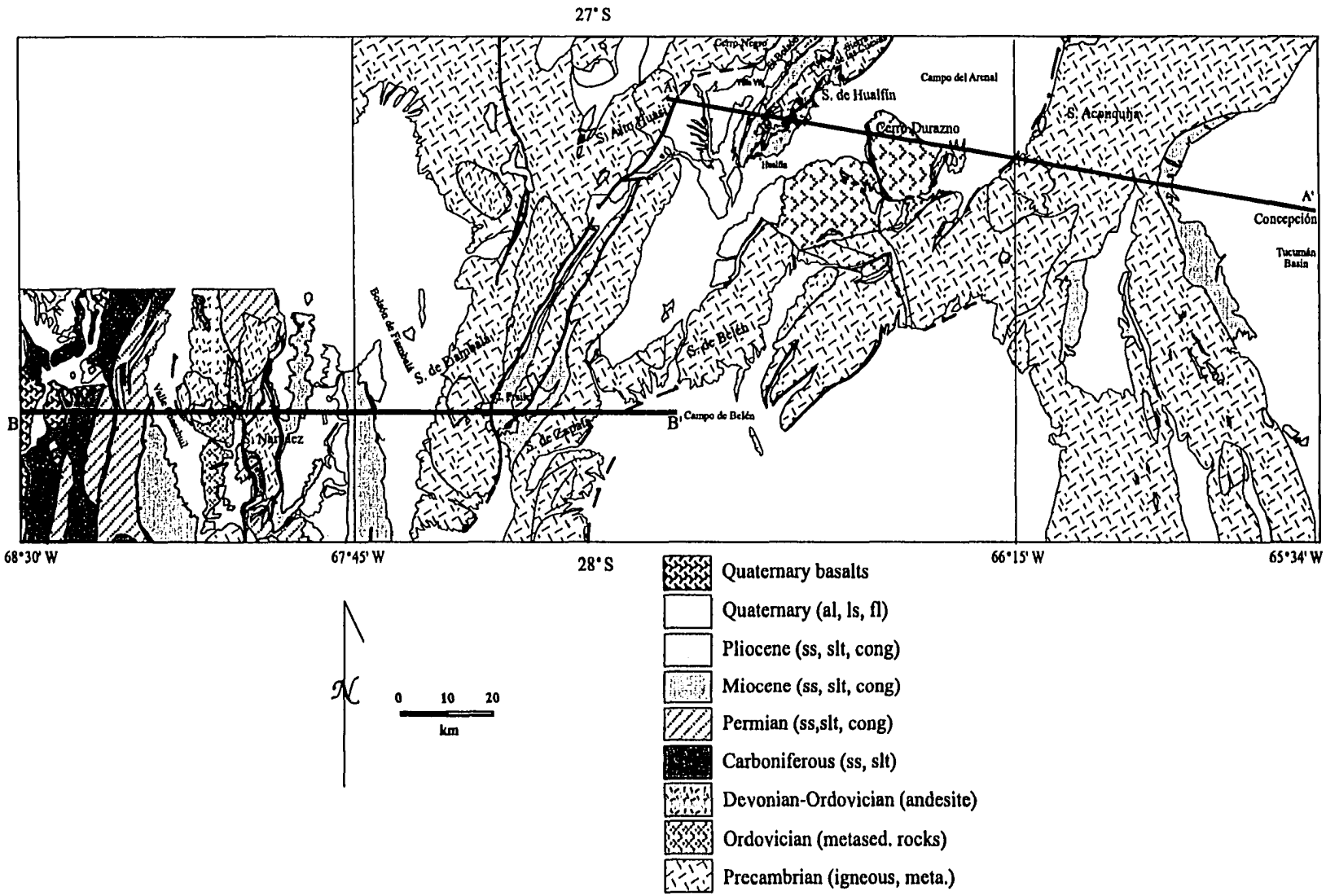

Figure 4.2. (c) Geologic map of the study area in the northern Sierras Pampeanas showing cross section locations.

Deformation in the west includes normal faulting, as well as compressional basement-involved structures. The westernmost normal faults are interpreted as older faults, cross-cut by younger thrust faults that elevated regional top of basement from 3 km below sea level in the east to 1.5 km above sea level in the west.

The interconnectedness of structures between provinces is one way to evaluate the relationship between provinces. Thrusts from one system may carry over into the other via similar detachment levels, or by way of lateral ramps which connect to a deeper common level of detachment. Alternatively, a vertical "suture" zone between each of these provinces could inhibit deformation (faults and folds) from one system to continue into the other. These relationships can be determined through kinematic and geometric analysis of surface and subsurface structures (decollement levels). In the Eastern Cordillera and Santa Barbara System (EC-SBS), thrust structures are more closely spaced and have shallower decollement levels than in the northern Sierras Pampeanas. Previous studies of Puna and northern Sierras Pampeanas kinematics (Marrett et al., 1994; Allmendinger, et al. 1997) show a continuous, eastward progression of the age of deformation and consistent kinematics between the provinces. These kinematics suggest a structural link between deformation in the Puna Plateau and deformation in the northern Sierras Pampeanas. In the regional cross sections presented, thrust systems at the eastern edge of the Puna are interpreted to join and interact with faults and structures of the northern Sierras Pampeanas. Faults in the Puna also are interpreted to sole into similar detachment levels (~16 km) as basement-cored uplift faults.

4.2. NORTHERN SIERRAS PAMPEANAS

Within the region of study in the northern Sierras Pampeanas there are seven main basement-cored uplifts, including the Sierra Aconquija, Cerro Durazno, Sierra de Quilmes, Sierra de Hualfín, Sierra de las Cuevas, Sierra Fiambalá, and Sierra de Zapata (Fig. 4.1). The basement in this region is composed of Precambrian and Paleozoic metamorphic rocks and Ordovician granitoid bodies (Omarini et al., 1984; Mendez et al., 1973). A common and important feature of the uplifts is the basement-cover unconformity that is preserved in many of the gently dipping backlimbs of the structures. This paleo-erosional surface is thought to have been formed over a 300-400 million year time span (Jordan et al., 1989). The unconformity (or basement-cover contact) is important in constraining the geometry of basement-cored uplifts and thus aids in the construction of regional cross sections.

4.2.1. Paleogeography, Tectonic Stratigraphy, and Stratigraphy

Paleogeography directly relates to depocenters in the region and is important as it helps to constrain the lateral extent of sedimentary strata in the regional cross section. A summary of sedimentation and related tectonic activity is given in Figure 4.3. Three major depositional events are represented in the region of study. An Ordovician basin located behind a west-facing continental-margin volcanic arc (Bahlburg, 1998), and currently preserved as meta-sedimentary strata, appears to have extended eastward only as far as the Sierra Narváez and does not exist in the Sierras Pampeanas proper. The Carboniferous-Permian Paganzo Basin, considered to be a foreland basin to Pacific Plate subduction under the margin of Gondwana (Ramos, 1988), represents the next major depositional period. Carboniferous deposits of the basin are from the post-glacial Lake Narváez (Buatois and Mangano, 1995). In the Permian, the region is thought to have evolved into a rift system (Buatois and Mangano, 1995). The northern part of the Paganzo Basin extended only as far

east as Sierra Narváez, as the northeastern regions were likely basement highs during the Carboniferous (Buatois and Mangano, 1995). In the middle to late Tertiary (Miocene) through Quaternary, continental deposits were accumulating in vast quantities in the northern Sierras Pampeanas, as the area was the site of a non-marine foreland basin (Jordan and Alonso, 1987). During the Miocene-Pliocene, the southern Eastern Cordillera was lower than the northern Sierras Pampeanas, as revealed by Miocene foreland basin deposition that began earlier in the already-low Eastern Cordillera than in the northern Sierras Pampeanas (Grier et al., 1991). Quaternary deposition of the Punaschotter unit, a boulder conglomerate composed mainly of crystalline rocks from the Puna, appear to mark the uplift of structures to the west (Penck, 1920; González Bonorino, 1950; Allmendinger , 1986; Muruaga, 1999).

Stratigraphic terminology for the area of the cross sections (Fig. 4.4) was drawn from several sources. For the northeastern cross section, stratigraphy and unit thicknesses from González Bonorino (1950), Allmendinger (1986), and Muruaga (1999) were used (Fig. 4.4). These include approximately 3 km of sedimentary strata beneath El Bolsón (area west of Sierra de Hualfín) and 4 km under the Campo del Arenal (basin east of Sierra de Hualfín) (Fig. 4.2c). Basin depths for the Tucumán basin are interpreted on the basis of reflection seismic profiles in Cristallini et al. (2001; 5 km depth), and in Gómez et al. (1999; greater than 3 km depth). For the southwestern cross section, in the areas of Valle de Chaschuil and Sierra de Fiambalá, stratigraphy from Turner (1967) was used (Fig. 4.4). The sedimentary rocks increase westward in thickness from ~4 km to ~ 8 km with the addition of Permian, Carboniferous, Devonian-Ordovician and Ordovician strata west of the Sierra de Fiambalá.

There is a change in thickness of the two Tertiary units in the cross section (Fig. 4.4). In the east, the lower Tertiary unit (Calchaquense or Tambería Formation) is only ~1000 m thick, whereas in the west, the unit is 2800 m thick. The overlying Araucanense

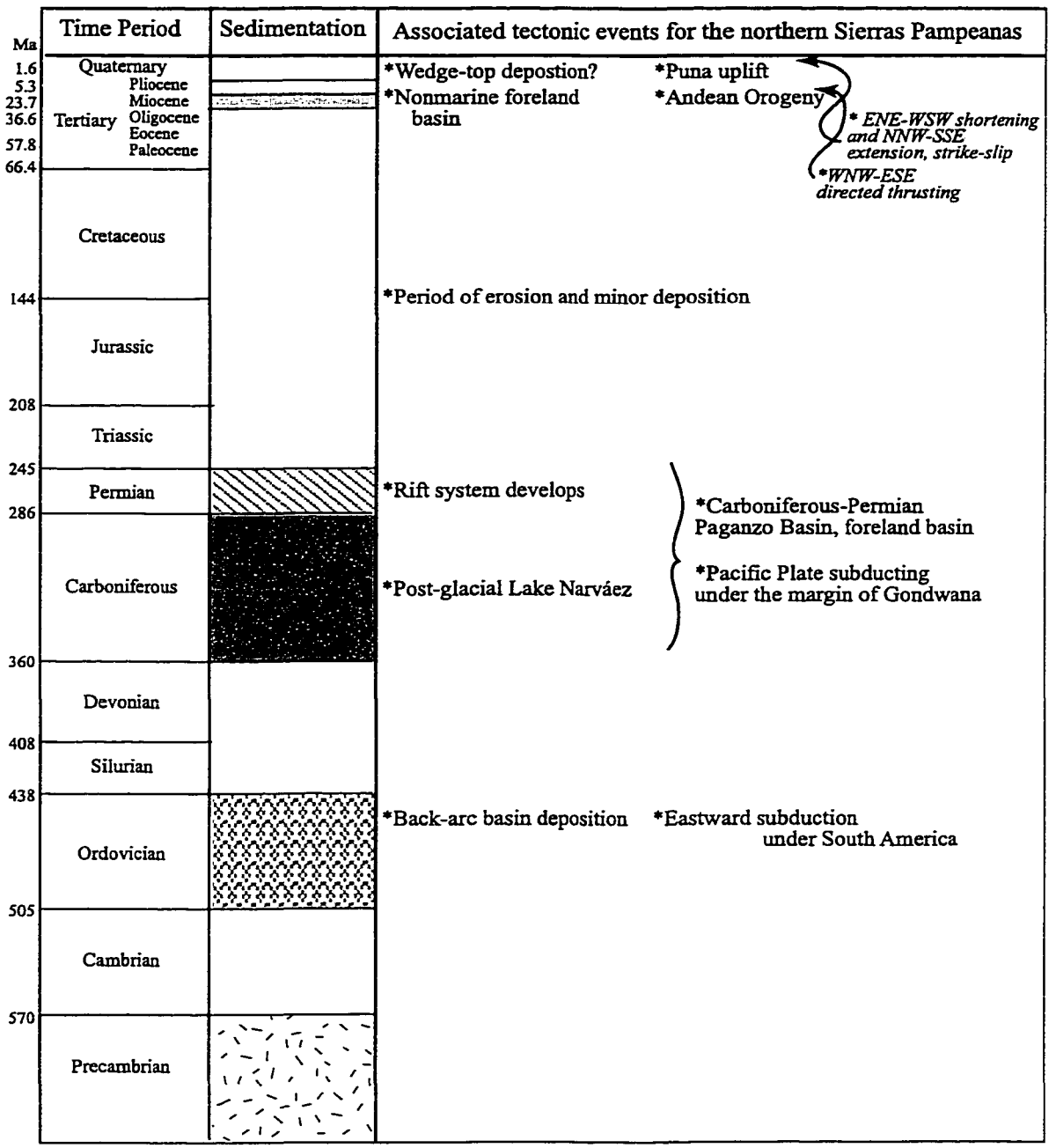

Figure 4.3. Tectonostratigraphic diagram showing major episodes of sedimentation and associated tectonic activity in the northern Sierras Pampeanas area. Kinematics from Marrett et al., (1994) and Allmendinger, et al. (1997).

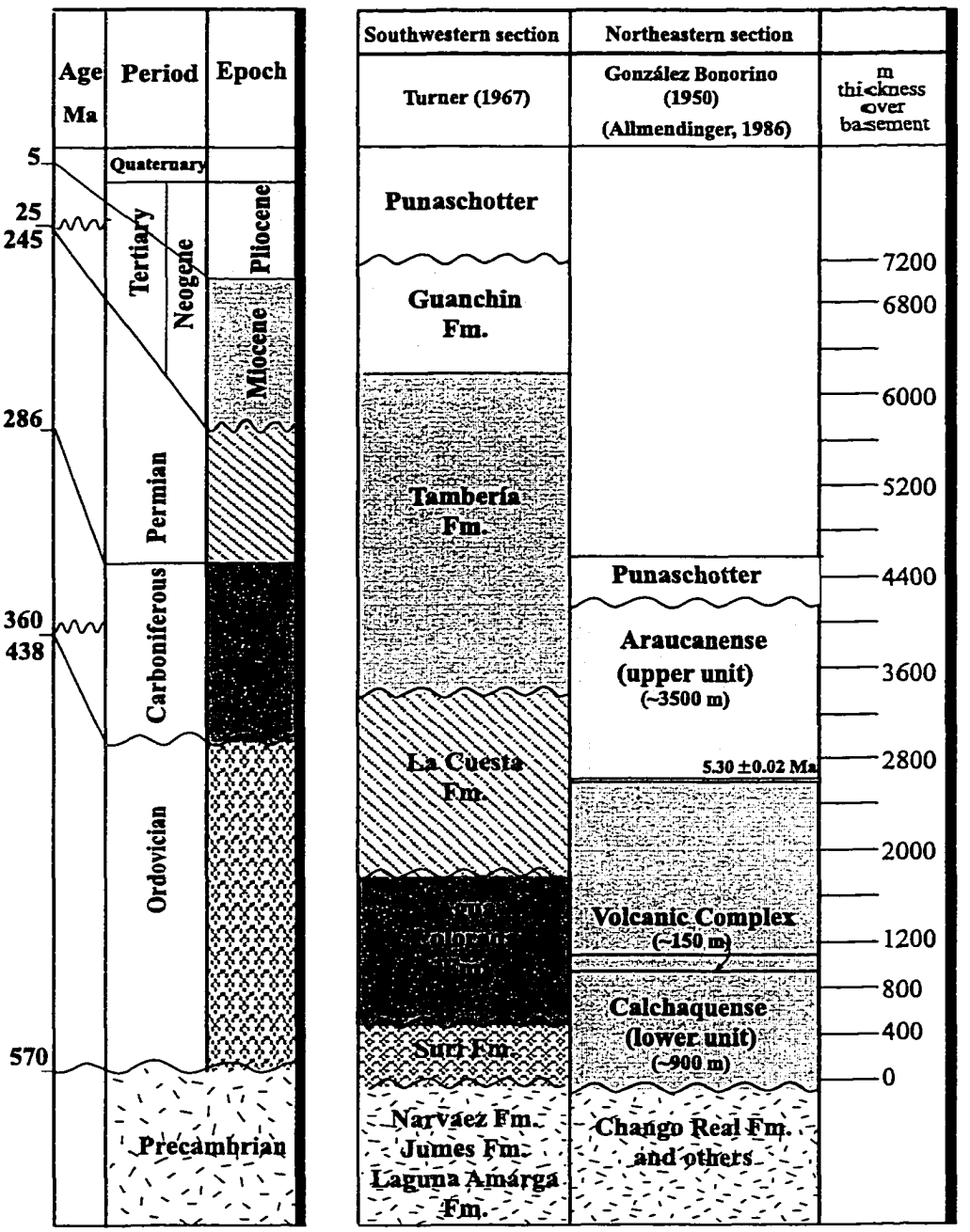

Figure 4.4. Stratigraphic column for the area of study encompassing the cross section. Time is scale on the left and unit thicknesses are scaled on the right. Strata are shown in meters above basement. Note the greater thickness of units in the area of the southern cross section which is due to the presence of Ordovician, Carboniferous, and Permian strata not present to the east of the Sierra de Fiambalá. 5.30 +/- 0.2 Ma dated tuff from Butler et al. (1984).

Formation (or Guanchín Formation) is ~ 3000 m thick (Allmendinger, 1986) in the east, and only 1000 m thick in the west. When compared in terms of time represented (shading of units in Fig. 4.4), the strata are more similar in thicknesses (2600 m and 2800 m for Tambería Formation; 1600 m and 1000 m for Guanchín Formation). If these units are correlative (González Bonorino, 1972; Turner, 1967), then a shift in depocenters from west to east during the Mio-Pliocene is implied.

4.2.2. Regional Cross Section

4.2.2.a. Methodology

The regional cross sections were constructed based on published map data, published reflection seismic profiles, and field work conducted for this study. Published maps are from the Instituto Nacional de Geología y Minería, República Argentina, at 1:200,000 scale. The published maps used for the cross sections and for Figure 2c are Hoja 12e Anconquija - González Bonorino (1951), Hoja 13e Villa Alberdi - González Bonorino (1950), Hoja 12d Capillitas - Hoja 12e Andalgala - González Bonorino (1950a), Hoja 12c Laguna Helada - Ruíz Huidobro (1975), Hoja 13c Sierra de Fiambalá - González Bonorino (1972), and Hoja 13b Chaschuil -Turner (1967). Mapping at a scale of 1:250,000 was carried out at approximately latitude 27° 42' S along Rt. 45 from ~ 67°40' to 68° 03' in detail, with reconnaissance mapping from 68°03' to 68°30'. Also, detailed mapping at a scale of 1:55,000 in the area of Sierra de Hualfín was used (García, 2001).

Cross sections were constructed at a scale of 1:250,000 and in two segments (Fig. 4.2a, b) in order to take advantage of available subsurface data from the literature and surface data collected for this study. Regional elevations for the top of basement were determined from known and estimated basin depths. The cross sections were balanced by

conserving line lengths and area in the deformed and the restored versions, and by reasonable depiction of observable structural geometries (Bally et al., 1966; Dahlstrom, 1969).

Depth to detachment for the basement-cored uplifts was calculated iteratively by restoring the individual structures using a flexural slip algorithm in a cross section restoration software program (2DMove from Midland Valley Exploration) (Fig. 4.5a), and by using the area balance method (Dahlstrom, 1969) (Fig. 4.5b). Iterative balancing of individual structures involved restoring the deformed state hanging wall shape, conserving line length and area, and matching the restored hanging wall geometry to the geometry of the (undeformed) footwall (Fig. 4.5a). This method yielded fault-bend fold geometries for basement-cored uplifts, and the detachment levels seen in the cross sections (Fig. 4.2a, b). The area balance method (Fig. 4.5b) uses the area above regional, which is the area between the fault, the hanging wall, and the regional elevation line. This area should be equal to the amount of shortening (*lo*-*lf*) multiplied by the depth to detachment (Dahlstrom, 1969; Fig. 4.5b, A=A'). The combination of these two techniques produces better constrained depth to detachment calculations; however, the calculations are non-unique. For example, for the Sierra de Aconquija, different fault geometries within an acceptable range produced depths to detachments of 23 to 31 km. A depth of 27 km was calculated for Figure 4.2a.

The main variables that affect depth to detachment calculations are the geometry of the top of basement and fault trajectory. The basement unconformity is often well exposed on the gently dipping backlimb of uplifts in the northern Sierras Pampeanas, and thus provides a rigid constraint for depth to detachment calculations. Studies in the Sierra de Hualfín (García, 2001; García and Davis, 2001), where the basement unconformity and overlying cover sediments are well-preserved, have served as a guideline for interpreting the geometry of the basement unconformity of other uplifts where the unconformity may

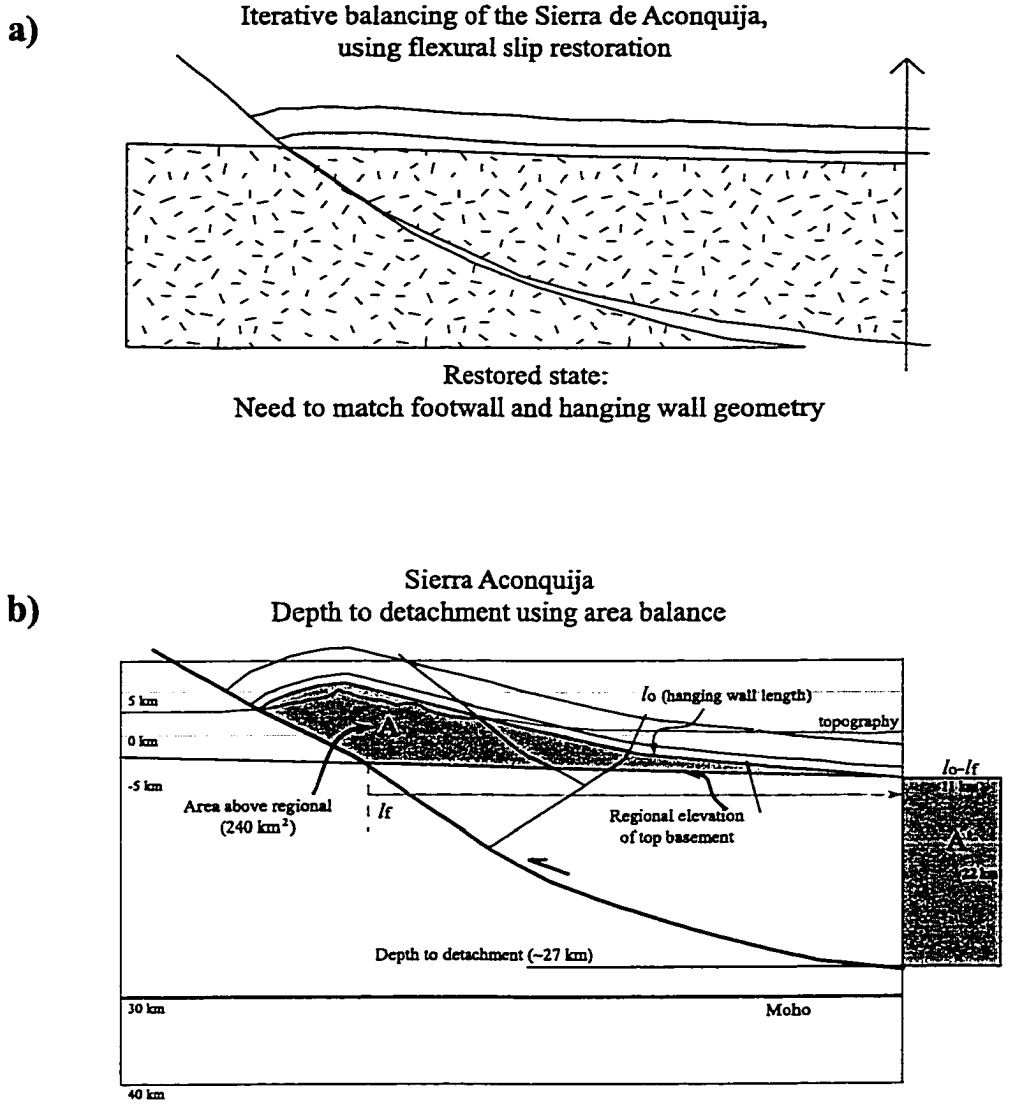

Figure 4.5. (a) Sample restoration step for the Sierra Aconquija showing footwall and hanging wall cut-offs. These cut-offs need to match in order to consider the cross section balanced. The cut-off geometry depends on the shape of the fault, and thus can help determine depth to detachment calculations. Steeper fault angles did not restore well, give the observed surface geometry of the top of basement and overlying sedimentary strata.

(b) Area balance method for determining depth to detachment for the Sierra Aconquija, after Dahlstrom (1969). Depth to detachment is obtained by calculating shortening (lo-lf), and dividing the shaded area A by shortening. This results in the vertical component (d) of area A', which is the depth to detachment.

not be exposed. Fault geometry was constrained by the geometry of the overlying sediments and the basement unconformity. In some areas of the Sierras Pampeanas, inversion of previous rift structures (e.g., Schmidt et al., 1995) has been cited as a way to explain steep dips on thrust faults. Within the northern Sierras Pampeanas of this study area, there is no sedimentological record that indicates previous rifting, in contrast to, for example, the region of the Santa Barbara System where Cretaceous sedimentation records a rifting event (Grier et al., 1991). Thus, low angle thrust faults are interpreted to be producing the basement-cored uplifts in the area of the cross sections.

4.2.2.b. Structure

The northeastern cross section line trends N80°W from the town of Concepción, Tucumán Province, to NW of the village of Villa Vil, Catamarca Province (Fig. 4.2a, c). The length of this section line is approximately 145 km. The section line crosses (from SE to NW) the western edge of the Tucumán basin, Sierra del Aconquija, Cerro Durazno, Campo del Arenal basin, Sierra de Hualfín, and the eastern edge of the Sierra de Alto Huasi. The cross section shows individual basement-cored uplifts separated from each other by intervening basins. There is a west-directed thrust system, represented by faults beneath the Sierra del Aconquija and the Cerro Durazno, and an east-directed fault system, represented by faults beneath the Sierra de Hualfín and the Sierra de Alto Huasi. Subsurface data from Cristallini et al. (2001) show several other minor structures, both east- and west-directed, that do not have a surface expression, but are interpreted as a fault system related to the larger uplifts. Regional elevation of the top of basement in the area of the northeastern cross section is at approximately 5 km below sea level on the east and 1 km below sea level on the west, and thus slopes 2°E. Shortening in this cross section is about 16 km or 11%.

The southwestern cross section line trends E-W at the latitude of ~ 27° 42' S. The cross section line is 145 km long, and from E to W passes through Campo de Belén, Sierra de Zapata, Cerro Fraile, Sierra de Fiambalá, Bolsón de Fiambalá, Sierra Narváez, and Valle de Chaschuil. In this section, the Sierra de Fiambalá and the basement-cored uplifts to the east are separated by relatively narrow and shallow basins. Cerro Fraile appears to be an imbricate thrust block of the Sierra de Fiambalá because its eastern-bounding fault is interpreted to join the thrust of Sierra Fiambalá to the south and to the north (Fig. 4.2c). West of the Sierra de Fiambalá (considered the westernmost uplift of the Sierras Pampeanas), folded and faulted Tertiary sedimentary rocks have been juxtaposed by a normal fault with the east-dipping backlimb of another basement-cored uplift, the Sierra de Narváez. The east flank of the Sierra de Narváez contains the eastern-most exposures of Carboniferous and Permian sedimentary units. In the footwall of the east-dipping Sierra de Narváez fault, Permian and Carboniferous strata are folded into an anticline-syncline-anticline geometry (Fig. 4.2b, c). It is unclear whether folding of these units was contemporaneous with thrusting of the Sierra Narváez, related to thrusting of Ordovician strata from the west, or a combination of both. Five kilometers west of the Sierra de Narváez, Ordovician metasedimentary rocks are thrust eastward over the folded Permian and Carboniferous strata, and Devonian-Ordovician rocks are thrust westward over Tertiary strata. In the cross section, the west-dipping thrust is interpreted as the major uplifting thrust whereas the east-dipping thrust is interpreted as a backthrust. West of the thrusted Ordovician rocks are a series of normal faults with variable offset that affect Precambrian through Tertiary rocks. These normal faults are interpreted as older faults, cut by a west-dipping thrust fault, and transported eastward in the hanging wall of the thrust fault.

Regional elevation of the top of basement in the east is ~ 3 km below sea level under the Campo de Belén, and would be 6.4 -8 km below sea level in the west, given the thickness of the Paleozoic through Cenozoic strata in the western region. However, the top of the basement in the westernmost area of the southern section is currently at 1.5 km above sea level, despite greater thickness of sedimentary cover units. Structural relief on the basement, thus, is ~ 7.9 - 9.5 km. In order to attain this structural elevation on the west, a large basement thrust is interpreted to lie beneath the normal faults in the west, thereby increasing the thickness of the basement underneath the western region and elevating regional top of basement.

Splicing the two cross sections together, the region of the northern Sierras Pampeanas at ~ 27° 30'S can be interpreted as shown in Figure 4.6. The sections are joined at the westernmost fault in the northeastern section (Cerro Negro-S. Alto Huasi fault, see Fig. 4.2c) which, along strike and to the south, becomes the fault of Sierra de Fiambalá. The combined sections show east- and west- directed fault systems which detach below ~ 25 km, near the base of the crust. There is also a midcrustal detachment at 16 km depth and a lateral ramp under Sierra de Hualfín at 5 km that is interpreted to join the midcrustal detachment farther to the west and south.

4.2.2.c. Crustal thickness

In order to help constrain the regional cross sections, it is important to interpret crustal thickness. Crustal thickness in the area between 27°S and 28°S latitude has not been directly measured. Estimates of depth to the Moho at 24.5° S and at 30°S latitude, obtained from broad band seismology studies (Whitman, 1994; Yuan et al., 2000) (Fig. 4.7), and gravity measurements and modeling (Introcaso et al., 1992), are the closest direct

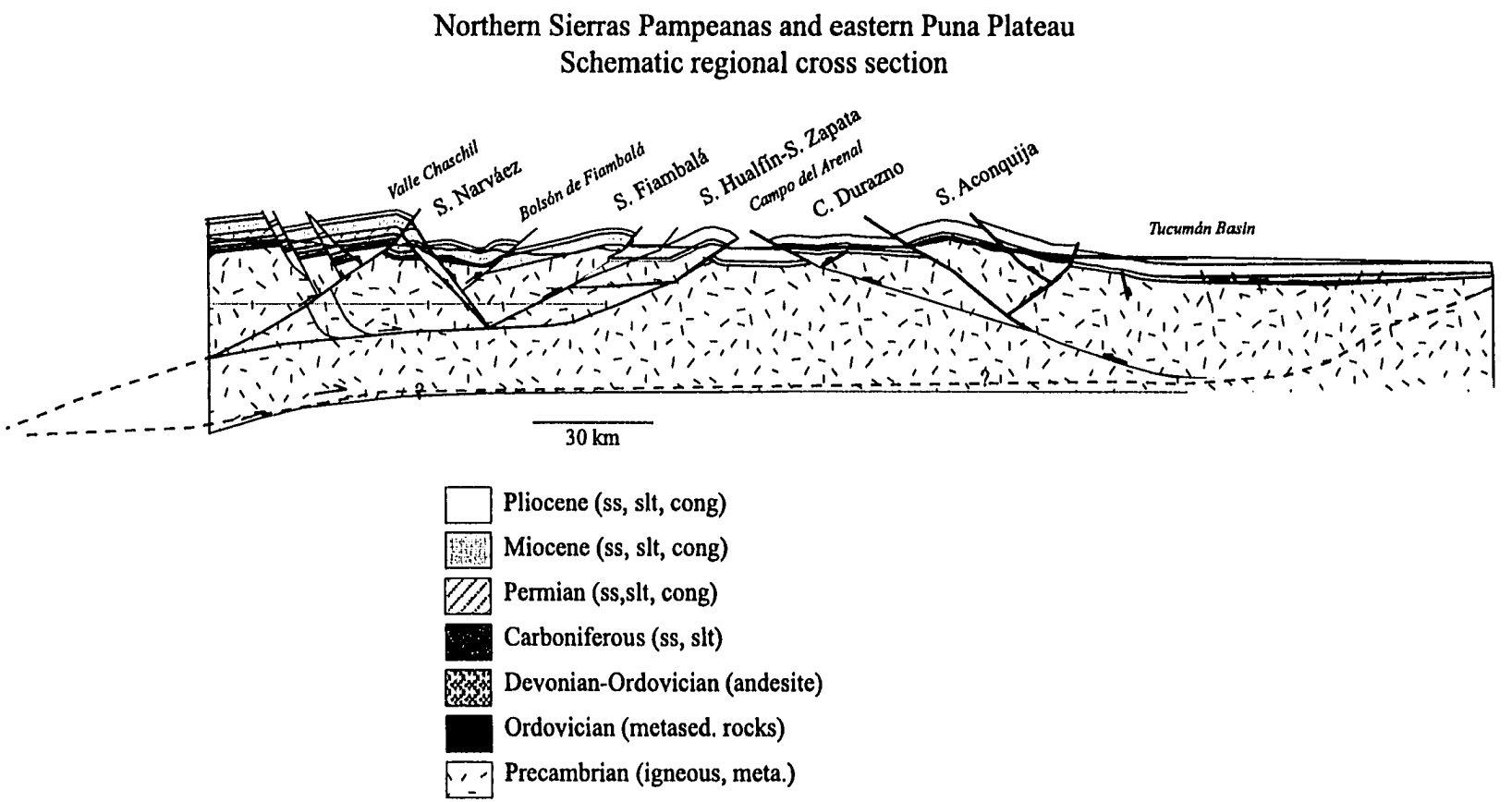

Figure 4.6. Schematic cross section combining northern and southern cross sections. Overlap between the two sections is at the Sierra de Alto Huasi fault and the Sierra de Fiambalá fault (see Figure 4.2c).

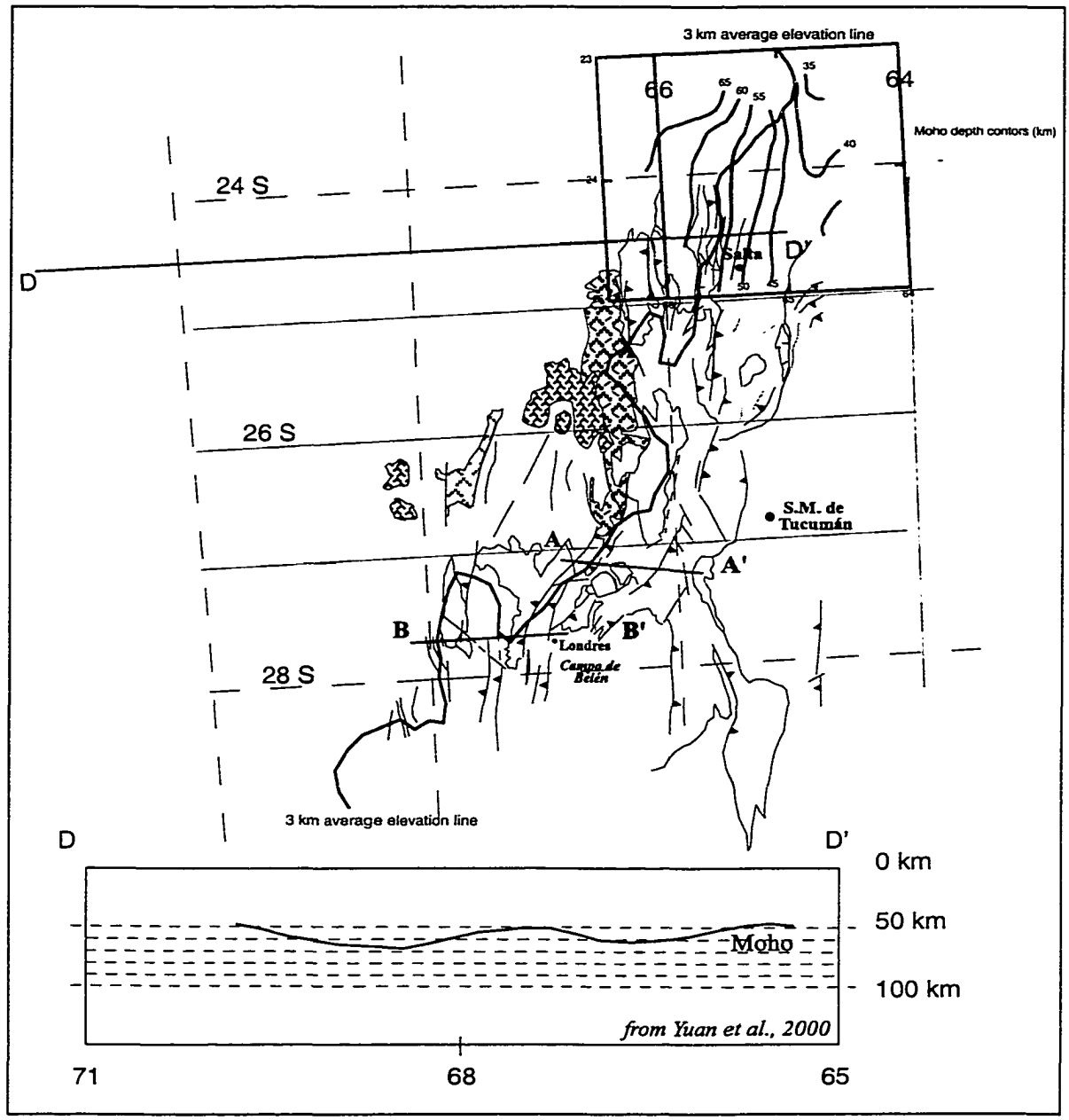

Figure 4.7. Crustal thickness map. Moho contours are from Whitman et al. (1994). Cross section D-D' (from Yuan et al. 2000) shows depth to Moho at 24.5° S. Geology is the same as Figure 4.1.

Area	Thickness (km)	Comments	Reference
Southern Altiplano	75-80	Predominantly felsic crust, relatively high velocity uppermost mantle	Zandt et al., 1994
		No recent delamination here, no large mafic magma component to thickening	
		Felsic crust--weaker, localizes deformation? or felsic product of thickening	
Lat. 20 deg S	70-74	Western Cordillera and Eastern Cordillera	Beck et al., 1996
(S. Altiplano)	32-38	Chaco Plain (200 km east)	
	60-65	Central Altiplano	
	55-60	16 deg lat, E. Cordillera	
	70-74	20 deg lat, E. Cordillera	
	43-47	Subandean zone	
		at boundary btw E. Cord. & Suband., & in Chaco-->	
		thinner than predicted by Airy isostacy modeling	
Lat. 30 deg S	70	Gravity modeling, MAXIMUM crustal depths	Introcaso et al., 1992
Lat. 32-33 deg S	65		
Lat 35 deg S	57		
Lat. 26 deg S*	~33	Cross section (their Fig. 11), no refs or constraints?	Kay et al., 1994
Near San Juan		*From portable local seismic network (converted waves)*	Regnier et al., 1994
	52	Sierras Pampeanas (S. Pie de Palo)	
	55-57	Eastern Precordillera	
	60	Central Precordillera	
	40	Brazilian shield	
Lat. 24 deg S		*From inverted seismic travel time residuals, eastern edge Puna,*	Whitman, 1994
		coupled with estimates of foreland flexural rigidity	
*	40-45	Flat beneath foreland	
		beneath eastern margin of Puna, dips 10-15 deg west	
	65	Flatens beneanth eastern Puna	
		SIMILAR to Moho modeled from refraction data on western side of Puna	Wigger et al., 1994
Lat. 30 deg S		*From cross sections*	Allmendinger et al., 1990
	~45	Under foreland (pre-deformation crustal thickness of 38km)	
	~65	Under high Andes	
	~45	Under Coastal Cordillera	
Lat. 24 deg S*	36	Cross section (their fig. 8, p.36) under Santa Barbara system	Whitman et al.,1996
Lat. 24.5 deg S	75	Altiplano	Yuan et al., 2000
*	50	Puna	
	30	Chaco plain at lat. 19 deg S, figure 3a	
Lithosphere			
	greater than 150	Altiplano	Whitman et al., 1992, 1993
	less than 100	Puna	

Table 4.1. Summary of the available crustal thickness values by location.

	Area	Elevation	Layer thickness	Density	Crustal thickness
		km	km	kg/m-3	km
1	Tucumán basin				
	low	-0.4	5.0	2300	
		4.6	19.0	2750	
		23.6	76.5	3300	
		100.0			24.0
	high	-0.4	5.0	2500	
		4.6	22.8	2800	
		27.4	72.6	3300	
		100.0			27.8
2	Aconquija-Campo Arenal-Hualfín				
1	low	-2.0	4.0	2300	
		2.0	30.4	2750	
		32.4	67.6	3300	
		100.0			34.4
2	high	-3.0	43.6	2750	
		40.6		3300	
					43.6
3	Campo de Belén-Fiambalá				
	low	-1.6	3.0	2300	
		1.4	29.8	2750	
		31.2	68.8	3300	
		100.0			32.8
	high	-2.0	37.6	2750	
		35.6		3300	
		100.0			37.6
4	Valle Chaschuil				
	low	-3.0	1.0	2500	
		-2.0	42.2	2750	
		40.2	59.8	3300	
		100.0			43.2
	high	-3.0	1.0	2500	
		-2.0	46.4	2800	
		44.4	55.6	3300	
		100.0			47.4

Notes:

Areas separated by changes in elevation or regions of more equal elevation (2 and 3 should be similar).

Elevation is negative above sea level and positive below (depth).

Table shows low and high calculations for crustal thickness based on average crustal densities for a simple, presumed crustal structure.

Average densities from Turcott and Schubert (1982)

mean upper mantle	3300 kg/m-3
granite and diorite	2650-2800
mean density cont. rocks	2750
sedimentary rocks: Ss	*2200-2700*

Isostatic balance calculated against a standard column:

Elev.	Thick.	Density
0	10	2670
10	10	2870
20	10	2950
30	70	3300
100		

1 Assumes basin elevation and basin fill across area.

2 Assumes negligible basin fill, uses and estimated average elevation.

Table 4.2. Airy isostatic calculations for an average crustal column for the Tucumán basin, Campo Arenal-Campo de Belén region and the eastern Puna in the Valle Chaschuil region

measurements available. A combination of general trends (i.e., crust is thicker under the Puna than in the foreland) and calculations of an isostatically balanced crust derived from normal crustal densities and average elevations were used for determining crustal thickness in the study area (Tables 4.1, 4.2). Studies of crustal thickness farther north at 20°S and 21°S (Beck and Zandt, 2001, submitted) show a strong correlation between crustal thicknesses, suggesting Airy isostatic compensation. However, studies carried out farther south suggest that the Puna is supported thermally as well as by a crustal root (Whitman et al., 1996), and thus the elevation of the Puna may not correspond entirely to the thickness of the crust. Recent studies showing a 50-km crust beneath the Puna at 24.5° S (Yuan et al., 2000) support the idea of a thermal root that elevates the Puna an average of ~ 1 km higher than the Altiplano to the north (Whitman et al., 1996). Isostatic calculations in the northern Sierras Pampeanas and southern Puna Plateau using the present day elevations may give a maximum thickness value for the crust in this area.

A summary of the available crustal thickness values by location is shown in Table 4.1. The general trends in the Central Andes include: crustal thickness in the foreland and Subandean zone is around 30 km (Yuan et al., 2000), with thinner crust under the foreland; thickness measurements under the Puna vary from 50 km (Yuan et al., 2000) to 65 km (Whitman, 1994; Wigger et al., 1994). Airy isostatic calculations for an average crustal column for the Tucumán basin, Campo Arenal-Campo de Belén region and the eastern Puna in the Valle Chaschuil region are presented in Table 4.2. The calculations range from 24 to 28 km in the Tucumán basin, and 43 to 47 km in the Valle Chaschuil (Table 4.2). These values are in agreement with the general trend of crustal thicknesses from published data of 30-35 km in the foreland to 50-55 km in the Puna (Table 4.1). The slightly lower values given in the isostatic calculations may suggest that the effects of a thermal root under the Puna farther north are not as great in this region.

4.3. COMPARISON TO OTHER PROVINCES

4.3.1. Setting and Relevance

At the latitudes of the northern Sierras Pampeanas, the main provinces that comprise the Central Andes are: the Puna Plateau (the westernmost region is an active volcanic arc, the central-northern region is an internally drained basin, the eastern edge is a basement-involved thrust system), the Eastern Cordillera (a basement-involved thrust belt) the Santa Barbara System (a foreland province, transitional thrust belt between the thin-skinned Subandean belt to the north and the thick-skinned Sierras Pampeanas to the south) and the Sierras Pampeanas (a foreland basement-cored uplift system).

The structure of the Puna Plateau, as well as the Eastern Cordillera and the Santa Barbara System, is important in considering the structure of the northern Sierras Pampeanas because the tectonomorphic provinces are contiguous and are the result of the same orogenic event. The Puna lies to the north and along-strike of the Precordillera thin-skinned fold-thrust belt, thus occupying a hinterlandward position relative to the northern Sierra Pampeanas. Geologic maps of western Argentina show that the Precordillera becomes or dies out to the north into the Puna region (Fig. 4.1). The Eastern-Cordillera and Santa Barbara System lie along-strike of the northern Sierras Pampeanas and are foreland provinces comparable to the Sierras Pampeanas.

4.3.2. Puna Plateau

The Puna Plateau is considered to be south of 23°S latitude (Whitman et al., 1996) and the area encompassed by elevations greater than 3 km (Isacks, 1988). Puna morphology is characterized by NNE-SSW-trending thrust-bounded Precambrian and Paleozoic basement ranges. The thrusts are east- and west-directed and are separated by

intervening Cenozoic intermontane basins (Coutand et al., 1998). Late Cenozoic sedimentary basins reach up to 5 km in thickness (Allmendinger et al., 1997). The structure of the Puna includes NW-trending Miocene and younger volcanic centers, which have been suggested to be related to preexisting NW-trending zones of weakness (Allmendinger et al., 1983, Alonso et al, 1984, Coira et al., 1982; Allmendinger et al., 1997). The Puna is also the site of the southernmost segment of the active magmatic arc of the Andes.

Deformation and uplift of the Puna have been cited as Neogene (20-15 Ma) in age (e.g. Allmendinger et al., 1983; Jordan and Alonso, 1987). However, recent studies showing syntectonic sedimentation in the Upper Eocene Casa Grande Formation argue for an earlier start of deformation (Coutand et al., 1998). Compression and thrusting in the Puna is thought to have lasted until 2-4 Ma, at which time shortening was mostly active in the Sierras Pampeanas and the Santa Barbara System (Allmendinger and Gubbels, 1996). The bulk of crustal shortening at these latitudes is thought to be in the Puna and not in the foreland (Allmendinger and Gubbels, 1996), although precise amounts are not known due to significant volcanic cover. Estimates of shortening across the Puna have been made on the basis of mass balance considerations (210 km , Isacks, 1988) and mass balance given a thinned lithosphere (150 km, Whitman et al., 1996). Reflection seismic profiles from the Puna at ~23° S (Coutand et al., 1998) (Fig. 4.8d) show that the easternmost basement-involved and other thrusts detach at approximately 2.5 s (TWT; ~ 7.5 - 8 km below the surface, with Vp = 6 - 6.4 km/s), and thus would relate to midcrustal detachment levels in the Santa Barbara system.

The Puna Plateau at ~27° 42' S is an elevated area, both topographically and structurally. A substantial increase in structural elevation is seen by the presence of Permian, Carboniferous, and Ordovician strata that have been raised significantly above their regional elevation. In the cross sections presented here, this increase in regional

elevation where strata are gently dipping or have minor structure and are not accompanied by the development of a fold-thrust belt, is accomplished by large thrust sheets expressed at the surface and in the subsurface. This is the simplest case scenario that balances the cross section and produces the observed surface geometries.

4.3.3. Eastern Cordillera and Santa Barbara System

The northern Sierras Pampeanas are along trend with the Eastern Cordillera in NW Argentina (Grier et al., 1991). The Eastern Cordillera is a basement-involved fold and thrust belt (e.g. Grier et al., 1991) with Precambrian and Paleozoic basement rocks and overlying sedimentary strata. The boundary between the Eastern Cordillera and northern Sierras Pampeanas appears to be the southern margin of the Cretaceous Salta Rift Basin (Grier et al., 1991). The significant change in composition of basement rocks and the amount of overlying sedimentary rocks related to the paleogeography of this region are accountable for the major change in structural styles seen across this boundary (Grier et al., 1991). However, because they lie along-strike, structures need to be compatible or there would be significant shear zones that have not been observed or recognized.

The Eastern Cordillera and the northern Sierras Pampeanas differ in the spacing of structures, in the amount of cover sedimentary units involved and in the composition, and therefore rheology, of the basement. The Eastern Cordillera has folds and faults spaced between 10 and 20 km consistently (Grier et al., 1991) whereas the northern Sierras Pampeanas have structures separated by 5 to 30 km randomly (20 km between S. Quilmes and Cumbres Calchaqui; 15 km between S. Hualfín and C. Durazno; 30 km between C. Durazno and S. Aconquija; less than 5 km in the area of Sierra Fiambalá-Sierra Zapata; see Fig. 2). Similarly, the change from the Subandean belt to the Santa Barbara System

Figure 4.8. Cross sections from the northern Sierras Pampeanas region and adjacent tectonic provinces. Sections are shown at the same scale and in relative spatial positions.

a) Balanced cross section from Grier et al. (1991) across the Eastern Cordillera and the Santa Barbara system at ~25°S.

b) Combined cross section from Figure 4.6, this study, across the northern Sierras Pampeanas and eastern edge of the Puna Plateau, ~27° 30'.

c) Western Sierras Pampeanas reflection seismic profile interpretation at ~ 30°S. From Smalley et al. (1993).

d) Seismic reflection interpretation from Coutand, et al. (1998) of thrust structures on the Puna Plateau at ~23 °S. Note both thin-skinned and basement-involved thrusting. Depth to detachments at the top of basement are approximately 2.5 s (TWT), ~ 7.5 - 8 km below the surface (Vp=6 - 6.4 km/s).

Figure 4.8

a)

Puna Plateau at ~23° S

from Coutand, et al. (1998)

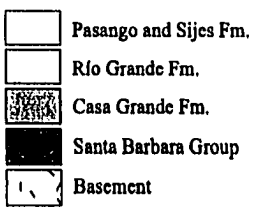

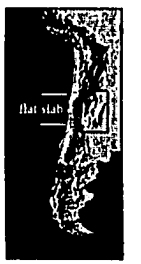

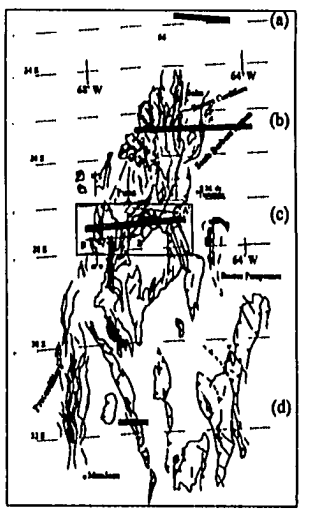

b)

Santa Barbara System and Eastern Cordillera at 25°30'S latitude

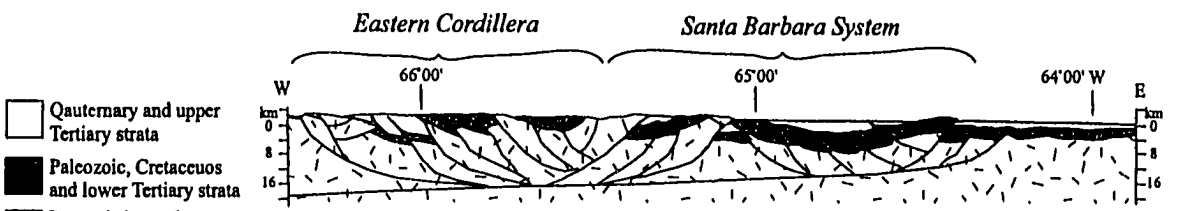

from Grier et al. (1991)

c)

Northern Sierras Pampeanas at ~27° 30' S

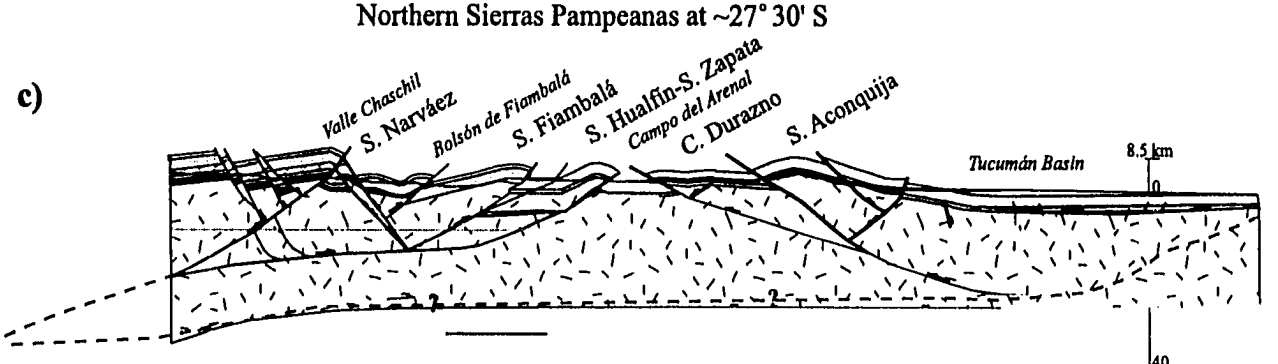

Western Sierras Pampeanas at ~31°40' S, between 68° and 67° W

Seismic reflection profile interpretation across the Sierra de la Huerta

d)

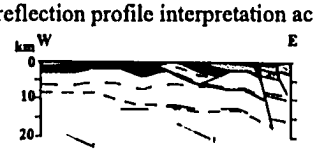

between 23-24°S is abrupt and occurs at the Orán low, the northern margin of the Cretaceous Salta rift (Kley and Monaldi, 1999a).

A cross section at 25°30' from Grier et al. (1991) provides the best comparison to structures in this study because of the proximity of their study area (Fig. 4.8a). They show a decollement level at 10-12 km in the eastern most part of their section under the Santa Barbara system, which deepens to 19 km under the Eastern Cordillera. Grier et al. (1991) suggest that the structures are completely controlled by the Cretaceous rift architecture, which accounts for the west- and east- vergence of the structures in the Eastern Cordillera and in the Santa Barbara System. Cross sections in the Santa Barbara System between 24° and 25°S, farther NE than Grier et al. (1991), similarly show a decollement in the Santa Barbara system at 10-12 km depth that continues to shallow towards the east (Kley and Monaldi, 1999a; their figure 5c). Additionally, reprocessing of a reflection seismic data from the Metán region near the study of Grier et al (1991) reveals a high reflectivity zone at 6 seconds (interpreted as 12 km depth) that is interpreted as the boundary between upper and lower crust, coincident with the decollement horizons in this area (Cristallini et al., 1997). Thus, in these foreland provinces there appears to be a common midcrustal detachment for thrust structures. However, the northern Sierras Pampeanas differ in that the larger uplifts, such as the Sierra Aconquija, require deeper detachment levels, given the geometric and structural assumptions related to detachment depth calculations.

4.3.4. Implications for Basement-Cored Uplift Formation

The combination of modeling of the Sierra de Hualfín from the first study and the regional cross sections with detachments ranging from 16 to 27 km depth suggests that, in this area basement-cored uplifts can be formed by gently-dipping faults detaching in the middle crust and near the base of the crust. Faults with ~30° dips have been imaged in the

Rocky Mountain foreland (e.g. Smithson et al., 1978, 1979) and dips have been corroborated by well data that gives vertical separation and horizontal separation. For example, in the Wind River Mountains there is 10.3 km of vertical separation and 19.5 km of horizontal separation, and in the Bighorn Mountains there is 4.26 km of vertical separation and 8 km of horizontal separation (Stone, 1993). These measurements give average fault angles of about 28° (arctan(vertical separation/horizontal separation) = fault dip) . The midcrustal and deeper detachment levels interpreted here for the northern Sierras Pampeanas also correspond well with detachment levels proposed for the uplifts in the Wyoming foreland (Stone, 1993; Erslev, 1993) (Fig. 4.9). Mechanisms for the formation of basement-cored uplifts must then account for varying levels of detachment for individual uplifts within the same province.

4.3.5. Lithospheric Considerations

Figure 10 shows a scaled lithospheric cross section across the Central Andes at 27°30' S, with the position of the subducting Nazca Plate beneath the South American continent. Foreland structure is represented by the combined cross sections from this study (Fig. 4.6), showing the relation of the study area with other crustal-scale elements. The distance from the active volcanic arc to the foreland is relatively small (under 100 km), and the structural geometries in the foreland, as presently known, do not show large amounts of shortening, although faults are know to exist over 300 km in board from the volcanic arc (Cristallini et al., 2001). This scenario implies that there are significant amounts of shortening under the Puna Plateau that have not been observed. The few seismic reflection profiles from the Puna that are available (at ~23°S, Coutand et al., 1998), suggest the presence of large thrust faults helping to accommodate shortening in the Puna.

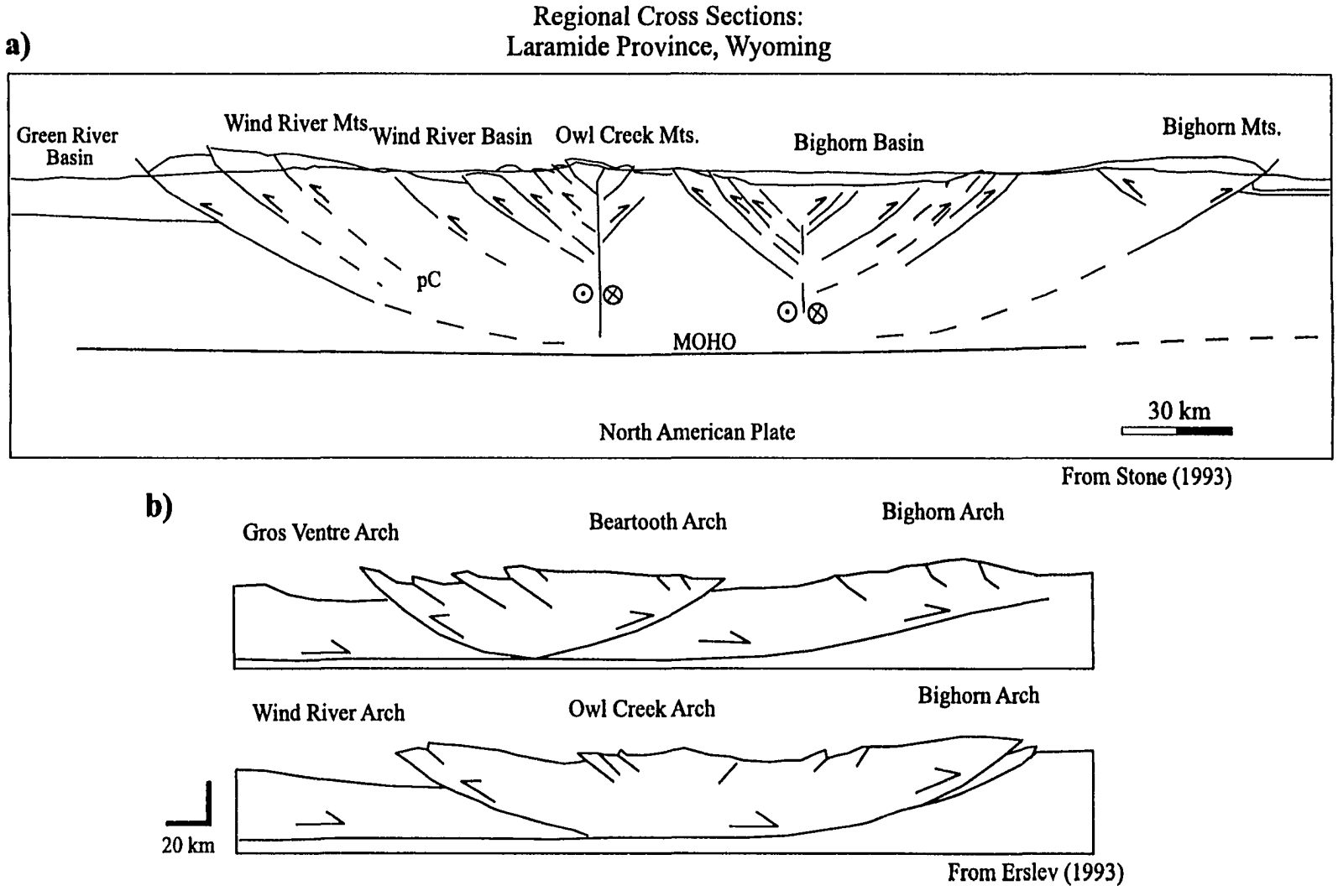

Figure 4.9. Regional cross sections across the Wyoming foreland, showing basement-cored uplifts with gently-dipping (~30°) thrust faults in the subsurface. These thrusts are interpreted to detach at or near the base of the crust. Midcrustal detachment levels are not interpreted although there are several faults shown terminating at midcrustal levels. (a) From Stone (1993). (b) From Erslev (1993).

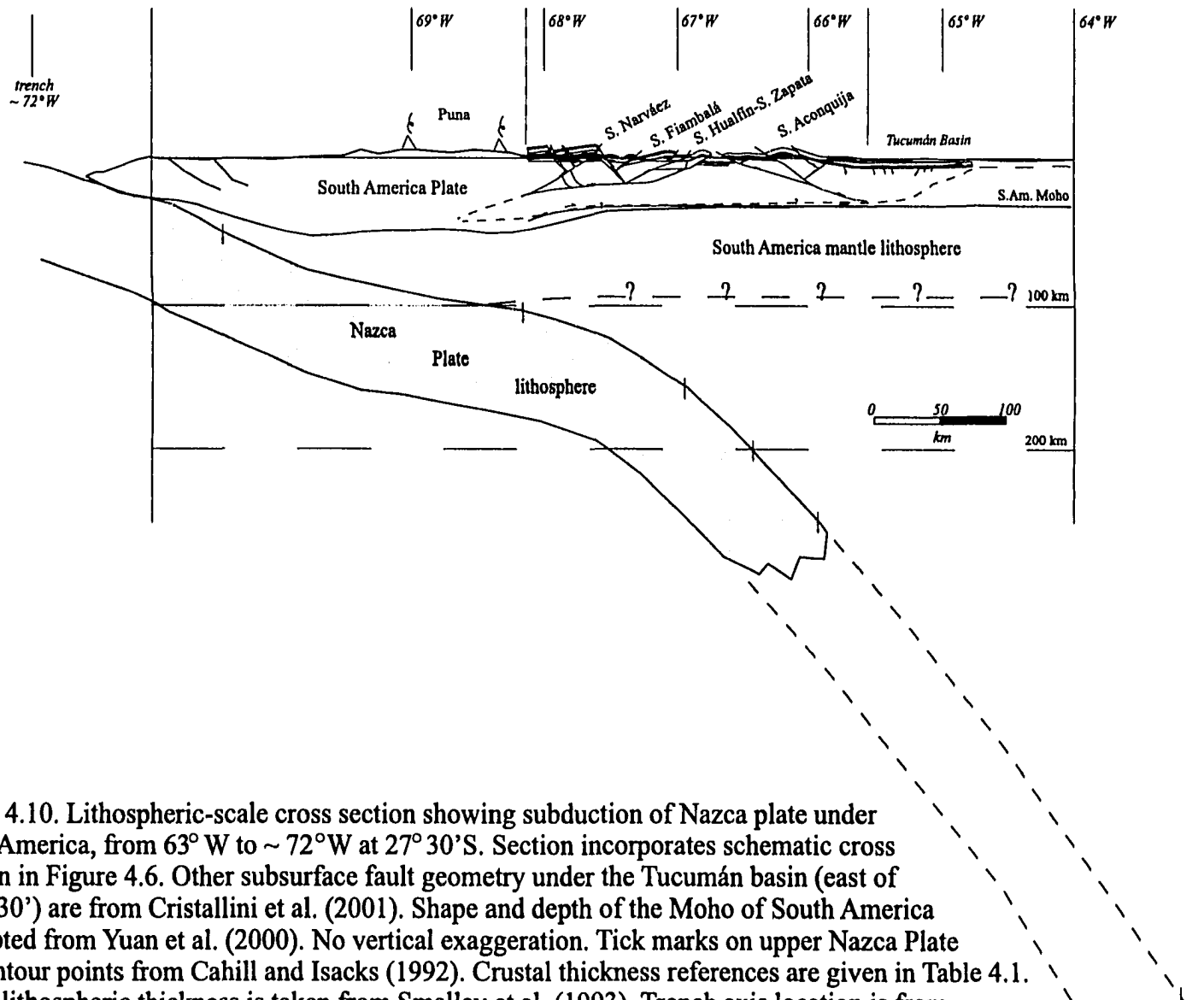

Figure 4.10. Lithospheric-scale cross section showing subduction of Nazca plate under South America, from 63° W to ~ 72°W at 27° 30'S. Section incorporates schematic cross section in Figure 4.6. Other subsurface fault geometry under the Tucumán basin (east of ~ 65° 30') are from Cristallini et al. (2001). Shape and depth of the Moho of South America is adapted from Yuan et al. (2000). No vertical exaggeration. Tick marks on upper Nazca Plate are contour points from Cahill and Isacks (1992). Crustal thickness references are given in Table 4.1. Nazca lithospheric thickness is taken from Smalley et al. (1993). Trench axis location is from Isacks (1988), Cahill and Isacks (1992).

4.5. CONCLUSIONS

1. The regional cross section across the northern Sierras Pampeanas and the eastern edge of the Puna Plateau shows that the northern Sierras Pampeanas have two main detachment levels at 16 km and ~25 km depth.

2. The 16 km depth of detachment in the western region, with a lateral ramp level at 5 km, corresponds well with detachment levels postulated for the Eastern Cordillera to the north. Smaller uplifts, such as the Sierra de la Huerta in the western Sierras Pampeanas, also have a mid-level detachment at ~ 10-12 km depth. In the Puna, 2.5 s (TWT) could be interpreted to be ~ 7.5 -8 km below the surface (Vp = 6 - 6.4 km/s), and thus would relate to midcrustal detachment levels in the Santa Barbara system.

3. The deeper detachment level in the eastern region underneath the Sierra de Aconquija is not seen in the adjacent provinces and seems to be characteristic of the large basement-cored uplifts of the Sierras Pampeanas.

4. Mechanisms for the formation of basement-cored uplifts must address or account for varying levels of detachment for individual uplifts within the same province.

5. The formation of the northern Sierras Pampeanas is not an isolated event and is related structurally (spatially and temporally) to the adjacent Puna Plateau and Eastern Cordillera-Santa Barbara thrust systems, and thus, to the development of the Andean Cordillera.

REFERENCES

Achili, F., Anselmi, G., Ardolino, A., Blasco, G., Caminos, R., Cobos, J., Chipulina, M.A., Dal Molin, C., Foluera, A., Franchi, M., Giai, S., González, O., González, P., Hugo, C., Leanza, H., Lizuain, A., Malumian, N., Martinez, L., Miró, R., Panza, J.L., Ragona, D., 1997, Mapa Geológico de la República Argentina: Servicio Geológico Minero Argentino, scale 1:2,500,000.

Allmendinger, R. W., Ramos, V.A., Jordan, T.E., Palma, M., Isacks, B.L., 1983, Paleogeography and Andean structural geometry, northwest Argentina: Tectonics, v. 2, no. 1, p. 1-16.

Allmendinger, R. W., 1986, Tectonic development, southeastern border of the Puna Plateau, northwestern Argentine Andes: GSA Bulletin, v. 97, p. 1070-1082.

Allmendinger, R. W., Figueroa, D., Snyder, D., Beer, J., Mpodozis, C., Isacks, B.L., 1990, Foreland shortening and crustal balancing in the Andes at 30 S latitude: Tectonics, v. 9, no. 4, p. 789-809.

Allmendinger, R. W., and Gubbels, T., 1996, Pure and simple shear plateau uplift, Altiplano-Puna, Argentina and Bolivia: Tectonophysics, v. 256, p. 1-13.

Allmendinger, R. W., Jordan, T. E., Kay, S. M., and Isacks, B. L., 1997, The evolution of the Altiplano-Puna Plateau of the central Andes: Annual Review of Earth & Planetary Science, v. 25, p. 139-74.

Allmendinger, R. W., 1998, Inverse and forward modeling of trishear fault-propagation folds: Tectonics, v. 17, no. 4, p. 640-656.

Assumpção, M., and Araujo, Mario, 1993, Effect of the Altiplano-Puna plateau, South America, on the regional intraplate stresses: Tectonophysics, v. 221, p. 475-496.

Bahlburg, H., 1998, The geochemistry and provenance of Ordovician turbidites in the Argentine Puna, in Pankhurst, R. J. a. R., C.W., ed., The Proto-Andean Margin of Gondwana: London, Geological Society, p. 127-142.

Bally, A. W., Gordy, P.L., Stewart, G.A., 1966, Structure, seismic data, and orogenic evolution of southern Canadian Rocky Mountains: Bulletin of Canadian Petroleum Geology, v. 14, no. 3, p. 337-381.

Barnes, C. W., and, and Houston, R. S., 1969, Basement response to the Laramide orogeny at Coad Mountain, Wyoming: Contributions to Geology, v. 8, no. 1, p. 37-41.

Beck, S. L., Zandt, G., Myers, S. C., Wallace, T. C., Silver, P. G., and, and Drake, L., 1996, Crustal-thickness variations in the central Andes: Geology, v. 24, p. 407-410.

Beck, S. L., and Zandt, G., 2001, The nature of orogenic crust in the Central Andes: Journal of Geophysical Research, submitted.

Blackstone, D. L., 1980, Foreland deformation; Compression as a cause: Contributions to Geology, v. 18, p. 83-101.

Blackstone, D. L., 1983, Laramide compressional tectonics, southeastern Wyoming: Contributions to Geology, v. 22, no. 1, p. 1-38.

Bossi, G. E., Ovejero, R., and, and Strecker, M., 1987, Correlación entre los Perfiles de Puerta de Corral Quemado-Hualfín y de Entre Ríos (Chiquimil), Pcia. de Catamarca, Argentina: Actas X Congreso Geológico Argentino, v. 2, p. 155-172.

Bossi, G., Muruaga, C., Sanagua, J., Hernando, A., and, and Ahumada, A. L., 1993, Geología y estratigrafía de la Cuenca Neógena Santa María-Hualfín (Dptos. Santa María y Belén, Provincia de Catamarca): XII Congreso Geológico Argentino y II Congreso de Exploración de Hidrocarburos, v. II, p. 156-165.

Bossi, G., Muruaga, C., Georgieff, S., Ahunada, A.L., Ibañez, L., and Vides, M.E., 1997, The Santa Maria Neogene Basin of the Pampeanas Ranges: an example of mixed tectonic evolution: I Congreso Latinoamericana de Sedimentología, Sociedad Venezolana de Géologos, v. 1, p. 97-104.

Brown, W. G., 1988, Deformational style of Laramide uplifts in the Wyoming foreland, in Schmidt, C. J., and Perry, W. J., eds., Interaction of the Rocky Mountain foreland and the Cordilleran thrust belt: Geological Society of America Memoir 171, p. 1-25.

Buatois, L. A., and Mangano, M. G., 1995, Sedimentary dynamics and evolutionary history of a Late Carboniferous Gondwanic lake in north-western Argentina: Sedimentology, v. 42, p. 415-436.

Butler, R. F., Marshall, L. G., Drake, R. E., and, and Curtis, G. H., 1984, Magnetic polarity stratigraphy and 40K-40Ar Dating of Late Miocene and Early Pliocene continental deposits, Catamarca Province, NW Argentina: Journal of Geology, v. 92, p. 623-636.

Caminos, R., 1979, Sierras Pampeanas noroccidentales. Salta, Tucumán, Catamarca, La Rioja y San Juan., Geología Regional Argentina, Segundo Simposio: Córdoba, Argentina, Academia Nacional de Ciencias de Córdoba, p. 225-292.

Chester, J. S., Spang, J.G., and Logan, J.M., 1988, Comparison of thrust fault rock models to basement-cored folds in the Rocky Mountain foreland, in Schmidt, C. J., and Perry, W.J., Jr., ed., Interaction of the Rocky Mountain foreland and the Cordilleran thrust belt: Geological Society of America Memoir 171, p. 65-74.

Coira, B. L., Davidson, J., Mpodozis, C., and Ramos, V.A., 1982, Tectonic and magmatic evolution of the Andes of northern Argentina and Chile: Earth Science Reviews, v. 18, p. 303-332.

Coney, P. J., 1976, Plate tectonics of the Laramide Orogeny, Tectonics and Mineral Resources of Southwestern North America: New Mexico Geological Society, Special Publication, p. 5-10.

Cook, D. G., 1988, Balancing basement-cored folds of the Rocky Mountain foreland, in Schmidt, C. J., and Perry, W. J., eds., Interaction of the Rocky Mountain Foreland and the Cordilleran Thrust Belt: Geological Society of America Memoir 171, p. 53-64.

Coughlin, T. J. O. S., P.B., Kohn, B.P., Holcombe, R.J., 1998, Apatite fission track thermochronology of the Sierras Pampeanas, central western Argentina: Implications for the mechanism of plateau uplift in the Andes: Geology, v. 26, no. 11, p. 999-1002.

Coutand, I., Cobbold, P., Chauvin, A., Rossello, E., Lopez-Gamundi, O., 1999, Cenozoic deformation and tectonic style of the Puna Plateau (northwestern Argentina, central Andes), in Fourth ISAG, Goettingen, Germany, p. 192-196.

Cristallini, E. C., 1997, Deep structure of the Metán region: Journal of South American Earth Sciences.

Cristallini, E. O., Comínguez, A., Ramos, V.A., 1998, Estructural profunda del sector occidental de la sierra del Aconquija, Sierras Pampeanas de Argentina: Congreso Latino Americano de Geología.

Cristallini, E. O., Cominguez, A. H., Ramos, V. A., and , and Mercerat, D. E., 2001, Basement double-wedge thrusting in western Sierras Pampeanas of Argentina (26°s): Constraints from deep seismic reflection: Thrust Tectonics Conference, Special Publication. Royal Holloway, University of London.

Dahlstrom, C. D. A., 1969, Balanced cross sections: Canadian Journal of Earth Sciences, v. 6, p. 743-757.

DeCelles, P. G., Gray, M.B., Ridgway, K.D., Cole,R.B., Srivastava, P., Pequera, N., Pivnik, D.A., 1991, Kinematic history of a foreland uplift from Paleocene synorogenic conglomerate, Beartooth Range, Wyoming and Montana.: Geological Society of America Bulletin, v. 103, p. 1458-1475.

Demorest, M., 1941, Critical structural features of the Bighorn Mountains, Wyoming: Geological Society of America Bulletin, v. 52, no. 2, p. 161-176.

Dickinson, W. R., and Snyder, W. S., 1978, Plate tectonics of the Laramide orogeny, in Matthews, V. I., ed., Laramide Folding Associated with Basement Block Faulting in the Western U.S., Geological Society of America Memoir 151, p. 355-366.

Erslev, E., 1986, Basement balancing of Rocky Mountain foreland uplifts: Geology, v. 14, p. 259-262.

Erslev, E. A., 1991, Trishear fault-propagation folding: Geology, v. 24, p. 617-620.

Erslev, E., and Rodgers, J., 1993, Basement-cover geometry of Laramide fault-propagation folds, in Schmidt, C. J., Chase, R.B., Erslev, E.A., eds., Laramide Basement Deformation in the Rocky Mountain Foreland of the Western United States: Geological Society of America Special Paper 280, p. 125-146.

Evans, J. P., 1985, Deformation mechanisms and textures in feldspar-rich rocks; Examples from Laramide fault zones, Wyoming: EOS Transactions of the American Geophysical Union, v. 66, p. 1068.

Evans, J. P., 1986, Development of a monocline due to compression and its relationship to Laramide basement thrusts: Geological Society of America Abstracts with Programs, v. 18, p. 354.

Evans, J. P., Dubois, M. A., Batatian, D., Derr, D. N., Harlan, S. S., Malizzi, L., McDowell, R. J., Nelson, G. C., Parke, M., Schmidt, C. J., and Weberg, E. D., 1993, Deformation mechanisms and kinematics of a Precambrian-cored fold and fault structure: Jakeys Fork structure, northeastern Wind River Range, Wyoming, in Schmidt, C. J., Chase, R. B., Erslev, E.A., eds., Laramide Basement Deformation in the Rocky Mountain Foreland of the Western United States: Geological Society of America Special Paper 280, p. 163-176.

Gapais, D., Cobbold, P., Bourgeois, O., Rouby, D., and Urreiztieta, M. d., 2000, Tectonic significance of fault-slip data: Journal of Structural Geology, v. 22, p. 881-888.

García, P. E., 1999, "Folding" of basement by faulting in a basement-cored uplift: Sierra de Hualfin, NW Argentina: Geological Society of America Cordilleran Section Meeting, p. A-56.

García, P. E., 2000, 3-Dimensional structure and mechanical stratigraphy of the Sierra de Hualfin, a Laramide-type basement-cored uplift in the Sierras Pampeanas of NW Argentina: Geological Society of America Abstracts with Programs, 1999 GSA Rocky Mountain Section Meeting.

García, P. E., and Davis, G. H., 2001, Mechanisms of basement deformation as revealed in the Sierra de Hualfín basement-cored uplift, NW Argentina: *in prep.*

García, P. E., 2001, Along-strike structural variations in the Sierra de Hualfín, NW Argentina: Clues to the formation of a basement-cored uplift: *in prep.*

Gomez, J. S., Mon, R., and Piccioni, L., 1999, Estructura de la Cuenca de Tucumán y de su subsuelo profundo, in XIV Congreso Geológico Argentino, Salta, Argentina, p. 209-211.

González Bonorino, F., 1950a, Geología y petrografía de las hojas 12d (Capillitas) y 13d (Andalgalá): Ministerio de Industria y Comercio de la Nacion, Direccion General de Industria Minera, Boletín, v. 70, p. 1-39.

González Bonorino, F., 1950b, Descripción geológica de la hoja 13e, "Villa Alberdi", provincia de Tucumán: Argentina, Direccion Nacional de Geologia y Mineria, Boletin., v. 74, p. 1-78.

González Bonorino, F., 1951, Descripción geológica de la hoja 12e, "Anconquija", Catamarca-Tucumán: Argentina, Direccion Nacional de Geologia y Minería, Boletin., v. 75, p. 1-50.

González Bonorino, F., 1972, Descripción geológica de la Hoja 13c, "Fiambalá": Direccion Nacional de Geología y Minería, Boletín, v. 127, p. 1-75.

Grier, M. E., Salfity, J.A., Allmendinger, R.W., 1991, Andean reactivation of the Cretaceous Salta rift, northwestern Argentina: Journal of South American Earth Science, v. 4, p. 351-372.

Introcaso, A., Pacino, M.C., and Fraga, H., 1992, Gravity, isostacy and Andean crustal shortening between latitudes 30 and 35 deg. S.: Tectonophysics, v. 205, p. 31-38.

Isacks, B. L., 1988, Uplift of the Central Andean Plateau and bending of the Bolivian orocline: Journal of Geophysical Research, v. 93, no. B4, p. 3211-3231.

Jordan, T. E., Isacks, B. L., Allmendinger, R. W., Brewer, J. A., Ramos, V. A., and Ando, C. J., 1983, Andean tectonics related to geometry of subducted Nazca plate: Geological Society of America Bulletin, v. 94, p. 341-361.

Jordan, T. E., and Allmendinger, R. W., 1986, The Sierras Pampeanas of Argentina: A modern analogue of Rocky Mountain foreland deformation: American Journal of Science, v. 286, p. 737-764.

Jordan, T. E., and Alonso, R. N., 1987, Cenozoic stratigraphy and basin tectonics of the Andes Mountains, 20-28 degrees south latitude: American Association of Petroleum Geologists, v. 71, no. 1, p. 49-64.

Jordan, T. E., Zeitler, P., Ramos, V., and Gleadow, A. J. W., 1989, Thermochronometric data on the development of the basement peneplain in the Sierras Pampeanas, Argentina: Journal of South American Earth Science, v. 2, no. 3, p. 207-222.

Kay, S. M., Coira, B., and, and Viramonte, J., 1994, Young mafic back arc volcanic rocks as indicators of continental lithospheric delamination beneath the Argentine Puna plateau, central Andes: Journal of Geophysical Research, v. 99, p. 24,323-24,339.

Kley, J., Monaldi, C. R., Salfity, J.A., 1998a, Along-strike segmentation of the Andean foreland: cause and consequences: Tectonophysics, v. 301, p. 75-94.

Kley, J., and Monaldi, C.R., 1998b, Tectonic shortening and crustal thickness in the Central Andes: How good is the correlation?: Geology, v. 26, no. 8, p. 723-726.

Kley, J., and Monaldi, C.R., 1999, Estructura de las Sierras Subandinas y del Sistema de Santa Barbara, in Congreso Geologico Argentino: Geología del noroeste Argentino, Salta, Argentina, p. 415-525.

Latorre, C., Quade, J., and McIntosh, W. C., 1997, The expansion of C4 grasses and global change in the late Miocene: Stable isotope evidence from the Americas: Earth and Planetary Science Letters, v. 146, p. 83-96.

Marrett, R. A., Allmendinger, R. W., Alonso, R. N., and Drake, R. E., 1994, Late Cenozoic tectonic evolution of the Puna Plateau and adjacent foreland, northwestern Argentine Andes: Journal of South American Earth Sciences, v. 7, no. 2, p. 179-207.

Marshall, L. G., Butler, R. F., Drake, R. E., Curtis, G. H., and, and Tedford, R. H., 1979, Calibration of the Great American Interchange: Science, v. 204, p. 272-279.

Marshall, L. G., and, and Patterson, B., 1981, Geology and geochronology of the mammal-bearing Tertiary of the Valle de Santa María and Río Corral Quemado, Catamarca Province, Argentina: Fieldiana-Geology, v. n.s. no. 9, p. 1-80.

Martinez, L. V., 1995, Mapa Geológico de la Provincia de Catamarca, República Argentina: Ministerio de Economía y Obras y Servicios Públicos, scale 1:500,000.

McConnell, D. A., and Wilson, T.G., 1993, Linkage between deformation of basement rocks and sedimentary rocks in basement-involved foreland folds, in Schmidt, C. J., Chase, R.B., Erslev, E.A., ed., Laramide Basement Deformation in the Rocky Mountain Foreland of the Western United States: Geological Society of America Special Paper 280, p. 319-333.

Mendez, V., Navarini, A., Plaza, D., and Viera, O., 1973, Faja eruptiva de la Puna oriental, in Actas, Congreso Geologico Argentina, 5th, October, 1972, Villa Carlos Paz, p. 89-100.

Miller, E. W., and Lageson, D. R., 1990, Laramide basement deformation in the northern Gallatin Range and southern Bridger Range, southwest Montana: Geological Society of America Abstracts with Programs, v. 22, no. 6, p. 39.

Mitra, G., and Frost, B.R., 1981, Mechanisms of deformation within Laramide and Precambrian deformation zones in basement rocks in the Wind River Mountains: Contributions to Geology, v. 19, p. 161-173.

Mitra, G., Hull, J., Yonkee, A., and Protzman, G., 1988, Comparison of mesoscopic deformational styles in the Idaho-Wyoming thrust belt and the Rocky Mountain foreland, in Schmidt, C. J., and Perry, W. J., eds., Interaction of the Rocky Mountain Foreland and the Cordilleran Thrust Belt: Geological Society of America Memoir 171, p. 119-141.

Mon, R., 1976, La tectónica del borde oriental de Los Andes en las Provincias de Salta, Tucumán y Catamarca, República Argentina: Revista de la Asociación Geologica Argentina, v. 21, p. 65-72.

Muruaga, C., 1998, Estratigrafía y sedimentología del Terciario superior, entre las localidades de Villavil y San Fernando, Provincia de Catamarca [Tesis Doctoral (unpublished) thesis]: Facultad de Ciencias Naturales e Instituto Miguel Lillo.

Muruaga, C., 1999, Estratigrafía de sedimentos terciarios aflorantes en la sierra de Hualfín, NE de Catamarca, in XIV Congreso Geológico Argentino, Salta, p. 479-482.

Narr, W., and Suppe, J., 1994, Kinematics of basement-involved compressive structures: American Journal of Science, v. 294, p. 802-860.

Omarini, R. H., Viramonte, J.G., Cordani, U., Salfity, J.A., Kawashita, K., 1984, Estudio geocronologico Rb/Sr de la Faja Eruptive de la Puna en el sector de San

Antonio de los Cobres, provincia de Salta, in Actas Congreso Geologico Argentino, 9th, S.C. de Bariloche, Argentina, p. 146-158/488.

Peirano, A., 1956, Observaciones generales sobre la tectonica y los depositos terciarios del cuadrangulo 26∞ S - 64 30 - 67 O en el noroeste argentino: Acta Geologica Lilloana, S.M. de Tucumán, v. 1, p. 61-144.

Penck , W., 1920, Der Südrand der Puna de Atacama (NW Argentinien):: Leipzig, Germany, Abhanlungen Mathematisch-Physiakalische Klasse der Sächsischen Akademie der Wisssenschaften, v. 37, 420 p.

Powell, J., Mule, P., Ortiz, P., Duarte, R., Sanagua, J., and Muruaga, C., 1998, Mamíferos del Huayqueriense (Mioceno superior) de la Formación Chiquimil (sector occidental de la Sierra de Hualfín), Catamarca, Argentina: Ameghiniana.

Ramos, V. A., 1988, Late Proterozoic-early Paleozoic of South America - a collisional history: Episodes, v. 11, no. 3, p. 168-174.

Regnier, M., Chiu, J., Smalley, R. J., Isacks, B. L., and Araujo, M., 1994, Crustal thickness variation in the Andean foreland, Argentina, from converted waves: Bulletin of the Seismological Society of America, v. 84, no. 4, p. 1097-1111.

Riggs, E. S., and, and Patterson, B., 1932, Stratigraphy of Late Miocene and Pliocene deposits of the province of Catamarca (Argentina) with notes on the faunae: Physics (Rev. Soc. Argent. Cien. Natur.), v. 14, p. 143-162.

Rodgers, J., 1987, Chains of basement uplifts within cratons marginal to orogenic belts: American Journal of Science, v. 287, p. 661-692.

Roering, J. J., Cook, M.L., Pollard, D.D., 1997, Why blind thrust faults do not propagate to the Earth's surface; numerical modeling of coseismic deformation associated with thrust-related anticlines: Journal of Geophysical Research, v. 102, no. 6, p. 11,901-11,912.

Ruíz Huidobro, O. J., 1975, Descripción geológica de la Hoja 12c, "Laguna Helada": Servicio Geologico Nacional, Boletín, v. 146, p. 1-57.

Sasso, A., 1997, Geological evolution and metallogenetic relationships of the Farallón Negro Volcanic complex, NW Argentina [Ph.D. thesis]: Queens University, 517 p.

Schmidt, C. J., and, and Garihan, J. M., 1983, Laramide tectonic development of the Rocky Mountain foreland of southwestern Montana, in Lowell, J. D., and,Gries, R., eds., Rocky Mountain foreland basins and uplifts, Rocky Mountain Association of Geologists, p. 271-294.

Schmidt, C. J., and Perry, W., J., 1988, Interaction of the Rocky Mountain Foreland and the Cordilleran Thrust Belt, Geological Society of America Memoir 171: Boulder, CO, Geological Society of America, 582 p.

Schmidt, C. J., Genovese, P.W., Chase, R.B., 1993, Role of basement fabric and cover-rock lithology on the geometry and kinematics of twelve folds in the Rocky Mountain

Foreland, in Schmidt, C. J., Chase, R.B., Erslev, E.A., ed., Laramide Basement Deformation in the Rocky Mountain Foreland of the Western United States, Geological Society of America Special Paper 280, p. 1-44.

Schmidt, C. J., and, and Erslev, E., A., 1993, Laramide basement deformation in the Rocky Mountain foreland of the western United States, Geological Society of America Special Paper 280: Boulder, CO, Geological Society of America, 365 p.

Schmidt, C. J., Astini, R. A., Costa, C. H., Gardini, C. E., and Kraemer, P. E., 1995, Cretaceous rifting, alluvial fan sedimentation, and Neogene inversions, southern Sierras Pampeanas, Argentina, in Tankard, A. J., S., R. S., and Welsink, H. J., eds., Petroleum Basins of South America: AAPG Memoir 62, p. 341-358.

Sheriff, R. E., and Geldart, L.P., 1995, Exploration Seismology: Cambridge, New York, Cambridge University Press, 592 p.

Smalley, R. J., Pujol, J., Regnier, M., Chiu, J., Chatelain, J., Isacks, B. L., Araujo, M., and Puebla, N., 1993, Basement seismicity beneath the Andean Precordillera thin-skinned thrust belt and implications for crustal and lithospheric behavior: Tectonics, v. 12, p. 63-76.

Snyder, D. B., Ramos, V. A., and Allmendinger, R. W., 1990, Thick-skinned deformation observed on deep seismic reflection profiles in western Argentina: Tectonics, v. 9, no. 4, p. 773-788.

Spang, J. H., Evans, J. P., and Berg, R., 1985, Balanced cross sections of small fold-thrust structures: The Mountain Geologist, v. 22, no. 2, p. 41-46.

Spang, J. H., and, and Evans, J. P., 1988, Geometrical and mechanical constraints on basement-involved thrusts in the Rocky Mountain foreland province, in Schmidt, C. J., and Perry, W. J., eds., Interaction of the Rocky Mountain Foreland and the Cordilleran Thrust Belt: Geological Society of America Memoir, Geological Society of America, p. 41-51.

Stearns, D. W., 1975, Laramide basement deformation in the Bighorn Basin - The controlling factor for structures in layered rocks, in 27th Annual Field Conference, Cody, Wyoming, p. 149-158.

Stone, D. S., 1993, Basement-involved thrust-generated folds as seismically imaged in the subsurface of the central Rocky Mountain foreland, in Schmidt, C. J., Chase, R.B., Erslev, E.A., ed., Laramide Basement Deformation in the Rocky Mountain Foreland of the Western United States, Geological Society of America Special Paper 280, p. 271-318.

Strecker, M., Bloom, A. L., Malizzia, D., Cerveny, P., Bossi, G., Bensel, C., and, and Villanueva García, A., 1987, Nuevos datos neotectónicos sobre las Sierras Pampeanas septentrionales (26∞ -27∞S): República Argentina, in X Congreso Geológico Argentino, Tucumán, p. 231-234.

Strecker, M. R., Cerveny, P., Bloom, A.L., Malizia, D., 1989, Late Cenozoic tectonism and landscape development in the foreland of the Andes: Northern Sierras Pampeanas (26 - 28 degrees S), Argentina: Tectonics, v. 8, p. 517-534.

Suppe, J., and Medwedeff, D.A., 1990, Geometry and kinematics of fault-propagation folding: Eclogae Geologicae Helvetiae, v. 83, p. 409-454.

Turner, J. C., 1967, Descripción geológica de la Hoja 13b "Chaschuil", Provincia de Catamarca y La Rioja: Boletín Instituto Nacional de Geológica Minería, v. 106, p. 1-.

Urreiztieta, M. d., Gapais, D., Le Corre, C., Cobbold, P. R., and Rossello, E., 1996, Cenozoic dextral transpression and basin development at the southern edge of the Puna Plateau, northwestern Argentina: Tectonophysics, v. 254, p. 17-39.

Whitman, D., 1994, Moho geometry beneath the eastern margin of the Andes, northwest Argentina, and its implications to the effective elastic thickness of the Andean foreland: Journal of Geophysical Research, v. 99, no. B8, p. 15,277-15,289.

Whitman, D., Isacks, B.L., Kay, S.M., 1996, Lithospheric structure and along-strike segmentation of the Central Andean Plateau: seismic Q, magmatism, flexure, topography and tectonics: Tectonophysics, v. 259, p. 29-40.

Wigger, P., Schmitz, M., Araneda, M., Asch, G., Baldzuhn, S., Giese, P., Heinsohn, W.D., Martínez, E., Ricaldi, E., Rower, P., Viramonte, J., 1994, Variation in the crustal structure of the southern Central Andes deduced from seismic refraction Investigations., in Reutter, K. J., Scheuber, E., P.J. Wigger, ed., Tectonics of the southern central Andes: Structure and Evolution of an Active Continental Margin: Berlin, Springer-Verlag.

Wise, D. U., Obi, C.M., 1992, Laramide basement deformation in an evolving stress field, Bighorn Mountain front, Five Springs area, Wyoming: American Association of Petroleum Geologists Bulletin, v. 76, no. 10, p. 1586-1600.

Yuan, X., Sobolev, S.V., Kind, R., Oncken, O., Bock, G., Asch, G., Schurr, B., Graeber, F., Rudloff, A., Hanka, W., Wylegalla, K., Tibi, R., Haberland, Ch., Rietbrock, A., Giese, P., Wigger, P., Rower, P., Zandt, G., Beck, S., Wallace, T., Pardo, M., Comte, D., 2000, Subduction and collision processes in the Central Andes constrained by converted seismic phases: Nature, v. 408, p. 958-961.

Zandt, G., Velasco, A.A., and Beck, S., 1994, Composition and thickness of the southern Altiplano crust, Bolivia: Geology, v. 22, p. 1003-1006.